



# **Properties of gap junctional coupling among glial cells in the central nervous system**

Dissertation zur Erlangung des akademischen Grades des  
Doktors der Naturwissenschaften (Dr. rer. nat.)

eingereicht im Fachbereich Biologie, Chemie, Pharmazie  
der Freien Universität Berlin

vorgelegt von

Nadine Richter  
aus Bernau bei Berlin

2015

Diese Arbeit wurde am Max-Delbrück-Centrum für Molekulare Medizin von November 2011 bis April 2015 unter der Leitung von Prof. Helmut Kettenmann angefertigt.

1. Gutachter: Prof. Helmut Kettenmann
2. Gutachter: Prof. Fritz Rathjen

Tag der Disputation: 24.07.2015

## I. Acknowledgements

*Meine Arbeit liegt hinter mir, wie Sie es selbst sagen. Niemand kann vorhersagen, wie spätere Zeiten sie einschätzen werden. Ich selbst bin nicht so sicher, von der Forschung ist ja der Zweifel unablässig, und mehr als ein Bruchstückchen der Wahrheit hat man gewiß nicht herausbekommen.*

Sigmund Freud (1856 - 1939)  
Österreichischer Psychiater und Begründer der Psychoanalyse  
Quelle: In einem Brief an Stefan Zweig

With this quote, I would like to thank Prof. Dr. Helmut Kettenmann for the great opportunity to work on my "electrifying" project, for the supervision and funding. Prof. Dr. Fritz Rathjen for being my supervisor from the Freie Universität Berlin. Dr. Christiane Nolte for her great guidance and support throughout my time as a PhD-student. I am thankful for the exciting collaborations with Prof. Dr. Christian Steinhäuser and Dr. Stephanie Griemsmann from the ZNE in Bonn and Dr. Tatyana Pivneva from the Bogomoletz Institute of Physiology in Kiev. Furthermore, I would like to thank Dr. Marta Maglione and Dr. Bruno Benedetti, my former supervisor during my Master thesis - where it all began. Particularly thanks to Birgit Jarchow, our indispensable secretary, for her exceptional organizational skills. Thanks to Dr. René Jüttner, Dr. Marcus Semtner and Stefan Wendt for the fruitful discussions. A special thanks also to Philipp Jordan for programming in R for me. Thanks for the technical support to Regina Piske, Michaela Seeger-Zografakis for genotyping and to Nadine Scharek. Not to forget my incredible lab members that accompanied me during my time in the lab. Thank you, Dr. Petya Georgieva, Dr. Maria Pannell, Daniele Mattei, Emile Wogram (my former "Patch-neighbor"), Dr. Katyayni Vinnakota, Dr. Feng Hu, Felipe Sassi, Dr. Frank Szulzewsky and all those who I did not mention here. It was a wonderful experience to work with you! Thank you also to my friends and their understanding for my limited time. Last but not least I want to thank Ronny Heinicke for his enduring support, his understanding, his inspiration and motivation during a demanding time. This thesis is dedicated to my family who I want to thank for all their support and understanding during my time of studies.

## II. Table of Contents

II. Table of Contents.....	IV
III. List of Abbreviations.....	VII
IV. Figure Legend.....	IX
V. Table Legend.....	XI
1 Introduction.....	12
1.1 Glial cells in the central nervous system.....	12
1.2 Astrocytes.....	12
1.3 Oligodendrocytes.....	14
1.4 NG2 cells.....	17
1.5 Microglial cells.....	18
1.5.1 Microglia/macrophages in pathology - Glioma.....	19
1.5.2 Microglia/macrophages in pathology - Stroke.....	20
1.6 Gap junctional communication.....	21
1.6.1 Metabolic coupling among glial cells in the CNS.....	24
1.6.2 Electrical coupling between glial cells in the CNS and regulation by neurotransmitters.....	26
1.7 Aims of the project.....	29
2 Materials and Methods.....	30
2.1 Equipment and Materials.....	30
2.2 Computer software.....	31
2.3 Chemicals.....	31
2.3 Animals.....	35
2.4 Genotyping.....	37
2.5 Acute brain slice preparation.....	39
2.6 The patch-clamp technique.....	40
2.6.1 Visualization and characterization of the different cell types and dye-filling.....	41
2.6.2 Electrophysiological recordings.....	43
2.7 Immunohistochemistry.....	44
2.8 <i>In vivo</i> glioma implantation and stab wound lesion.....	45
2.9 Cell isolation and fluorescence-activated cell sorting (FACS).....	46
2.10 RNA isolation, cDNA preparation and qPCR.....	47
2.11 Connexin primers for PCR and qRT-PCR.....	47

---

2.12	Stroke mouse model - Middle Cerebral Artery Occlusion .....	48
2.13	Statistical analysis .....	49
3	Results .....	50
3.1	Astrocytes form panglial networks in the CNS and express a unique antigen profile .....	50
3.2	Does the panglial network provide energy for axons? .....	54
3.3	Pair recordings of oligodendrocytes in the mouse white matter - corpus callosum .....	59
3.3.1	Gap junctional coupling between oligodendrocytes is low and shows no voltage dependence.....	59
3.3.2	Kainate application does not significantly influence the junctional conductance between oligodendrocyte pairs .....	62
3.4	Electrophysiological characterization and dye-coupling experiments of microglia under normal physiological conditions as well as pathology-associated microglia and macrophages/monocytes .....	66
3.4.1	Microglial cells are not part of the panglial network under normal physiological conditions .....	67
3.4.2	Glioma-associated microglia and macrophages/monocytes express a different membrane current profile.....	68
3.4.3	The membrane potential of GAMs is more negative and the membrane area is increased as compared to control microglia ...	72
3.4.4	Glioma-associated microglia/ macrophages are not coupled by gap junctions.....	72
3.4.5	FACS isolated GAMs, GAMPs and control microglia do not express Cx43 .....	74
3.4.6	Stroke associated microglia/ macrophages show distinct electrophysiological properties.....	74
4	Discussion.....	79
4.1	Astrocytes form panglial networks in the CNS and express a unique antigen profile .....	79
4.2	Does the panglial network provide energy for axons? .....	81
4.3	Oligodendrocytes are electrically coupled in the corpus callosum and display voltage independent gap junctional conductance which could not be inhibited by kainate .....	84

4.4 Glioma-associated microglia and macrophages/monocytes display distinct electrophysiological properties and do not communicate via gap junctions .....	86
4.5 Stroke-associated microglia and macrophages/monocytes display distinct electrophysiological properties .....	88
5 Summary.....	91
6 Zusammenfassung .....	93
7 Eidesstattliche Erklärung.....	96
8 References.....	97
9 Curriculum Vitae .....	106

**III. List of Abbreviations**

ACSF	Artificial cerebrospinal fluid
ADP	Adenosine diphosphate
AMPA	$\alpha$ -Amino-3-hydroxy-5-methyl-4-isoxazolepropionic acid
ATP	Adenosine triphosphate
BSA	Bovine serum albumin
CAP	Compound action potential
CNPase	2', 3'-Cyclic nucleotide-3'-phosphohydrolase
CNS	Central nervous system
CO <sub>2</sub>	Carbondioxide
Cx	Connexin
dKO	Double knock out
DMEM	Dulbecco's modified Eagle's medium
et al.	Et alii (lat.: and others)
e.g.	Exempli grantia (lat.: for example)
EGD	Exogenous glucose deprivation
eGFP	Enhanced green fluorescent protein
EYFP	Enhanced yellow fluorescent protein
FACS	Fluorescence-activated cell sorting
FCS	Fetal calf serum
fEPSP	Field excitatory postsynaptic potential
GABA	$\gamma$ -aminobutyric acid
GAMs	Glioma-associated microglia
GAMPs	Glioma-associated macrophages
GFAP	Glial fibrillary acidic protein
GJ	Gap Junction
GJN	Gap junction network
HBSS	Hank's balanced salt solution
I	Current
Iba1	Ionized calcium-binding adapter molecule
IFN- $\gamma$	Interferon - $\gamma$
IP <sub>3</sub>	Inositol triphosphate
LPS	lipopolysaccharide

MCAo	Middle cerebral artery occlusion
Mt	Mutant
NGS	Normal goat serum
NG2	NG2 chondroitin sulphate proteoglycan
2NBDG	2-[N-(7-nitrobenz-2-oxa-1,3-diazol-4-yl)amino]-2-deoxy-d-glucose
p	Postnatal day
PFA	Paraformaldehyd
PBS	Phosphate buffered saline 1x
PNG	Peptidoglycan
PNS	Peripheral nervous system
PCR	Polymerase chain reaction
qPCR	Quantitative polymerase chain reaction
RT	Room temperature
R <sub>p</sub>	Pipette resistance
TNF- $\alpha$	Tumor necrosis factor - $\alpha$
U	Voltage
V <sub>m</sub>	Membrane potential
WT	Wildtype

## IV. Figure Legend

Figure 1: Illustration of all 3 glial elements in the CNS by Del Rio-Hortega.....	14
Figure 2: Glial metabolic support for myelinated axons.....	15
Figure 3: Morphology and membrane current patterns of rat spinal cord glial cells.....	16
Figure 4: Relationship between polydendrocytes and oligodendrocytes.....	17
Figure 5: Comparison of microglia currents in different activation states.....	19
Figure 6: Gap junctional coupling in the CNS.....	22
Figure 7: Gap junction proteins expressed by oligodendrocytes and astrocytes...	23
Figure 8: Effect of GABA, glutamate, aspartate and glycine on the membrane potential of astrocytes.....	27
Figure 9: The ionotropic- and metabotropic glutamate receptors.....	27
Figure 10: The patch-clamp technique.....	40
Figure 11: Visualization of the brain area of interest and setup.....	42
Figure 12: Voltage commands for whole-cell patch-clamp recordings and pair recordings.....	43
Figure 13: Middle cerebral artery occlusion (MCAo) and timeline for stroke experiment setup.....	48
Figure 14: Astrocyte dye-coupling in the neocortex and corpus callosum of <i>hGFAP/eGFP</i> mice.....	51
Figure 15: Immunostaining of gap junctional networks with Olig2 in the neocortex and corpus callosum of <i>hGFAP/eGFP</i> mice.....	52
Figure 16: Cx43-ECFP+ cells expressing Olig2, a transcription factor expressed by both precursor and mature oligodendrocytes.....	53
Figure 17: NG2 cell staining in biocytin networks in the neocortex of <i>hGFAP/eGFP</i> mice.....	53
Figure 18: Astrocytes supply axons with metabolites via a panglial network in the corpus callosum.....	55
Figure 19: Oligodendrocytes supply axons with metabolites via a panglial network in the corpus callosum of an <i>hGfap/RFP</i> mouse.....	57
Figure 20: Oligodendrocytes supply axons with metabolites via gap junctional network in the corpus callosum of a wildtype mouse.....	58
Figure 21: Pair recording of two oligodendrocytes in the mouse corpus callosum.....	60

---

Figure 22: Average IV-curves of oligodendrocyte pair recordings. ....	61
Figure 23: Current responses of stimulated and receiving cells of a paired recording from oligodendrocytes, over a time course of 150 seconds. ....	63
Figure 24: Conductance of stimulated and receiving cells of oligodendrocyte pair recordings after application of the specific kainate/AMPA receptor ligand kainate. ....	65
Figure 25: Lack of gap junctional coupling in microglia under normal physiological conditions. ....	67
Figure 26: Morphology and membrane currents of control microglia, GAMs, GAMPs and stab wound-associated microglia. ....	70
Figure 27: Specific membrane conductance, membrane capacitance and membrane potential of control microglia, GAMs, GAMPs and stab wound-associated microglia. ....	71
Figure 28: Lack of coupling of GAMs, GAMPs and stab wound-associated microglia. ....	73
Figure 29: Comparison of intrinsic microglia and invading macrophages 7 to 9-days after middle cerebral artery occlusion in MacGreen mice. ....	76
Figure 30: Membrane resistance [R <sub>m</sub> ], membrane capacitance [C <sub>m</sub> ], membrane potential [U <sub>m</sub> ] and specific membrane conductance [G] of stroke associated microglia and macrophages. ....	78
Figure 31: Averaged EGD results under control conditions and previous oligodendrocyte network filling. ....	82

---

## V. Table Legend

Table 1: List of equipment and materials.....	30
Table 2: Filter sets.....	31
Table 3: List of computer software .....	31
Table 4: List of chemicals.....	31
Table 5: Solution for acute brain slices and standard intracellular solution for electrical coupling experiments and experiments injecting microglia in the glioma- or stroke context .....	32
Table 6: Solution for acute brain slices and standard intracellular solution for panglial gap junctional and metabolic coupling experiments. ....	33
Table 7: List of primary antibodies.....	33
Table 8: List of secondary antibodies .....	34
Table 9: Solutions for immunohistochemistry .....	34
Table 10: Solutions for cell isolation and FACS.....	35
Table 11: Antibodies for Fluorescence-activated cell sorting (FACS).....	35
Table 12: List of primer sequences .....	37
Table 13: Solutions for PCR reactions .....	37
Table 14: PCR programs for different mouse strains .....	38

## 1 Introduction

### 1.1 Glial cells in the central nervous system

There are two types of cells in the brain, the neurons and the glial cells. Rudolf Virchow was the first one to mention the glial cells in his lecture in 1858. Although back then he presented the brain connective tissue as the `nerven Kitt`, which he termed `neuroglia` (Kettenmann and Verkhratsky, 2008). Up till now there is a debate on the ratio of neurons vs. glia cells in the brain. The most recent evidence of a 1:1 ratio comes from a study by Azevedo (Azevedo *et al.*, 2009) using a new method of counting cells which they applied to four human brains. However, in contrast to this study a publication by Allen and Barres (Allen and Barres, 2009) states that the proportion of glial cells correlates with the size of the animal, e.g. the nematode worm has only a few glial cells, the fruit fly approximately 25%, the mouse brain about 65% and last but not least, the human brain consists of up to 95% glial cells.

In the central nervous system (CNS) glial cells are essential for normal information processing. They play an important role during development of the CNS, and during injury and disease. They are also important for the physiology of the "normal brain", by modulating synaptic transmission, blood flow, ionic homeostasis and metabolic trafficking. Furthermore, glial cells secrete neuroactive substances like adenosine triphosphate (ATP) and D-serine which are known to be involved in synaptic function. However, these studies are still elusive and have yet to be further investigated; for review see (Barres, 2008). There are four main types of glial cells in the CNS: astrocytes, oligodendrocytes, NG2 cells and microglial cells.

### 1.2 Astrocytes

Astrocytes which are also called astroglia, are a heterogeneous population that can be divided into three morphological phenotypes: fibrous, protoplasmic, and radial astrocytes. In the grey matter, mainly protoplasmic astrocytes (Figure 1 A) can be found whose processes ensheath synapses and blood vessels (Barres, 2008). The fibrous astrocytes are preferentially located in the white matter (Figure 1 B). Via their long unbranched cellular processes they contact nodes of Ranvier at the myelinated axons and blood vessels. The radial cells are arranged in a flat

surface perpendicular to the axis of the ventricles (Barres, 2008). In the developing nervous system, radial glia function both as neuronal progenitors and as a scaffold upon which newborn neurons migrate (Campbell and Gotz, 2002). A rather specialized form of astrocytes are the Müller cells of the retina and Bergmann glia cells in the cerebellar grey matter that ensheat many synapses (Barres, 2008). Most astrocytes have a star-shaped morphology with primary processes that originate from the cell soma. The intermediate filament protein glial fibrillary acidic protein (GFAP) is specifically expressed in the cytoplasm of (the majority of) astrocytes and serves therefore as a classical marker for identification of this cell type. Recently, another marker called Aldh1L1 (aldehyde dehydrogenase 1 family member L1) has been identified by a transcriptional profiling study for astrocytes and astrocytic precursors (Cahoy *et al.*, 2008). Aldh1L1 also labels those astrocytes in the cortex which are negative for the otherwise so frequently used GFAP-marker. Astrocytes can be easily identified by their low input resistance and typical passive, non-inactivating potassium current (Verkhratsky and Steinhauser, 2000) (Figure 14, first column).

Astrocytes play a major role in controlling and maintaining the extracellular potassium homeostasis following axonal activity. This is achieved through a mechanism called “spatial buffering” which makes it possible for astrocytes to take up potassium where concentrations exceed regular levels. The potassium is then distributed through the coupled astrocytes and released in areas where potassium concentrations are too low (Wallraff *et al.*, 2006). Furthermore astrocytes are capable of taking up glutamate, which has been released as a result of neuronal activity, from the extracellular space; accumulation of which could lead to toxic effects. The close contact of astrocytic cell processes with blood vessels and neurons gives them the ability to control local blood flow and easily provide metabolites, such as lactate to neurons (as shown in Figure 2 taken from Saab *et al.* 2013) (Kettenmann and Verkhratsky, 2008).

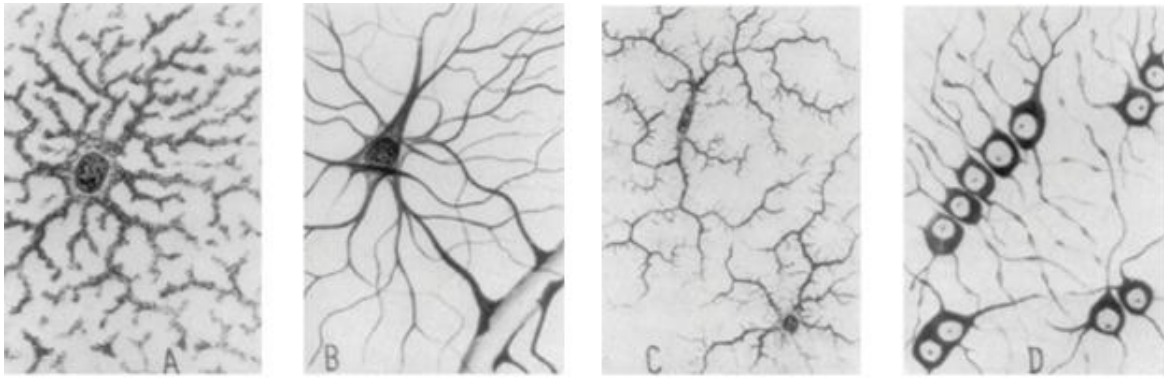
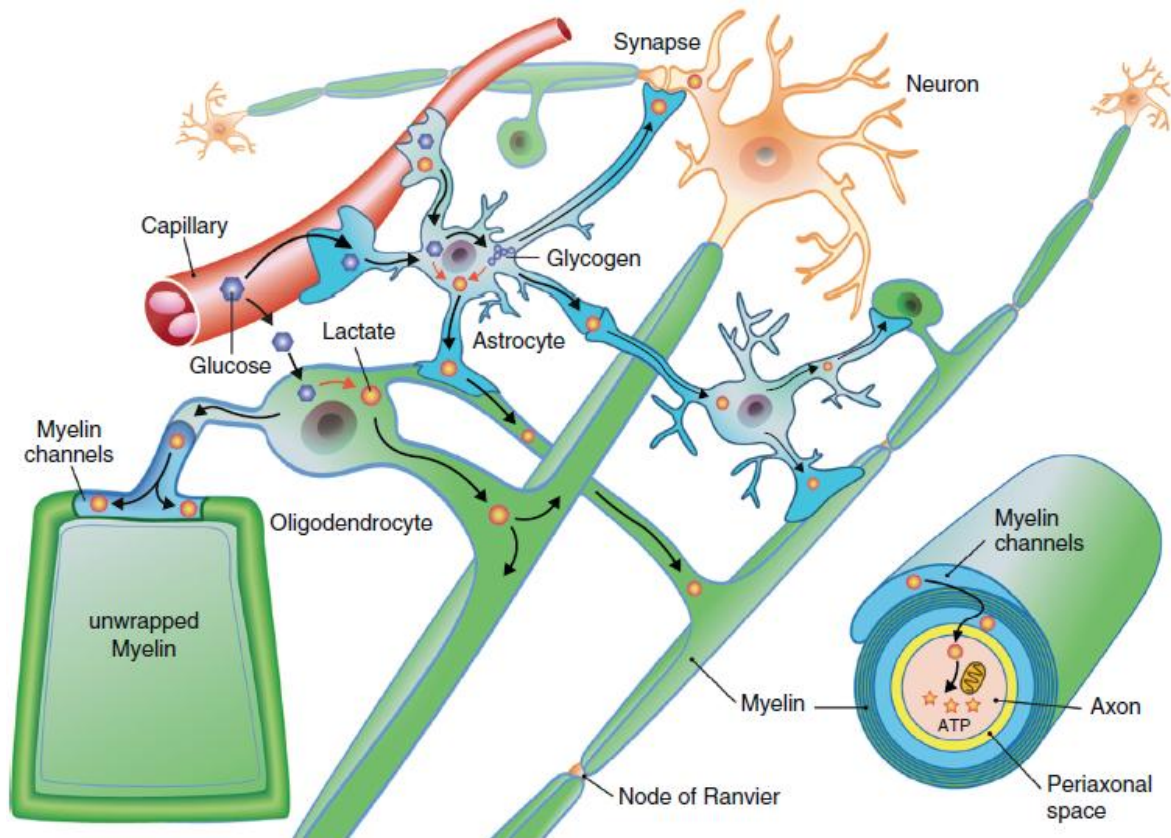


**Figure 1: Illustration of all 3 glial elements in the CNS by Del Rio-Hortega.**

(95) A: protoplasmic astrocytes from grey matter. B: fibrous astrocytes from white matter. C: microglia. D: interfascicular glia, or oligodendrocytes, from white matter. Images drawn by Del Rio-Hortega (Del Rio-Hortega, 1920; Verkhratsky *et al.*, 1998).

### 1.3 Oligodendrocytes

Oligodendrocytes, another major glial cell population, are defined by their primary function of forming myelin sheaths around the neuronal axons. Myelin is a lipidprotein membrane structure which ensures electrical isolation of axons. This myelination is a prerequisite for high conductance and therefore allows the saltatory propagation of action potentials. Depending on the region in the CNS, oligodendrocytes can myelinate up to 50 axonal segments (Baumann and Pham-Dinh, 2001). The myelinating glial cells play an important role in the nervous system function, shaping the structural and electrical properties of axons by controlling their diameter, as well as the spacing and clustering of ion channels at nodes of Ranvier by covering the axon at intervals (internodes) and leaving segments unmyelinated (nodes of Ranvier) (Figure 1 D, Figure 2; Barres 2008).



Current Opinion in Neurobiology

**Figure 2: Glial metabolic support for myelinated axons.**

Oligodendrocytes (green) myelinate and insulate long axons. Capillaries and astrocytes (blue) provide continuously glucose, which enters oligodendrocytes and undergoes glycolysis. Lactate (or pyruvate) diffuses through glial cytoplasmic channels, and reaches the periaxonal space (yellow) via mono-carboxylate transporters (MCT1). Astrocytes, oligodendrocytes and myelin are gap junction coupled (Cx47/Cx30). This panglial network provides via its physical connection ions and metabolites between capillaries and axons. Astrocytic processes enwrap synapses, and provide metabolic support. In case of decreased concentration of glucose, astrocytes can hydrolyze glycogen and maintain the supply of glucose and lactate to oligodendrocytes, axons and synapses. (Image taken from Saab *et al.* 2013)

When myelination takes place during early postnatal brain development, oligodendrocytes undergo significant molecular, morphological, and physiological changes. Additionally, they provide insulation and trophic support to neurons (Barres, 2008). The so-called satellite oligodendrocytes represent a subtype of oligodendrocytes. These cells are preferentially found in the grey matter of the brain and remain opposed to neurons and regulate the extracellular fluid (Baumann and Pham-Dinh, 2001). There is an array of markers that can be used to identify oligodendrocytes by immunohistochemistry: for example, the CNS myelin proteins PLP (proteolipid protein, 50% of myelin protein) and MBP (myelin basic

protein, 30% of myelin protein). Other proteins expressed by oligodendrocyte processes and cell bodies in the CNS are CNPase (2',3'-cyclic nucleotide-3'-phosphodiesterase) and the myelin glycoproteins MOG (myelin oligodendrocyte glycoprotein), a CNS-specific protein, as well as MAG (myelin associated glycoprotein) which is also expressed by Schwann cells in the peripheral nervous system (PNS). (Butt, 2013) Electrophysiological properties of oligodendrocyte precursor cells have been studied by (Berger *et al.*, 1995) and showed a delayed rectifier potassium current and inward rectifying currents. Mature oligodendrocytes are characterized by the presence of voltage independent membrane currents with some decay during voltage steps and sometimes large symmetrical tail currents (Figure 3, B&C) (Berger *et al.*, 1991; Pastor *et al.*, 1995; Maglione *et al.*, 2010).

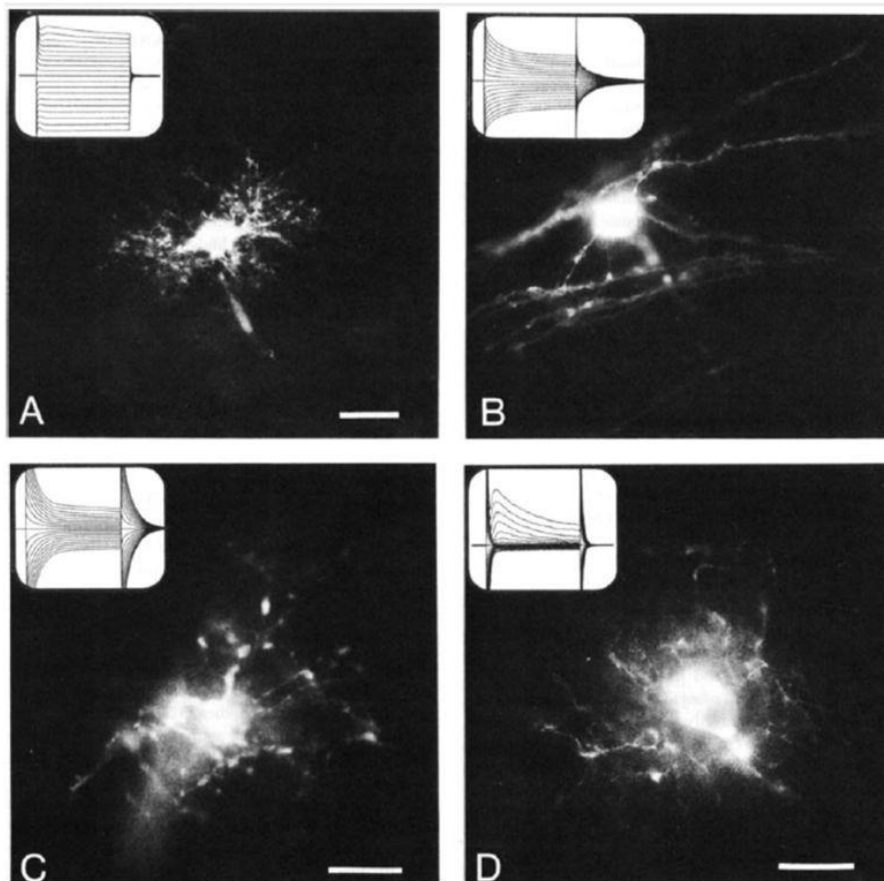


**Figure 3: Morphology and membrane current patterns of rat spinal cord glial cells.**

Image shows lucifer yellow filled glial cells from spinal cord slices. Four types are presented by Pastor *et al.* (1995) based on their distinct channel patterns as shown in the insets. (A) Astrocyte, characterized by a passive current pattern. (B) Oligodendrocyte, identified by its passive decaying currents and rarely branched processes which are aligned in parallel. (C) An oligodendrocyte precursor cell, characterized by voltage-gated  $K^+$  channels. (D) Glial cell with  $Na^+$  currents. (Taken from Pastor *et al.* 1995)

## 1.4 NG2 cells

NG2 cells, also named polydendrocytes, are defined by expression of the NG2 proteoglycan, a type 1-transmembrane protein expressed by an array of cell types inside and outside the mammalian nervous system (Trotter *et al.*, 2010). Moreover, they express alpha receptor PDGF (alpha receptor for platelet-derived growth factor) and the transcription factors Olig2 and Sox10 (Figure 4). They are stellate cells and form multiple contacts with neurons, astrocytes, oligodendrocytes and myelin (Butt *et al.*, 2005). In the postnatal CNS, they are the major proliferating cell population. They proliferate rapidly in response to defects in oligodendrocytes or myelin and give rise to oligodendrocytes and a subpopulation of astrocytes during normal development (Nishiyama, 2007). In the last couple of years the synaptic association and modulation between NG2 cells and neurons in several different regions of the developing and adult CNS has been shown (Bergles *et al.*, 2000; Jabs *et al.*, 2005; Kukley *et al.*, 2007). In acute brain slices these cells are characterized by a complex current profile. Upon depolarization a delayed, inactivating outward current is triggered while hyperpolarization evokes inwardly rectifying currents (Wang *et al.*, 2008).

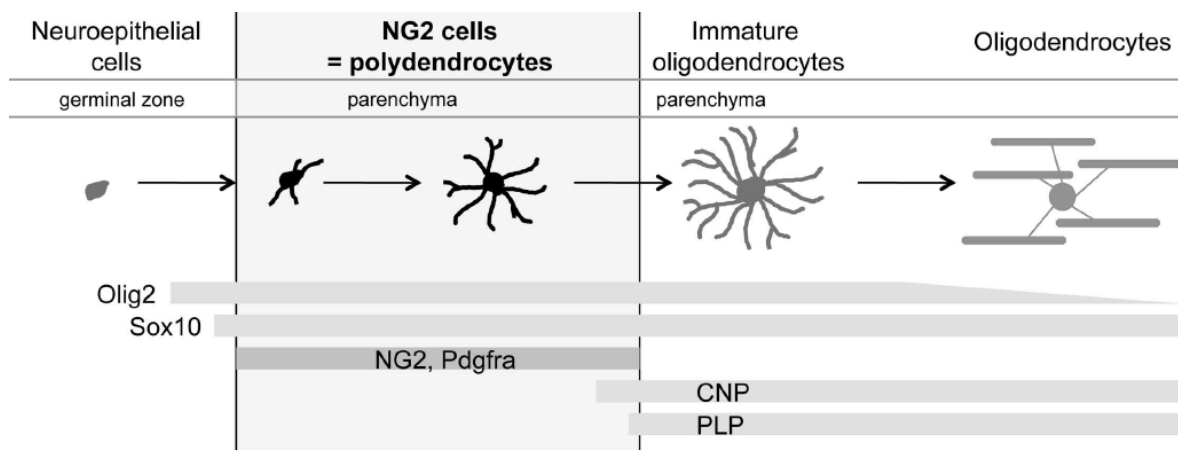


**Figure 4: Relationship between polydendrocytes and oligodendrocytes.**

Box indicates polydendrocytes that are process-bearing cells that express NG2 and Pdgfra. Bold grey lines specify the duration of expression of the indicated markers. (Taken from (Nishiyama, 2013)).

## 1.5 Microglial cells

Microglial cells are the innate immune cells of the CNS that participate in adaptive immune responses. They constitute about 5-20% of the CNS glial cells (Streit, 2013). An *in vivo* lineage tracing study showed that microglia are of mesenchymal origin, namely arise from myeloid progenitor cells and enter the brain early during development (embryonic day 8.5 and 9.5) migrating from the yolk sac (Ginhoux *et al.*, 2010). In the normal brain they acquire a specific ramified morphological phenotype, characterized by a small cell body with long, thin processes that constantly move, thereby scanning their local environment (Nimmerjahn *et al.*, 2005). Microglial cells are considered susceptible sensors of brain pathology. In response to any pathological change, such as neuronal injury, infection or neurodegeneration, ramified microglia are converted into an activated phenotype that can migrate to the site of injury, phagocytose dying cells and release a large number of molecules, cytokines (e.g. TNF- $\alpha$  (tumor necrosis factor- $\alpha$ )), nitric oxide (NO) and reactive oxygen species (ROS) (Mantovani *et al.*, 2004; Kettenmann and Verkhratsky, 2008; Kigerl *et al.*, 2009; Perry and O'Connor, 2010; Li and Graeber, 2012). The ability of microglia to migrate toward a site of lesion is supported by the upregulation of receptors that sense signals associated with tissue damage or inflammation (Tambuyzer *et al.*, 2009). This trait is accompanied by an enhanced ability to proliferate. Furthermore microglia are known to phagocytose as well as to interact with the peripheral immune system through antigen presentation (Kettenmann *et al.*, 2011).

The typical membrane current profile of microglia cells allows to draw conclusions about their activation state. Ramified microglia in acute brain slices have a high input resistance and show no voltage gated currents (Figure 5 A), while upon activation they typically develop inactivating inward currents, as shown in microglia of the facial nucleus after facial nerve axotomy (FNA) (Boucsein *et al.*, 2000). One day after FNA additional outward currents can be seen that decrease in amplitude with time (Figure 5 C). In comparison, in cultured microglia the potassium inward currents are much more prominent, probably due to the stressful isolation procedure of the cells (Figure 5 B) (Boucsein *et al.*, 2000).

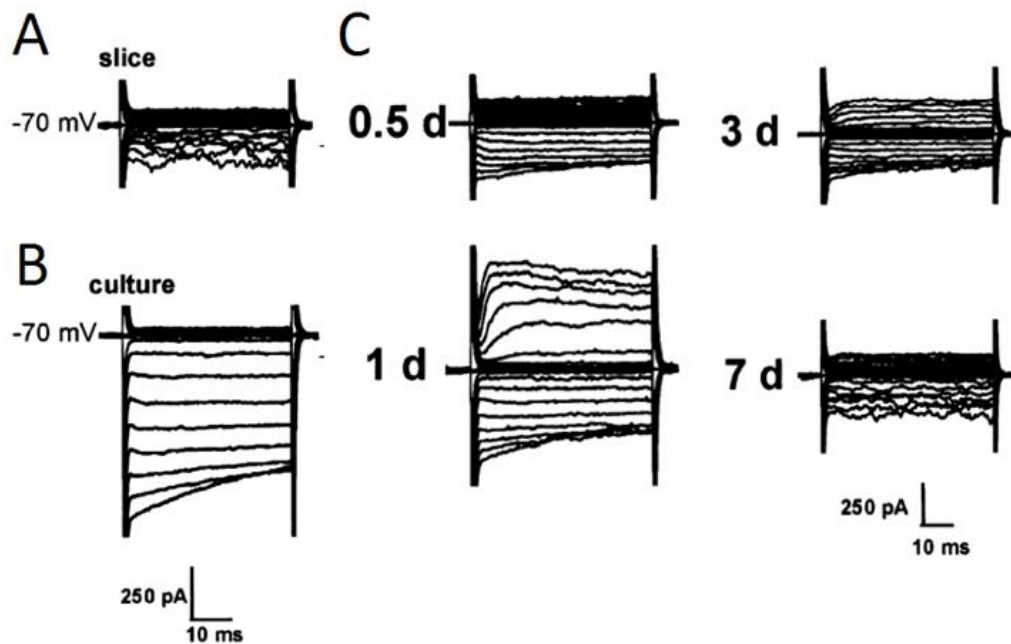


**Figure 5: Comparison of microglia currents in different activation states.**

Current profiles in response to de- and hyperpolarizing voltage steps of a resting microglia in an acute brain slice (A), a neonatal cultured microglia (B) and microglia after different time periods of an induced facial nerve axotomy (C). Figure modified from (Boucsein *et al.*, 2000).

### 1.5.1 Microglia/macrophages in pathology - Glioma

As mentioned above, microglia cells are highly sensitive detectors of several pathological signals and undergo functional changes in all types of brain diseases, injuries, as well as during the formation of brain tumors. Gliomas belong to the most malignant tumors in the brain.

Glioblastoma multiforme (GBM) is the most common and aggressive form of glioma and graded by the WHO as grade IV glioma. Patients suffering from grade IV glioma have an average survival time of about 12-15 months after diagnosis, regardless of surgical removal, radio-, and chemotherapy (Wen and Kesari, 2008). As the glioma damages the blood brain barrier, tumor-infiltrating cells like peripheral macrophages/monocytes invade the tumor. Together with the resident activated microglial cells they can amount up to one third of the total tumor mass (Charles *et al.*, 2011; Li and Graeber, 2012). Glioma-associated microglia (GAM) show an amoeboid morphology and accumulate in the glioma. GAMs and glioma-associated macrophages (GAMPs) have been shown to support glioma growth, invasion by degrading the extracellular matrix and glioma angiogenesis (Kerber *et al.*, 2008; Markovic *et al.*, 2009; Gabrusiewicz *et al.*, 2011; Vinnakota *et al.*, 2013).

Factors released by the tumor seem to reprogram microglial cells into a tumor-supporting, immuno-suppressive phenotype that participates in remodeling the extracellular matrix to promote infiltrative growth of glioma (Hanisch and Kettenmann, 2007). Studies on animal models have further underlined that CD11b+ microglia/macrophages - a specific marker for resident microglial cells as well as invading macrophages/monocytes - support the tumor growth. Upon depletion of CD11b+ cells from the experimental mouse glioma a prolonged survival of animals could be observed (Markovic *et al.*, 2009).

### **1.5.2 Microglia/macrophages in pathology - Stroke**

Strokes are categorized into two subtypes: ischemic and hemorrhagic (Brain Basics: Preventing Stroke, National Institute of Neurological Disorders and Stroke. (Institute, 2009)). Interruption of blood supply leads to ischemic strokes whereas the damage of a blood vessel or abnormal vascular structure results in hemorrhagic strokes due to leakage of blood into the brain parenchyma. Approximately 87% of strokes are ischemic and only 12% are of hemorrhagic origin (Donnan *et al.*, 2008). After an ischemic insult of the brain microglia are activated and participate in the inflammatory response. Following the ischemia, peripheral macrophages invade into the injured brain area via a leaky blood brain barrier (Lyons *et al.*, 2000). Furthermore, Lyons *et al* (2000) have shown that 48h after the insult, microglia and macrophages in the stroke area exhibit a membrane current pattern resembling those of activated microglia *in vitro* or after FNA (See Figure 5). To provide deeper insight into the different activational states of microglial cells and macrophages in the stroke context, I used electrophysiological techniques to characterize the differences and tested whether the cells in the stroke area can be discriminated on the basis of their membrane current profile. For that purpose, stroke was induced in MacGreen mice (Sasmono *et al.*, 2003), in which the intrinsic, activated microglia cells express eGFP under control of the murine CSF-1 receptor promoter, and can thus be distinguished by their green fluorescence. Invading macrophages, which express tandem dimer red fluorescent protein (tdRFP) were transplanted before induction of the stroke and could thus be visualized in the stroke area due to their red fluorescence (Luche *et al.*, 2007). More details on the stroke insult procedure can be found in the methods paragraph.

## 1.6 Gap junctional communication

Gap junctions (GJs) are dense aggregates of pore channels. They extend from one cell to an adjacent cell and mediate direct cytoplasm-to-cytoplasm communication. GJ channels are formed by a family of proteins, called connexins (Cxs). Six Cxs assemble into one hemichannel that can either interact with another hemichannel on an opposing cell to form a GJ channel or remain unopposed (Figure 6). Over 20 Cxs have been described in mammals and depending on the cellular partners, GJs can be composed of either identical Cx-types (homotypic) or different Cx-types (heterotypic) (Figure 6), which leads to a variety of possible GJ formations (Willecke *et al.*, 2002). GJs are channels which allow the diffusional exchange of ionic and biochemical molecules, with a size of up to 1-2 kDa, between cells (Bruzzone *et al.*, 1996). Furthermore, they allow diffusion of intracellular messengers, such as calcium, nucleotides, inositol triphosphate (IP<sub>3</sub>), and diverse metabolites like glycogen and pyruvate (Eugenin *et al.*, 2012). After neuronal axon excitation, GJs mediate the rapid clearance of potassium and other ions, and are therefore important for brain homeostasis and electrical coupling (Nualart-Marti *et al.*, 2013). The communication pathway of electrical coupling will be explained in detail in paragraph 1.6.2.

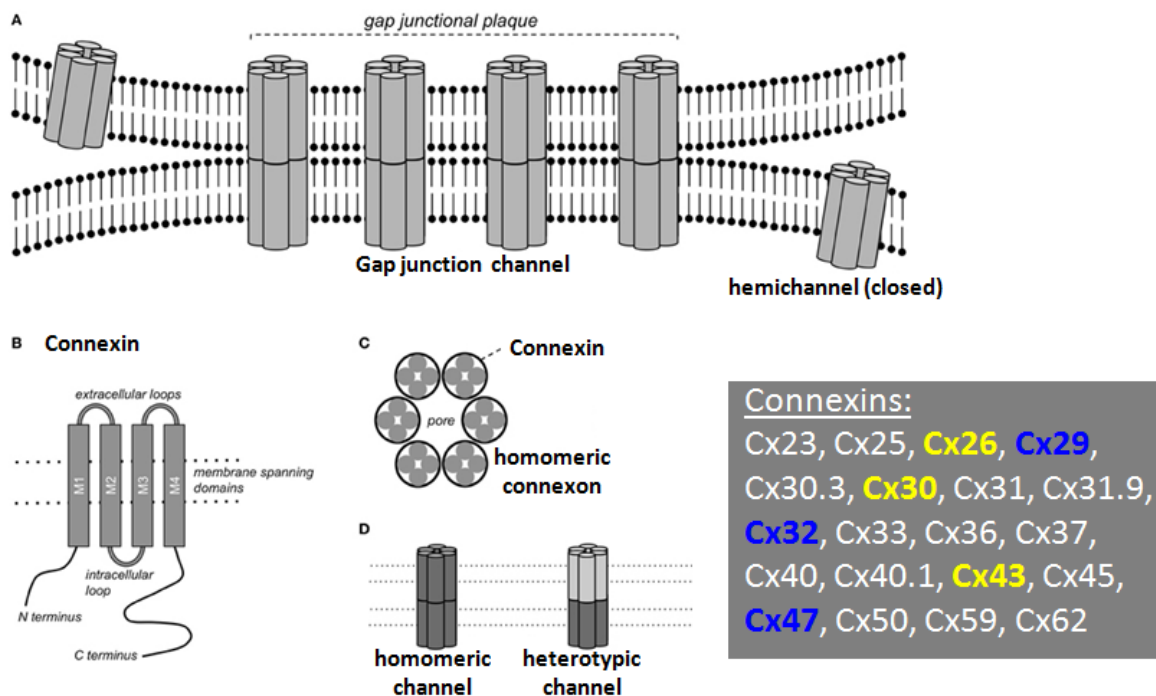


**Figure 6: Gap junctional coupling in the CNS.**

Twenty connexin genes have been identified in the mouse and 21 in the human genome. Connexins indicated in blue are expressed by oligodendrocytes, such as shown yellow by astrocytes. Six connexin proteins contribute to one hemichannel (connexon) and two connexons of adjacent cells can dock to each other to form a GJ channel. Depending on the cellular partners, GJs can be composed of either identical connexintypes (homotypic) or different connexin types (heterotypic) which leads to a variety of possible GJ formations (Willecke *et al.*, 2002). Image from: [http://www.frontiersin.org/files/Articles/53434/fphar-04-00081-HTML/image\\_m/fphar-04-00081-g001.jpg](http://www.frontiersin.org/files/Articles/53434/fphar-04-00081-HTML/image_m/fphar-04-00081-g001.jpg);

Oligodendrocytes express Cx47, Cx32 and Cx29, while astrocytes express Cx43, Cx30 and Cx26 (Orthmann-Murphy *et al.*, 2008) (Figure 7). Glial networks are not only formed interastrocytic (A:A) and interoligodendrocytic (O:O). Several studies show that coupling can also occur between astrocytes and oligodendrocytes (A:O), termed panglial coupling, in the white and grey matter (Maglione *et al.*, 2010; Wasseff and Scherer, 2011; Tress *et al.*, 2012). Interestingly, Maglione *et al.* (2010) showed that oligodendrocytes in the mouse corpus callosum can also be coupled to NG2 cells.

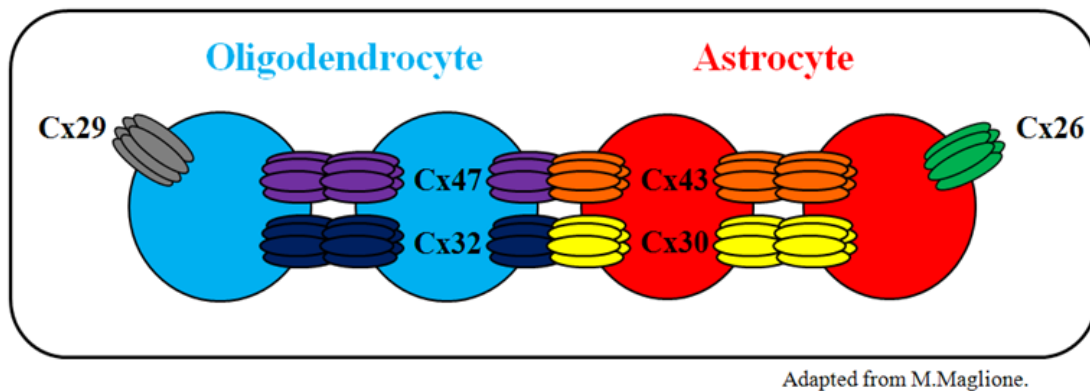


**Figure 7: Gap junction proteins expressed by oligodendrocytes and astrocytes.**

Oligodendrocyte-to-astrocyte (O:A; panglial coupling) GJs can be formed by Cx47/Cx43 and Cx32/Cx30, while interoligodendrocytic (O:O) GJs are formed by homotypic Cx47/Cx47 or Cx32/Cx32-channels and interastrocytic (A:A) GJs are composed of homotypic Cx30/Cx30 or Cx43/Cx43-channels. The unopposed hemichannels Cx29 and Cx26 allow the release of different intracellular factors (Eugenín *et al.*, 2012).

Besides, the intercellular communication via GJs is not only important for the rapid transfer of information between cell and brain regions, they furthermore have been shown to play an important role in different diseases of the CNS. For example, the dysfunction of the GJ communication based on gene defects or mutations in these connexin proteins is linked to demyelinating diseases as well as hypomyelinating diseases such as leukodystrophies. The demyelinating disease, Charcot-Marie-Tooth disease, is induced by the human Cx32 gene mutation and is characterized by a reduction in motor nerve conduction velocities and distal muscle weakness (Abrams and Freidin, 2014). Pelizaeus-Merzbacher-like disease is distinguished by hypomyelination, nystagmus, impaired psychomotor development and progressive spasticity. It is caused by mutations in the human Cx47 gene (Orthmann-Murphy *et al.*, 2008; Tress *et al.*, 2011).

So far, GJ communication is already well established between macroglial cells (astrocytes, oligodendrocytes). But it is not yet known whether microglia cells, the resident macrophages of the CNS, express connexins to form functional GJs among each other or with other cells of the brain and thereby participate in the gap junctional communication network of the brain, or whether they form hemichannels to exchange small bioactive molecules (such as neurotransmitters or inflammatory mediators). It is also largely unknown whether connexin expression and function in microglia is regulated by pathological states of the CNS. So far, connexins have

been mainly studied in microglia *in vitro* (Mika and Prochnow, 2012). Under normal conditions, cultured rat and mouse microglia show little expression of Cx43. An increase of Cx43 mRNA expression and the formation of functional GJ channels (activation-induced dye coupling) has been demonstrated *in vitro* after treatment with inflammatory agents like interferon- $\gamma$  and tumor necrosis factor- $\alpha$ , and *Staph.aureaus*-derived peptidoglycane (Eugenin *et al.*, 2001; Garg *et al.*, 2005). Cx36 expression in microglia has been shown, using immunohistochemistry and RT-PCR in unstimulated cultured mouse microglia (Parenti *et al.*, 2002). Moreover, Dobrenis (Dobrenis *et al.*, 2005) showed the expression of Cx36 and formation of GJs between neuronal and microglia cells in culture. While GJ communication/dye-coupling was not detected in unstimulated microglia, the incidence of coupling was increased after activation. Dye-transfer was observed to an average of three neighbouring cells (Saez *et al.*, 2005). Furthermore, Orellana (Orellana *et al.*, 2011) showed that low concentrations of A $\beta$ <sup>25-35</sup> increases Cx43 hemichannel activity in microglia which leads to opening of hemichannels and subsequent release of glutamate and ATP that induced neuronal death by activating Cx36 hemichannels in neurons.

Even though GJ coupling of microglia could not be confirmed in dye-coupling experiments in acute mouse brain slices, neither in direct brain injury (stab wound model) nor in an A $\beta$  pathology (Wasseff and Scherer, 2014), it might be possible that microglia/macrophages in other pathologies, such as stroke or in tumor microenvironment, use the GJ communication, since it has been shown that glioma cells are coupled via GJs with host astrocytes by (Zhang *et al.*, 1999).

### **1.6.1 Metabolic coupling among glial cells in the CNS**

Astrocytes are considered to be the energy storage units of the brain with glycogen exclusively found in astrocytes. Via their processes and perivascular endfeet they take up glucose from the blood vessels and release it in form of lactate to support neurons with energy (Brown and Ransom, 2007). This metabolic supply is also supported by the astrocytes characteristic to form extensive networks through the GJ proteins specific for astrocytes, namely Cx43 and Cx30, which are highly enriched in the perivascular endfeet of astrocytes in the mouse hippocampus (Rouach *et al.*, 2008). Furthermore Rouach *et al.* (2008) demonstrated that glucose once taken up by astrocytes from the blood vessel by their glucose trans-

porter-1, traffics through the gap junctional astroglial network because spread of the glucose derivative 2NBDG was completely abolished in the Cx30/Cx43 double knockout mice. Astrocytes comprise a heterogeneous population of cells regarding their morphology, expression of antigens and gap junctional network formation in different brain areas (Griemsmann *et al.*, 2014). Hence, heterogeneity might also exist concerning their metabolic support in different brain regions, e.g. the corpus callosum, in comparison to the studied hippocampus. As already pointed out in Figure 2, oligodendrocytes are in close contact with axons in the white matter tract. They could presumably fulfill a similar role in fast metabolic supply of neurons because they are GJ coupled to astrocytes via heterotypic Cx47/Cx30 GJ channels. Under a high demand of nutrients by neurons this glial network is important for the balance of potassium ions, water transport for ionic homeostasis (Menichella *et al.*, 2006) and is therefore most likely the first glucose support for axonal energy metabolism (Saab *et al.*, 2013).

The importance of astrocytes communicating to oligodendrocytes was already shown in development (Sutor and Hagerty, 2005) and has been confirmed in the early onset of death in Cx30/Cx47 double knockout model. These mice lack oligodendrocyte to astrocyte coupling, are hypomyelinated, and display vacuolisation in electron microscope images, suggestive for osmotic problems within the oligodendrocyte network (Tress *et al.*, 2012; Saab *et al.*, 2013). Due to these observations it will be essential to study the transfer of glucose in a glial network in the white matter. For that purpose 2-[N-(7-nitrobenz-2-oxa-1,3-diazol-4-yl)amino]-2-deoxy-d-glucose (2NBDG), a green fluorescent glucose derivative was used as a tracer in this thesis. 2NBDG was injected via the patch pipette into glial cells and imaged for its spread in the acute mouse brain slice as done in the work of Rouach *et al.* 2008. This will provide insights into the role of astrocytes and oligodendrocytes for metabolic supply of neuronal axons in the corpus callosum, a white matter tract of the CNS.

### 1.6.2 Electrical coupling between glial cells in the CNS and regulation by neurotransmitters

Electrical coupling presents a further pathway of glial gap junctional communication in the brain and has been shown to be important for a stable intracellular and extracellular ionic homeostasis (Ransom and Ye, 2005, *Neuroglia* 2nd ed.). Oligodendrocytes express a distinct set of connexins, namely Cx47 (Menichella et al., 2003; Odermatt et al., 2003), Cx32 (Dermietzel et al., 1989), and Cx29 (Altevogt and Paul, 2004) whereas only Cx47 and Cx32 form functional GJs. Early studies in the eighties showed that oligodendrocytes form functional junctions in mammalian nervous system cultures to a small degree (Kettenmann et al. 1983, 1984) and furthermore are weakly electrically coupled not only to one another (Von Blankenfeld *et al.*, 1993) but also to astrocytes *in vitro* (Kettenmann and Ransom 1988). By now we know that oligodendrocytes form large dye-coupled, gap junction mediated networks in the corpus callosum and that these networks are mainly formed by homotypic GJs composed of Cx47 (Maglione *et al.*, 2010; Wasseff *et al.*, 2010). In 1992 it was shown for the first time that oligodendrocytes in mouse corpus callosum slices elicit whole-cell currents activated upon glutamate and kainate application (Berger *et al.*, 1992). It was believed that glutamate triggers exclusively a response in neurons because depolarization of glial cells upon transmitter application *in situ* was attributed to the release of potassium from surrounding neurons (Somjen G.G., 1975). This view was first challenged by a series of studies in the 1980's on cell culture demonstrating that astrocytes (Figure 8) and oligodendrocytes respond to excitatory and inhibitory amino acids with depolarization in the absence of neurons (Bowman and Kimelberg, 1984; Kettenmann *et al.*, 1984a; Kettenmann *et al.*, 1984b). Moreover, an *in situ* study on rat spinal cord slices by Pastor *et al.* showed that glial cells respond to the inhibitory neurotransmitters glycine and  $\gamma$ -aminobutyric acid (GABA); and therefore implicating that these cells are able to detect synaptic activity (Pastor *et al.*, 1995).

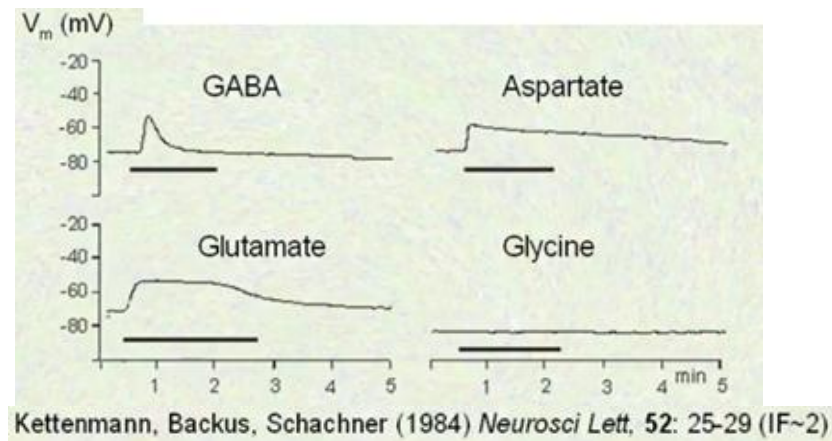


**Figure 8: Effect of GABA, glutamate, aspartate and glycine on the membrane potential of astrocytes.**

Transmitters were used at a concentration of 1 mM each and applied to the bath solution indicated by the black bar below the recording of the membrane potential ( $V_m$  (mV)) trace. All astrocytes, except one, reacted to glutamate, GABA and aspartate with depolarization, whereas glycine had no effect on the membrane potential. Taken from Kettenmann *et al.* 1984.

Kainate being a ligand for the  $\alpha$ -Amino-3-hydroxy-5-methyl-4-isoxazolepropionic acid (AMPA)- and Kainate ionotropic receptors which are a subtype of the glutamate receptors (Figure 9 dashed white square) has been shown to increase cytosolic  $Ca^{2+}$  and therefore affects junctional conductance in glial cells (Müller *et al.*, 1996).

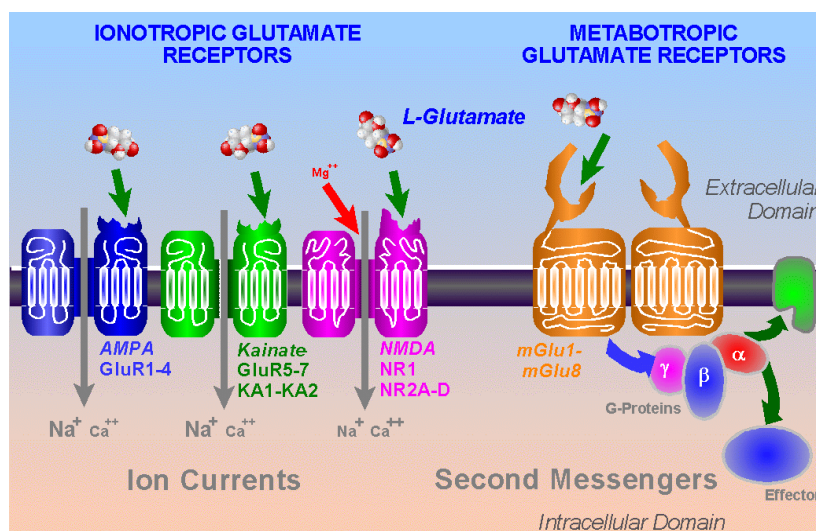


**Figure 9: The ionotropic- and metabotropic glutamate receptors.**

Classification based on pharmacological property: Alpha-amino-3-hydroxy-5-methyl-4-isoxazolepropionic acid (AMPA), KA (Kainate) and N-methyl-D-aspartate (NMDA). Ionotropic glutamate receptors incorporate ion channels and are therefore permeable to cations ( $Na^+$ ,  $Ca^{2+}$ ). The metabotropic glutamate receptors are G-protein linked and function by releasing second messengers into the cytoplasm. <http://www.ucl.ac.uk/~smgxt01/frameh.htm?page=glutamat.htm>

Up till now only a few studies have dealt with electrical coupling among glial cells. In addition to the studies mentioned above: for example it was shown that endothelin inhibits gap junctional communication in hippocampal astrocytes (Blomstrand *et al.*, 2004). Anandamide which is released by neurons and activates cannabinoid receptors was revealed to be an effective inhibitor of gap junctional conductance and dye permeability in astrocytes of the mouse striatum (Venance *et al.*, 1995). Furthermore, Meme *et al.* demonstrated electrical coupling between hippocampal astrocytes in rat brain slices and showed that the activation of purinergic receptors by ATP and adenosine diphosphate (ADP) leads to a decrease in junctional conductance of cortical and striatal astrocytes cultured from newborn rats and mice (Meme *et al.*, 2004; Meme *et al.*, 2009).

On the other hand, oligodendrocytes which are in close contact to axons by ensheathing them with myelin are like neurons very sensitive to damage by oxidative stress, the activation of apoptotic pathways and excitatory amino acids (Dzamba *et al.*, 2013). This sensitivity for glutamate has been pointed out in a review by Matute in 2011, describing the consequences of altered neurotransmitter signaling and its importance to disease.

To shed more light on the mechanisms that lie behind electrical coupling among oligodendrocytes in the white matter corpus callosum, I first focused on the characteristics under normal physiological conditions in the brain. The mouse strain *Plp-GFP* (Fuss *et al.*, 2000) or *Plp-GFP x hGfap-RFP* (cross breeding of *Plp-GFP mouse* with a transgenic mouse in which astrocytes express *RFP* under control of the human *hGfap*-promoter (Hirrlinger *et al.*, 2005)) was used to identify oligodendrocytes by their GFP fluorescence in the corpus callosum. The coupling ratio, the junctional conductance as well as the modulation of gap junctional conductance upon kainate exposure was studied in the following results part.

## 1.7 Aims of the project

In this doctoral thesis I addressed the topic of gap junctional communication among macroglial cells and microglia cells in the central nervous system in different brain regions with the main focus on the white matter corpus callosum of *Mus musculus*.

Specifically I addressed the following questions:

1. Heterogeneity of pangling networks in the white matter vs. grey matter and the properties of antigen expression of astrocytes.
2. The energy substrate support of axons via astrocytes and oligodendrocytes in the corpus callosum using the glucose derivative 2NBDG.
3. Electrical coupling as another alternative for glial gap junctional dye-coupling and its modulation by neurotransmitters.
4. The electrophysiological properties and gap junctional coupling of microglia cells under normal physiological conditions as well as in pathologies, such as the tumor microenvironment and in the stroke context.

## 2 Materials and Methods

### 2.1 Equipment and Materials

**Table 1:** List of equipment and materials

**Equipment:**

- Amplifier (EPC-10); HEKA Electronic, Lambrecht, Germany
- Confocal microscope Leica TCS SP5 and SPE; Leica, Solms, Germany
- Centrifuges 5417R and 5810R; Eppendorf, Hamburg, Germany
- Digital camera (Sensi Cam); PCO Computer Optics GmbH, Kelheim, Germany
- FACS Aria™ II ; BD Bioscience, Heidelberg, Germany
- Micromanipulator (Patchman); Eppendorf, Hamburg, Germany
- Microscope (Axioskop); Zeiss, Jena, Germany
- Monochromator Polychrome IV; Till photonics, Gräfelfing, Germany
- Objective 20x – numerical aperture 0.5w ; Olympus, Hamburg, Germany
- Objective 63x – numerical aperture 1.0 Vis IR; Zeiss, Jena, Germany
- Pipette Puller Model P-97; Sutter Instrument, Novato, CA, USA
- qPCR machine 7500 Fast Real Time PCR System; AB Applied Biosciences, Foster City, USA
- Spectrophotometer Nanodrop 1000; Wilmington, USA
- Stereotactic head holder; Stoelting, Wood Dale, USA
- Thermomixer Compact; Eppendorf, Hamburg, Germany
- Vibratome (HM 650V); Microm International GmbH, Walldorf, Germany

**Materials**

- Capillaries (borosilicate); Hilgenberg, Malsfeld, Germany
- Cell strainer, 70µM; NeoLab, Heidelberg, Germany
- Filtertips for intracellular solution; Millipore, Carrigtwohill, Ireland
- Superfrost Plus slides; Menzel GmbH & Co. KG, Braunschweig, Germany
- 24-well plate; BD Biosciences, Heidelberg, Germany
- RNeasyPlus Mini Kit; Qiagen, Hilden, Germany
- Neural Tissue Dissociation Kit; MiltenyiBiotec, Bergisch-Gladbach, Germany

**Table 2:** Filter sets

- Filter set Leica set GFP for (e)GFP and 2NBDG; Leica, Solms, Germany
- Filter set Multi band XF53 for EGFP and Alexa Fluor 594; Omega Optical, Austin, TX, USA

## 2.2 Computer software

**Table 3:** List of computer software

- Adobe® Photoshop® CS 8.0; Adobe Systems Inc., San Jose, CA, USA
- Adobe® Illustrator® CS 11.0; Adobe Systems Inc., San Jose, CA, USA
- Imaging Cells Easily (ICE) 3.6.1; own development, Max-Delbrück-Center for Molecular Medicine, Berlin, Germany
- LAS AF Lite; Leica, Solms, Germany
- FIJI, ImageJ; National Institutes of Health, USA
- Microsoft Office 2007; Microsoft, Redmond, WA, Germany
- SPSS 11.5.1; SPSS Inc, Chicago, IL, USA
- TIDA Version 5.24; HEKA Electronics, Lambrecht, Germany

## 2.3 Chemicals

**Table 4:** List of chemicals

Reagent	Company
Alexa Fluor 488 and 594 hydrazide	Invitrogen Molecular Probes, Karlsruhe, Germany
Aqua Poly/Mount	Polyscience Inc., Eppelheim, Germany
Biocytin	Sigma-Aldrich, Munich, Germany
Bovine Serum Albumin (BSA)	Carl Roth GmbH, Karlsruhe, Germany
Calciumchlorid (CaCl <sub>2</sub> )	Carl Roth GmbH, Karlsruhe, Germany
DAPI (4',6-Diamidin-2-phenylindol)	Sigma-Aldrich, Munich, Germany
Donkey Serum (DS)	Gibco, Eggenstein, Germany
DMEM	Gibco, Invitrogen, Darmstadt, Germany
Ethylene glycol tetraacetic acid (EGTA)	Sigma-Aldrich, Munich, Germany
FCS	Life technologies, Darmstadt, Germany
α-D(+)-Glucose-Monohydrat (C <sub>6</sub> H <sub>12</sub> O <sub>6</sub> )	Carl Roth GmbH, Karlsruhe, Germany

HBSS	Gibco Invitrogen, Carlsbad, USA
Sodium chlorid (NaCl)	Carl Roth GmbH, Karlsruhe, Germany
Hepes (C <sub>8</sub> H <sub>18</sub> N <sub>2</sub> O <sub>4</sub> S)	Carl Roth GmbH, Karlsruhe, Germany
Potassium chlorid (KCl)	Carl Roth GmbH, Karlsruhe, Germany
Kainic acid	AbcamBiochemicals, Cambridge, UK
Di-Potassium-hydrogenphosphate-Trihydrate (K <sub>2</sub> HPO <sub>4</sub> )	Merck KGaA, Darmstadt, Germany
Magnesium chlorid (MgCl <sub>2</sub> )	Carl Roth GmbH, Karlsruhe, Germany
Sodium hydrogencarbonate (NaHCO <sub>6</sub> )	Carl Roth GmbH, Karlsruhe, Germany
Oligo DT	Life technologies, Darmstadt, Germany
Paraformaldehyde	Merck KGaA, Darmstadt, Germany
Percoll	Th. Geyer, Renningen, Germany
Pentobarbital-sodium	Narcoren, Pharmazeutischen Handelsgesellschaft
Sulforhodamine B	Invitrogen, Karlsruhe, Germany
Sulforhodamine 101	Invitrogen, Karlsruhe, Germany
Superscript-II-reverse-transcriptase	Life technologies, Darmstadt, Germany
SYBR green Select Mastermix	Life technologies, Darmstadt, Germany
Triton X-100 (TX-100)	Carl Roth GmbH, Karlsruhe, Germany

**Table 5:** Solution for acute brain slices and standard intracellular solution for electrical coupling experiments and experiments injecting microglia in the glioma- or stroke context

	Artificial cerebrospinal fluid (aCSF) Buffer [mM]	Standard Intracellular Solution [mM]
NaCl	134	4
KCl	2.5	120
MgCl <sub>2</sub>	1.3	4
CaCl <sub>2</sub>	2	0.5
K <sub>2</sub> HPO <sub>4</sub>	1.25	-
C <sub>6</sub> H <sub>12</sub> O <sub>6</sub>	10	5
NaHCO <sub>6</sub>	26	-
HEPES	-	10
EGTA	-	5
Biocytin	-	0.5 - 0.6%
pH	7.4	7.4
Osmolarity (mmol/kg)	340	285

**Table 6:** Solution for acute brain slices and standard intracellular solution for panglial gap junctional and metabolic coupling experiments.

	Artificial cerebrospinal fluid (aCSF) Buffer [mM]	Standard Intracellular Solution [mM]
NaCl	126	-
K-Gluconate C <sub>6</sub> H <sub>11</sub> KO <sub>7</sub>	-	130
KCl	3	-
MgCl <sub>2</sub>	-	1
MgSO <sub>4</sub> - 7H <sub>2</sub> O	2	-
CaCl <sub>2</sub> -6H <sub>2</sub> O	2	-
C <sub>6</sub> H <sub>12</sub> O <sub>6</sub> (anhydrous)	10	-
NaH <sub>2</sub> PO <sub>4</sub> (anhydrous)	1.25	-
NaHCO <sub>3</sub>	26	-
HEPES	-	20
EGTA	-	10
Biocytin	-	0.5 - 0.6%
pH	7.4	7.4
Osmolarity (mmol/kg)	310	298

**Table 7:** List of primary antibodies

Name	Company
Cy3-conjugated streptavidin	Jackson Immuno Research/Dianova, Hamburg, Germany
Cy2-conjugated streptavidin	Jackson Immuno Research/Dianova, Hamburg, Germany
Mouse monoclonal anti-CNPase	Sigma-Aldrich, Munich, Germany
Rabbit polyclonal anti-GFAP	DAKO, Hamburg, Germany
Rabbit polyclonal anti-Iba1	Wako, Pure Chemicals, Japan
Rabbit monoclonal anti-Olig2	Millipore, Darmstadt, Germany
Rabbit polyclonal anti-NG2	Millipore, Darmstadt, Germany
Goat anti-EGFP	Acris Antibodies GmbH, Germany

**Table 8:** List of secondary antibodies

Name	Company
Cy5-conjugated donkey anti-mouse IgG	Jackson Immuno Research/Dianova, Hamburg, Germany
405-conjugated donkey anti-rabbit DyeLight	Jackson Immuno Research/Dianova, Hamburg, Germany
Cy5-conjugated donkey anti-rabbit IgG	Jackson Immuno Research/Dianova, Hamburg, Germany
Fluorescein (FITC)-conjugated donkey anti-goat IgG	Jackson Immuno Research/Dianova, Hamburg, Germany

**Table 9:** Solutions for immunohistochemistry

Solution	Substances
Fixation solution	4% paraformaldehyde + 0.1M phosphate buffer (PB), pH 7.4
Blocking and Permeabilisation for CNPase, GFAP and eGFP	2% TritonX-100 + 10% DS + 0.1M PB
Antibody dilution for CNPase, GFAP and eGFP	2% TritonX-100 + 5% DS + 0.1M PB
Blocking and Permeabilisation for NG2 staining	5% TritonX-100 + 10% DS + 2% BSA + 0.1M PBS
Antibody dilution for NG2 staining	0.1% TritonX-100 + 5% DS + 2% BSA + 0.1M PBS
Blocking and Permeabilisation for Olig2 staining	5% TritonX-100 + 10% DS + 5% BSA + 0.1M PBS
Antibody dilution for Olig2 staining	5% TritonX-100 + 5% DS + 2% BSA + 0.1M PBS
Washing buffer/ Phosphate buffer 0.1M	100mM $\text{Na}_2\text{HPO}_4$ + 100mM $\text{NaH}_2\text{PO}_4$

**Table 10:** Solutions for cell isolation and FACS

Solution	Substances
ACK lysis buffer	8.29 g/l NH <sub>4</sub> Cl, 1 g/l KHCO <sub>3</sub> , 37.2 mg/l Na <sub>2</sub> -EDTA, pH 7.2 – 7.4
Dissocation buffer	HBSS + 45%Glucose + 1M HEPES
Myelin gradient buffer	NaHPO <sub>4</sub> H <sub>2</sub> O 5.66 mM, Na <sub>2</sub> HPO <sub>4</sub> 2H <sub>2</sub> O 11.8mM, NaCl 137mM, KCl 5.36mM, Glucose 10mM
Percoll solution	1x Myelin gradient buffer, 22% Percoll, 36mM NaCl
FACS buffer	PBS + 2% FCS
DMEM complete	DMEM, 10% FCS, 2mM L-glutamin, 100U/ml penicillin, 100µg/ml streptomycin
HBSS	15mM HEPES, 0.5% Glucose

**Table 11:** Antibodies for Fluorescence-activated cell sorting (FACS)

Name	Company
CD45-e450	eBioscience, San Diego, CA, USA
Ly6G-PE	eBioscience, San Diego, CA, USA
Ly6C-PerCpCy5.5	eBioscience, San Diego, CA, USA
CD11b-APC	eBioscience, San Diego, CA, USA

### 2.3 Animals

All animals were kept and bred, under standard housing conditions with a 12-hour/12-hour dark-light cycle and with food and water ad libitum, at the animal facility of the Max-Delbrück-Center. Animal protocols for surgery were approved by the Landesamt für Gesundheit und Soziales (LaGeSo) of the Berlin Senate (G0438-12).

For immunohistochemistry and identification of Olig+ cells in the cortex and corpus callosum, as well as gap junctional dye transfer experiments, the *hGFAP/eGFP* mouse line was used. In this strain astrocytes are labeled by the eGFP protein under the control of the human GFAP promoter (Nolte *et al.*, 2001). Another reporter mouse used for the identification of astrocytes, is the *Cx43ki/eCFP* mouse (Degen *et al.*, 2012). In this mouse strain one allele of *Gja1* is replaced by *eCFP* which is in particular expressed by astrocytes and not by NG2 cells.

For pair recording experiments the *Plp-GFP* mouse, generated by (Fuss *et al.*, 2000), was used. In this mouse strain oligodendrocytes express GFP under the *Plp* promoter. Cross-breeding the *Plp-GFP* mouse with a transgenic mouse in which astrocytes express *RFP* under control of the human *Gfap*-promoter (Hirrlinger *et al.*, 2005) allowed us to distinguish oligodendrocytes from astrocytes and could possibly be used for future experiments investigating electrical coupling among these two glial cell types. The *hGfap-RFP* mouse strain was used for metabolic coupling experiments injecting astrocytes in the mouse corpus callosum.

To identify microglia either the *Cx3cr1<sup>GFP/wt</sup>* (Jung *et al.*, 2000) or the MacGreen mouse line (Sasmono *et al.*, 2003) was used. In the *Cx3cr1<sup>GFP/wt</sup>* mouse line one *Cx3cr1* allele is replaced by the enhanced green fluorescent protein reporter gene, while in the MacGreen mouse, the *eGFP* gene is expressed under the promoter of the *Csf1r/c-fms* (colony stimulating factor) gene.

By crossbreeding *Cx3cr1<sup>GFP/GFP</sup>* (the Jackson laboratory #008451) and *Ccr2<sup>RFP/RFP</sup>* mice (the Jackson laboratory #017586), a mouse line was generated to distinguish between glioma-associated microglia and invading monocytes and monocyte-derived macrophages. The *Ccr2* gene is expressed by blood monocytes and is replaced in one allele by a monomeric *RFP* (red fluorescent protein) reporter gene (*Ccr2<sup>RFP/wt</sup>*), therefore allowing visualization of CCR2+ monocyte-derived macrophages in glioma (Saederup *et al.*, 2012).

For FACS-isolation of microglia and macrophages/monocytes from GL261-implanted and control mice, C57BL/6 wildtype mice (Charles River Laboratories, Wilmington, MA, USA) were used (Animal protocol: Lageso G0268-10).

For electrophysiological characterization (and to a minor extent dye coupling experiments) of microglia cells after induction of stroke, I used the MacGreen mice (Sasmono *et al.*, 2003) in which intrinsic, activated microglia cells can be distinguished by their eGFP-fluorescence. Using irradiation and bone-marrow transplantation, invading bone-marrow-derived macrophages in these mice expressed a tandem dimer red fluorescent protein (tdRFP), for details see (Luche *et al.*, 2007). Irradiation, bone-marrow transplantation and middle cerebral artery occlusion (MCAo) were conducted by Dr. Karen Gertz at the Charité.

## 2.4 Genotyping

After birth, a tailcut from the required mouse was lysed with DirectPCR<sup>®</sup> Lysis Reagent Tail. Subsequently the tailcut was incubated for 3 h at 55°C in 100 µl DirectPCR<sup>®</sup> Ear, supplemented with 10 µl 0.2 mg/ml proteinase K. Afterwards the reaction mix was incubated for 50 min at 85°C for proteinase inactivation. For the PCR reaction (Table 13), 1 µl of the resulting lysate was used and primers as shown in table 12.

**Table 12:** List of primer sequences

Mouse strain	Primer sequence 5' → 3'	
<i>Cx3cr1-GFP</i>	TTC ACG TTC GGT CTG GTG GG	IMR3945
	GGT TCC TAG TGG AGC TAG GG	IMR3946
	GAT CAC TCT CGG CAT GGA CG	IMR3947
<i>Ccr2 -RFP</i>	TAA ACC TGG TCA CCA CAT GC	Common
	GGA GTA GAG TGG AGG CAG GA	Wt reverse
	CTT GAT GAC GTC CTC GGA G	Mt reverse
<i>hGfap-RFP</i>	GGC CGT CGG AGG GGA AGT T	Forward
	AGG AGC GAG CAG AGC CAG AGC	Reverse
<i>PLP-GFP</i>	ATG CGT ACC TGA CTT TCT CCT TCT	Forward
	CTC GGC GCG GGT CTT GTA GTT GC	Reverse

**Table 13:** Solutions for PCR reactions

<i>Cx3cr1-GFP</i>	ko	10x		wt	10x
H <sub>2</sub> O	17.25 µl	172.5µl	H <sub>2</sub> O	17.25 µl	172.5µl
Puffer	2.5 µl	25 µl	Puffer	2.5 µl	25 µl
MgCl <sub>2</sub>	1.5 µl	15 µl	MgCl <sub>2</sub>	1.5 µl	15 µl
dNTP	0.5 µl	5 µl	dNTP	0.5 µl	5 µl
IMR 3946	0.5 µl	5 µl	IMR 3946	0.5 µl	5 µl
IMR 3947	0.5 µl	5 µl	IMR 3945	0.5 µl	5 µl
Taq	0.25 µl	2.5 µl	Taq	0.25 µl	2.5 µl
	Size: 1200 bp			Size: 970 bp	
Subtotal	23 µl				
DNA	2 µl				

<b><i>Ccr2-RFP</i></b>	
H <sub>2</sub> O	16.4 µl
Puffer	2.5 µl
dNTP mixture each	2 µl
IMR13505 (10 pmol/µl)	1 µl
IMR13506 (10 pmol/µl)	1 µl
IMR13507 (10pmol/µl)	1 µl
Taq (TaKaRa)	0.125 µl
	Size WT: 494 bp, Size KO: 320 bp
Subtotal	24 µl
DNA	1 µl

	<b><i>hGfap-RFP</i></b>	<b><i>PLP-GFP</i></b>
H <sub>2</sub> O	17.75 µl	17.75 µl
Puffer	2.5 µl	2.5 µl
MgCl <sub>2</sub>	1.5 µl	1.5 µl
dNTP	0.5 µl	0.5 µl
Fw Primer	0.5 µl	0.5 µl
Rev Primer	0.5 µl	0.5 µl
Taq DNA Pol.	0.25 µl	0.25 µl
	Size: 510 bp	Size: 400 bp
Subtotal	23.5 µl	
DNA	1.5 µl	

**Table 14:** PCR programs for different mouse strains

<b><i>Cx3cr1-GFP</i></b>	<b><i>Ccr2-RFP</i></b>	<b><i>hGfap-RFP</i></b>	<b><i>PLP-GFP</i></b>
Lid 95°C	Lid 99°C	Lid 99°C	Lid 99°C
1. 94°C 3 min	1. 94°C 2 min	1. 94°C 3 min	1. 95°C 3 min
2. 94°C 30 s	2. 94°C 20 s	2. 94°C 30 s	2. 95°C 30 s
3. 60°C 30 s	3. 65°C 15 s	3. 66°C 30 s	3. 57°C 30s
4. 72°C 2 min	(1.5°C/ cycle)	4. 72°C 1 min	4. 72°C 35 s
35 cycles	4. 68°C 15 s	29 cycles	35 cycles
5. 72°C 2 min	5. Go to step 2-4, 10x	5. 72°C 10 min	5. 72°C 10 min
6. 10°C Pause	6. 94°C 15 s	6. 4°C Pause	6. 4°C hold
	7. 50°C 15 s		
	8. 72°C 10 s		
	9. Go to step 6-8, 25x		
	10. 72°C 2 min		
	11. 10°C hold		

## 2.5 Acute brain slice preparation

Acute coronal brain slices of 150  $\mu\text{m}$  thickness were prepared from mice of different ages (depending on the project) after decapitation as described in (Haas *et al.*, 1996). Mice were decapitated, the cranium was opened and the brain carefully removed. The brain stem and cerebellum were removed from the cerebrum. Then the cerebrum was fixed with conventional superglue on a metal disc in the vibratome chamber (Microm HM 650). Slice preparations were carried out in ice cold bicarbonate-buffered artificial cerebrospinal fluid (ACSF) (Table 5 Table 6). Subsequently, the brain slices were transferred in continuously gassed (95%  $\text{O}_2$ , 5%  $\text{CO}_2$ ) ACSF at room temperature for approximately 30 min before conducting the experiments. Depending on the set of experiments, the region of interest was either the corpus callosum, cingulum, striatum or cortex (Figure 11).

Time points (age of animals) for different experiments:

- Dye coupling experiments injecting astrocytes in the corpus callosum: postnatal day 15-20
- Dye coupling experiments injecting astrocytes in the cortex: postnatal day 30
- Dye coupling and electrophysiological experiments injecting microglia or macrophages: 10 to 12 weeks old mice and 14-16 days after tumor inoculation or stab wound lesion
- Metabolic coupling experiments injecting astrocytes or oligodendrocytes: postnatal day 12-18
- Electrical coupling experiments injecting oligodendrocytes: postnatal day 15-23

## 2.6 The patch-clamp technique

The patch-clamp technique is an electrophysiological method that allows to measure the current in single ion channels of cells in their natural environment. In the 1970s, Erwin Neher and Bert Sakmann established this method as a refinement of the voltage clamp technique which approaches the membrane currents of the entire cell. For all the experiments and obtained data of this doctoral project the whole-cell configuration was used. This configuration is based on a very strong glass-membrane seal that is established by placing the patch pipette very close to the cell membrane and applying a weak negative pressure at the end of the pipette via a syringe. The electrical resistance between the glass pipette's opening and the cell membrane increases to  $>1\text{G}\Omega$  and is therefore also called gigaseal. By further applying negative pressure to the pipette via suction, the membrane under the pipette opening is ruptured while the gigaseal remains intact (Figure 10). In just a few minutes, the cytoplasm of the cell is dialyzed almost completely with the pipette solution and the tracer in the solution can spread to adjacent cells if the cell is coupled via GJs (Hamill *et al.*, 1981). As an extension of the whole-cell configuration, pair recordings in the mouse corpus callosum were used to characterize the biophysical properties of oligodendrocyte: oligodendrocyte junctions and whether these properties are modulated by neurotransmitters.

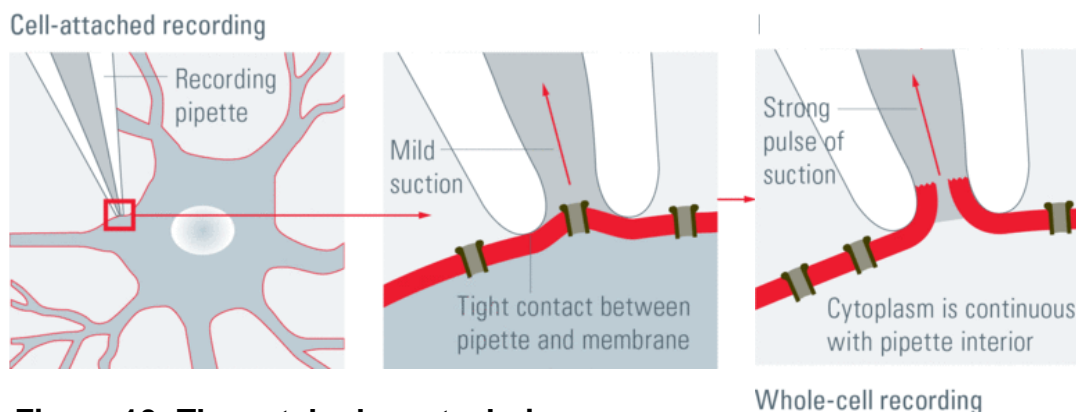


**Figure 10: The patch-clamp technique.**

Approach of a very small glass pipette to the cell membrane, application of small negative pressure to build a gigaseal between pipette and cell membrane, this tight bond can be ruptured by pulsed suction applied via a mouth piece. This type of recording technique is called the whole-cell patch-clamp technique and allows the recording of electrical potentials and currents from the entire cell as well as dialysis of the cell in a few minutes.

(<http://www.leica-microsystems.com/science-lab/the-patch-clamp-technique/>)

### 2.6.1 Visualization and characterization of the different cell types and dye-filling

For dye-coupling experiments and electrophysiological recordings the following procedure was applied. The acute coronal brain slices were mounted on a glass cover slip via a u-shaped platinum grid lined with very thin nylon threads and was then carefully placed in a bathing chamber (Figure 11 a-1). Throughout the electrophysiological recordings the chamber was constantly supplied with ACSF. For paired recordings, the neurotransmitter kainate was applied for 30 s in an 8 min recording, to see modulations of the biophysical properties. To find the area of interest and the fluorescence expressing glial cells in cortex, corpus callosum or striatum, magnifications of 20x or 63x water immersion objectives were used. In *hGFAP/eGFP* mice, astrocytes were identified by the expression of eGFP at an excitation and emission wavelength of 488 and 530 nm  $\pm$  10 nm, respectively (Nolte *et al.*, 2001). The excitation beam was generated by a Polychrome IV monochromator, controlled by TIDA software with an EPC 10 amplifier and visualized by the appropriate filter (Table 2) of an upright light microscope Axioskop 2 FS plus (Figure 11a). These settings were also used for eGFP+ microglia cells in *Cx3cr1<sup>GFP/wt</sup>*, MacGreen or *Cx3cr1<sup>GFP/wt</sup>/Ccr2<sup>RFP/wt</sup>* mice, as well as for the oligodendrocytes patched in *Pip-GFP* mice. The *Cx3cr1<sup>GFP/wt</sup>/Ccr2<sup>RFP/wt</sup>* strain provided the possibility to image blood monocytes from the periphery by their RFP fluorescence which had an excitation and emission wavelength of 584 and 607 nm, respectively. For these experiments a multi band filter was used (Table 2). The RFP fluorescent astrocytes (under the *hGfap*-promoter) used for metabolic coupling experiments had the same wavelength and settings.

Additionally, each glial cell type could be recognized by its characteristic current profile. To assess gap junctional coupling, the patch pipette was filled with standard intracellular solution (Table 5), biocytin (0.5-0.6 %) and depending on the project furthermore Sulforhodamine B (SB) (10  $\mu$ g/ml), Sulforhodamine 101 (SR101) (10  $\mu$ g/ml), Alexa594 (10  $\mu$ g/ml) or 2NBDG (5 mg/ml) was added to confirm intracellular access and/or dye-coupling. Before entering the pipette into the bath solution the intracellular solution was filtered and positive pressure was applied via a syringe to avoid clogging of the pipette tip. Then the pipette was mounted on a Cl<sup>-</sup> coated silver electrode which is held in a preamplifier and subsequently guided towards the selected cell of interest with a micromanipulator. During experiments

the electrical potential and current flow between the micropipette electrode and bath electrode were recorded and monitored (details follow in the next chapter). Images of chosen and dialyzed cells were taken with a Sensi Cam digital camera (Figure 11 a-3) and adjusted with the Imaging Cells Easily software. Single cells for the coupling experiments were dialyzed for 20 min (for paired recordings only one cell of the two was dialyzed with biocytin, detailed electrophysiological recording protocols will be explained in next paragraph) and subsequently de-and hyperpolarizing voltage steps were quickly applied to interrupt the seal and remove the pipette with a fast movement of the manipulator in order to leave the cell in the tissue. Slices were then fixed with 4 % PFA at 4 °C for 1 h and later transferred to PBS 0.1 M before biocytin uptake was revealed by Cy3-conjugated streptavidin and staining for the specific glial marker and analyzed with a confocal microscope.

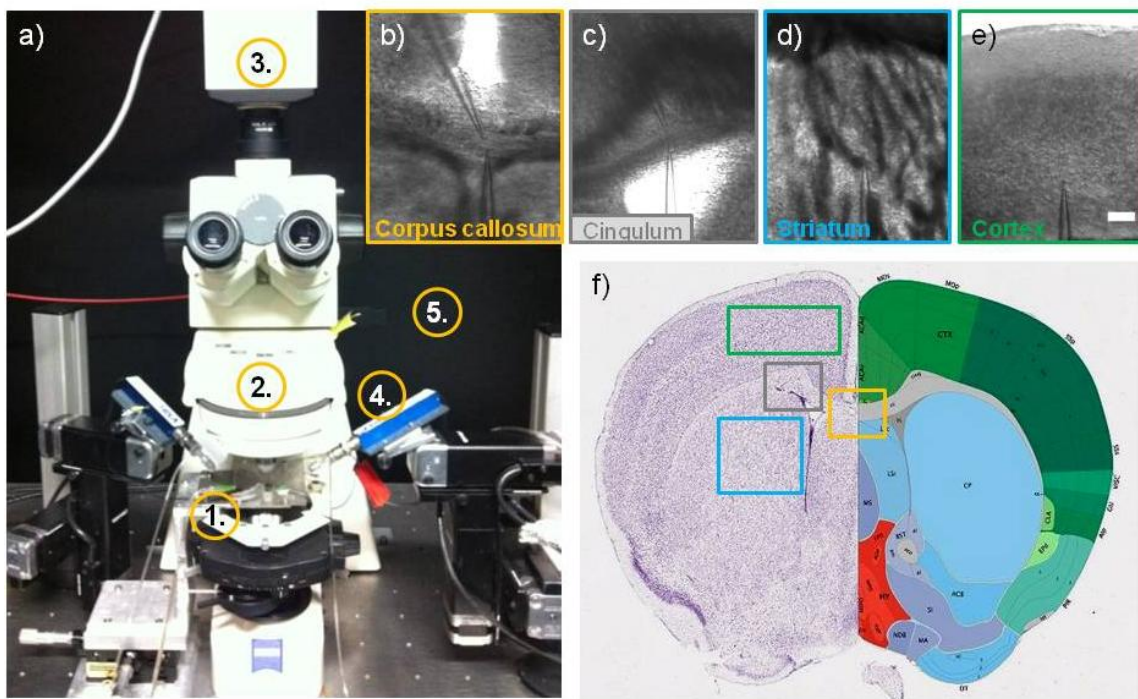


**Figure 11: Visualization of the brain area of interest and setup.**

a) Picture of setup 1. Microscope table with perfused bathing chamber and ground electrode, 2. Filters of an upright light microscope Axioskop 2 FS plus, 3. Sensi Cam digital camera, 4. Pipette holder connected directly to amplifier, 5. Faraday cage for electrical shielding. b-e) The different areas of interest and their localization in the acute brain slice (f). Scale bar in e) 100 $\mu$ m.

### 2.6.2 Electrophysiological recordings

Whole-cell patch-clamp recordings were performed using an EPC 10 patch-clamp amplifier combined with the TIDA software. Patch pipettes were pulled from borosilicate capillaries with a Sutter Instrument Pipette Puller (inner diameter  $\sim 1\text{-}3\ \mu\text{M}$ ) and filled with standard intracellular solution (Table 5, 6). The resistance of the patch pipettes (opening) ranged from 3-7  $\text{M}\Omega$ . To confirm intracellular access a fluorescent dye was added to the pipette solution as described above. The capacitive transients of the whole-cell recordings were compensated by TIDA 5.24 software. Membrane currents were recorded with a series of voltage steps (10 mV each, filtered with 2.9 kHz) from a holding potential of -70 mV to de- and hyperpolarizing potentials ranging from -170 mV to +50 mV for 50 ms (Figure 12 a, R50). For the pair recording experiments, a modified R50 was used, meaning that in one cell the voltage steps were applied and the current was measured in the other cell. If the cells were electrical coupled an additional protocol, termed 'Rev Sequence' was applied, demonstrated in Figure 12 b. In alternating steps, the two electrodes applied either a specified voltage (-50 mV, -100 mV, +50 mV, +100 mV, for 200 ms each) or were used to record the current response of one or the other cell.

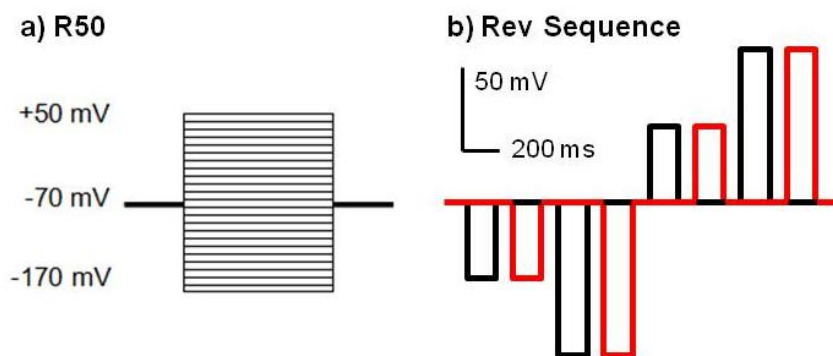


**Figure 12: Voltage commands for whole-cell patch-clamp recordings and pair recordings.**

Cells were clamped to -70 mV, voltage steps for the current induction were 50 ms pulses from -170 mV to +50 mV at 10 mV increments. For pair recordings an alternating Rev Seq was applied with -50 mV, -100 mV, +50 mV, +100 mV for 200 ms with 2 s interval before the next set of alternating steps was applied.

After recording and filling of cell(s), hyperpolarizing voltage steps were quickly applied for 0.1-10 ms (called zap) to interrupt the seal. Subsequently the patch pipette was quickly removed.

The input resistance was calculated with the following equation, derived from the Ohms law:  $R_{in} = \Delta U / I_{off}$ .  $I_{off}$  was measured from the steady state current in response to a depolarizing voltage step at 10 mV and a holding potential of -70 mV for 50 ms. The ability to load charges on a cell membrane depends on the channels that are patched via the pipette tip. Therefore the membrane capacitance ( $C_m$ ) was calculated integrating the capacitive current and applying the formula  $C_m = \int I \cdot dt / \Delta U$ . The transient currents, induced by response to a depolarizing +10 mV step from a holding potential of -70 mV for 50 ms, were measured with the TIDA software. The  $I \cdot dt$  was calculated using the TIDA-Analyze-Tool and by setting the integration baseline when the transient ends. For glioma-associated microglia and macrophages the cell surface was calculated based on the median membrane capacitance [pF], assuming a specific membrane capacitance of 1  $\mu\text{F}/\text{cm}^2$ . The specific outward conductance of glioma-associated microglia and macrophages was calculated from currents activated at 0 and -20 mV, and the inward conductance from currents activated at -100 and -120 mV. Finally, the conductance was normalized with the cell capacitance.

For the electrical coupling experiments among oligodendrocytes the conductance  $G$  [nS] of the stimulated cell was calculated by  $1/R$  and taken from the linear IV-curve between -120 mV to -20 mV. When the cell pair was electrically coupled, the voltage gradient in the first cell induced a junctional current ( $I_j$ ) flowing through GJ channels from cell 1 to cell 2 and therefore was compensated by an opposite current ( $I_2$ ) given by the feedback amplifier connected to the second cell. Hence the junctional conductance  $G_j$  [nS] could be calculated by dividing  $I_2$  by the amplitude of the  $V_1$  pulse. As the conductance was calculated using the rev sequence (shown above), the series resistance ( $R_s$ ) had to be taken into account. If  $R_s$  increased more than 30 % (own defined threshold) between the control response before and after the kainate peak, the measured cell pair was not used for statistical analysis. Moreover the coupling ratio was calculated by dividing the current response of cell 2 by the current of cell 1, at the voltage step of +30 mV.

## 2.7 Immunohistochemistry

After patch-clamp experiments acute brain slices were transferred to an Eppendorf tube containing 4% paraformaldehyde in PBS and fixed for one hour on ice. Subsequently, slices were rinsed once with washing buffer and incubated in blocking

and permeabilisation solution (See Table 9, can be variable depending of antibodies used) for 4 hours at room temperature. The blocking and permeabilisation solution was used to block nonspecific binding of the primary antibodies. To identify the tracer (biocytin) filled cells or the single filled cell, biocytin labeling with Cy3- or Cy2-conjugated streptavidin was combined with immunostaining for the following antigens, depending on the project: the oligodendrocytic marker CNPase or Olig2; astrocytic marker GFAP, NG2 as an NG2 cell marker and microglia/macrophages marker, Iba1 (ionized calcium-binding adapter molecule) and an EGFP antibody (Table 7) to amplify staining of eGFP or GFP expression. The following antibody dilutions were used: Cy3- or Cy2-conjugated streptavidin (1:200), rabbit-anti-GFAP astrocyte cell marker (1:500), mouse-anti-CNPase oligodendrocyte cell marker (1:200) and rabbit-anti-Olig2 (1:1000), rabbit-anti-NG2 (1:100), rabbit-anti-Iba1 microglia/macrophages marker (1:600) and goat-anti-EGFP (1:200). Antibodies were diluted in antibody dilution buffer (See Table 9) and 250 µl solution was added to each floating slice in a 24- well plate. The floating slices with the primary antibodies were incubated for 24 h at 4°C on shaker in a cold room. The next day the slices were washed three times for 10 minutes in washing buffer (phosphate buffer 0.1M at pH 7.4) to remove non-specifically bound primary antibodies. The primary antibody for the rabbit-anti-GFAP cell marker was visualized by application of DyLight 405-conjugated donkey anti-rabbit IgG (1:200); Cy5-conjugated donkey anti-mouse IgG (1:200) was used for mouse-anti-CNPase cell marker, Cy5-conjugated donkey anti-rabbit IgG (1:200) for rabbit-anti-Olig2, rabbit-anti-NG2, and rabbit-anti-Iba1. FITC donkey anti-goat was applied to visualize goat-anti-EGFP. All secondary antibodies (Table 8) were diluted in the antibody dilution buffer and hence incubated for two hours at room temperature on a shaker. Afterwards slices were rinsed three times for 10 minutes in washing buffer and mounted on superfrost microscope slides with Aqua Poly/Mount mounting medium. For negative control, the primary antibody was omitted. No unspecific cross reaction was observed. Images were obtained by confocal microscopy (Leica TCS SP5 or SPE) with Leica software (LCS Lite).

## 2.8 *In vivo* glioma implantation and stab wound lesion

GL261 glioma cells were implanted into 8 to 10-week-old mice as described previously (Vinnakota *et al.*, 2013). In brief, mice were anesthetized and mounted onto

a stereotactic head holder (Stoelting, Wood Dale, USA) in the flat-skull position. After making skin incision, the skull was carefully drilled with a 20-gauge needle tip 1 mm anterior and 2 mm lateral to the bregma. A 1  $\mu$ l Hamilton syringe with a blunt tip (Hamilton, Reno, NV, USA) was inserted to a depth of 4 mm and retracted to a depth of 3 mm from the dural surface into the right caudate putamen. Over 2 min, 1  $\mu$ l ( $2 \times 10^4$  cells/ $\mu$ l) GL261 glioma cell suspension was slowly injected into the brain. After surgery the mice were kept warm until they woke up and their post-operative condition was monitored daily. A stab wound was induced by inserting the syringe, without tumor cells, into the cortex. This served as a control for microglia activation. Glioma implantation and stab wound lesion were performed by our technician Regina Piske.

## **2.9 Cell isolation and fluorescence-activated cell sorting (FACS)**

For qRT-PCR validation of *Cx43* (*Gja1*) gene expression in GAMs and GAMPs cells were isolated from brain tissue and FACS sorted. GL261-implanted mice were sacrificed 20 days post-injection, while C57BL/6 wildtype littermate mice served as controls. Animals were anesthetized by intraperitoneal injection of 200  $\mu$ M pentobarbital-sodium (Narcoren, Pharmazeutischen Handelsgesellschaft), perfused with 0.9% NaCl solution and subsequently the brain was carefully removed and placed in ice-cold HBSS (Gibco-Invitrogen, Carlsbad, USA). For each brain the olfactory bulb and the cerebellum were disposed while in the tumor injected brains only the visible tumor area around the injection site was excised and stored in ice-cold HBSS. Samples were dissociated with the Neural Tissue Dissociation Kit (MiltenyiBiotec, Bergisch-Gladbach, Germany) and myelin was removed by mixing the cell suspension with 25 ml of a 22% Percoll (Th.Geyer, Renningen, Germany) solution and adding on top a layer of 5 ml cold PBS (Gibco Invitrogen). Then the samples were centrifuged at 950 rcf with slow acceleration and no break. This created a gradient which allowed to nicely separate the cell pellet on the bottom from the myelin floating in the tube. For further details please see Olah *et al.* (Olah *et al.*, 2012). The cell pellet was subjected to erythrocyte lysis by adding 5 ml of 1x RBC lysis buffer (Cat# 420301, Biolegend, San Diego, CA, USA). The lysis was carried out by shaking the tube mildly for 5 min at room temperature and stopped with 20 ml of PBS. The pellet was washed once with PBS and resuspended in PBS, containing 2% FCS (FACS buffer) for subsequent FACS isolation.

Cells were immunolabeled with dye-coupled CD45-e450, Ly6G-PE, Ly6C-PerCpCy5.5 and CD11b-APC antibodies (all from eBioscience, San Diego, CA, USA) for 30 min at 4°C. After washing and resuspension in FACS buffer (1x10<sup>7</sup> cells/ml), cells were sorted in a BD FACSAria™ II (BD Bioscience) to distinguish between resident microglia (CD11b<sup>+</sup>/CD45<sup>low</sup>) and invading macrophages/monocytes (CD11b<sup>+</sup>/CD45<sup>high</sup>/Ly6G<sup>-</sup>/Ly6C<sup>high</sup>). Compensation was calculated with single-stained beads (552844, BD Bioscience, Franklin Lakes, USA) and unstained cells.

### 2.10 RNA isolation, cDNA preparation and qPCR

Total RNA was isolated using the RNeasyPlus Mini Kit (Qiagen, Hilden, Germany), eluted in RNase-free water, measured with Nanodrop 1000 (Nanodrop, Wilmington, USA) spectrophotometer and stored at -80°C until further use. Complementary DNA was synthesized with 200U/μl Superscript-II-reverse-transcriptase and for mRNA transcription 0.5 μg/μl oligo-dT<sub>12-18</sub> primers (Life technologies, Darmstadt, Germany) were used. Until further use the cDNA was stored at -20°C. Gene amplification experiments were performed with 1 ng transcribed RNA per reaction with SYBR-green select master mix (Applied Biosystems, Foster City, USA) and the 7500 Fast-real time system (Applied Biosystems). The program used was: holding stage: 95°C for 15 min (one cycle), cycling stage: 95°C for 15 s and 60°C for 1 min (45 cycles). Quality of the amplification was assessed via the melting curve. Analysis was performed using the 2<sup>(-ΔΔCT)</sup> value method. Target gene expression was normalized to expression levels of the housekeeping gene β-actin.

### 2.11 Connexin primers for PCR and qRT-PCR

Primers specific for mouse *Cx43* (*Gja1*) were designed to recognize all validated mRNA splice variants of the gene, relying on the RefSeq sequences of the UCSC genome browser (<http://genome.ucsc.edu/>). The Primer-Blast tool (<http://www.ncbi.nlm.nih.gov/tools/primer-blast/>) was used to create the primer sequences. Using BLAST search (<http://blast.ncbi.nlm.nih.gov/Blast.cgi>), amplification of unintended targets was excluded. Unfavorable secondary structures and primer-dimer amplification were calculated via the IDT-oligo-analyzer (<http://eu.idtdna.com/analyzer/applications/oligoanalyzer/>). Two Primer sequences

for *Cx43* were tested: *Cx43FW1*: CAGGTTGTCCTACATCCCCG, *REV1*: TCCACACCTAGAGGGTCAGG (Product length 95bp); *FW2*: ACAGCGGTTGAGTCAGC TTG, *REV2*: GAGAGATGGGGAAGGACTTGT (Product length 106bp).

## 2.12 Stroke mouse model - Middle Cerebral Artery Occlusion

Surgery was performed by our collaborator, Dr. K. Gertz (Klinik und Poliklinik für Neurologie, Charité – Universitätsmedizin Berlin), for details please see (Wang *et al.*, 2008). MacGreen mice which furthermore expressed a tandem dimer red fluorescent protein in macrophages were provided 7 days after surgery for electrophysiological analysis of microglia/macrophages. In brief, mice were anesthetized with 1.5 % isoflurane and maintained in 1.0% isoflurane in 69 % N<sub>2</sub>O and 30 % O<sub>2</sub> via a vaporizer. The MCAo was induced with the use of a silicone-coated 8.0 nylon monofilament for 30 min on the left hemisphere (Figure 13). The filament was entered into the internal carotid artery up to the anterior cerebral artery and thereby occluded the middle cerebral artery. Subsequently the filament was removed to allow reperfusion. The temperature of the animals was maintained at 36.5 ± 0.5 °C with a control unit. (Gertz *et al.*, 2012)

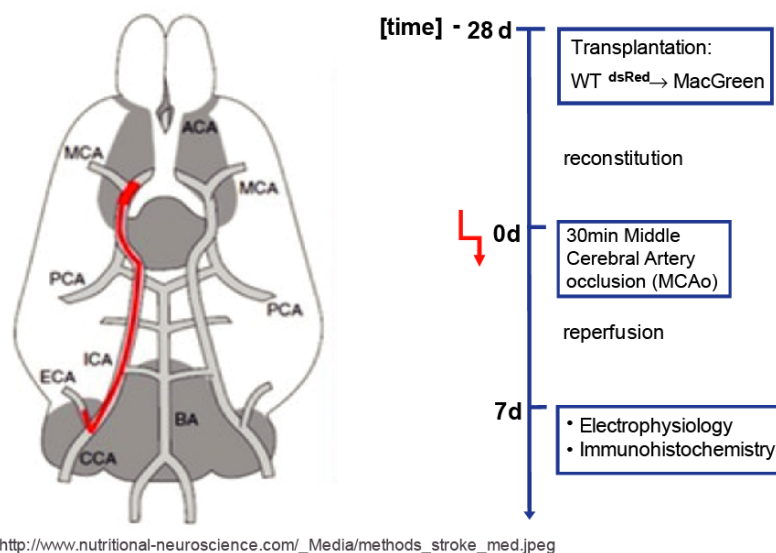


**Figure 13: Middle cerebral artery occlusion (MCAo) and timeline for stroke experiment setup.**

### 2.13 Statistical analysis

Electrophysiological recordings were analyzed with the TIDA software and Microsoft Excel. Additionally the programming software R was used for the analysis of pair-recordings. Dye-coupling was analyzed in sequentially acquired confocal stacks with FIJI (ImageJ). For examination of significance the SPSS software 11.5.1 (Chicago, IL, USA) was used. To analyze the differences in the specific conductance (G) and membrane capacitance (Cm), significances were examined by applying the non-parametric Mann-Whitney-U-Test. The Mann-Whitney-U-test combines and places the values from two groups in order and compares the mean ranks between the groups. The median and 25<sup>th</sup>/75<sup>th</sup> percentiles have to be stated while the 25<sup>th</sup> and 75<sup>th</sup> percentile values were taken from Tukey's Hinges meaning the values are approximations that can be obtained with little calculations. For the cell membrane potential of glioma-associated microglia and macrophages the One-way ANOVA and Bonferroni *Post hoc* test were used. P-values of <sup>###</sup>p<0.001, <sup>##</sup>p<0.01, <sup>#</sup>p<0.05 were considered statistically significant.

The two paired Student's t-Test was used to determine if kainate increases the conductance of electrical coupled oligodendrocytes in the corpus callosum and is presented as mean ± Standard Error of the Mean. While for the receiving cells the Mann-Whitney-U-Test was applied.

### 3 Results

Gap junctional communication in the central nervous system is an important aspect for the brain homeostasis but also for the exchange of ions, metabolites and second messengers. In this work I investigated the gap junctional communication among astrocytes and oligodendrocytes in the mouse brain as well as gap junctional coupling of microglia cells under normal physiological conditions and in the diseased brain.

#### 3.1 Astrocytes form panglial networks in the CNS and express a unique antigen profile

In this project, I investigated the astrocytic participation in panglial networks in the cortex and corpus callosum as a part of a collaboration project with the lab of Prof. Steinhäuser. This project gives insight to the heterogeneity of astrocytes whose physiological importance still has to be characterized. The data for the cortex were published in the paper (Griemsmann *et al.*, 2014) whereas the corpus callosum data is not yet published.

To assess gap junctional coupling of astrocytes in the neocortex and corpus callosum of acute brain slices, a single astrocyte was dialysed via the whole-cell patch-clamp technique with the GJ permeable tracer biocytin. Astrocytes were distinguished by their eGFP expression and their typical passive membrane current (Figure 14) obtained by application of a voltage protocol of de- and hyperpolarizing steps (+50 mV to -170 mV) in 10 mV increments for 50 ms.

In the neocortex of *hGFAP/eGFP* mice, biocytin spread to approximately  $102 \pm 25$  cells and 31% (SEM = 4.3) of the labeled cells were GFAP/eGFP-positive exclusively ( $n = 8$ ,  $p30$ ). In contrast, in the corpus callosum on average only  $31 \pm 5$  cells were biocytin filled ( $n = 5$ ,  $p15$ ). In these networks 21% (SEM = 3.2) of the cells were GFAP/eGFP-positive. The little insets of Figure 14 show the spread of Alexa Fluor 594 into multiple branches of the astrocyte. After 20 min of dialysis the brain slice was fixed and subsequently labelled with streptavidin-Cy3 to visualize tracer spread (Figure 14, 2nd column). The biocytin filled networks in the neocortex usually showed a circular biocytin-spread while the networks in the corpus callosum were more densely packed and oriented along the fibre tracts and therefore revealed an elongated biocytin spread (Figure 14). For characterization of the bio-

cytin coupled cells I used the oligodendrocyte marker Olig2, which is a transcription factor expressed by both precursors and mature oligodendrocytes (Lu *et al.*, 2002; Marshall *et al.*, 2005; Nishiyama *et al.*, 2009; Trotter *et al.*, 2010). In the neocortex,  $60 \pm 7$  of  $102 \pm 25$  ( $60 \pm 15$  %) biocytin filled cells ( $n = 8$ ) were Olig2+, and in the corpus callosum  $12 \pm 4$  out of  $28 \pm 4$  ( $44 \pm 15$  %) biocytin filled cells expressed Olig2 ( $n = 5$ ) (Figure 15). These experiments indicated that astrocytes in the neocortex as well as in the corpus callosum of *hGFAP/eGFP* mice are coupled to oligodendrocytes and form a pangiial network.

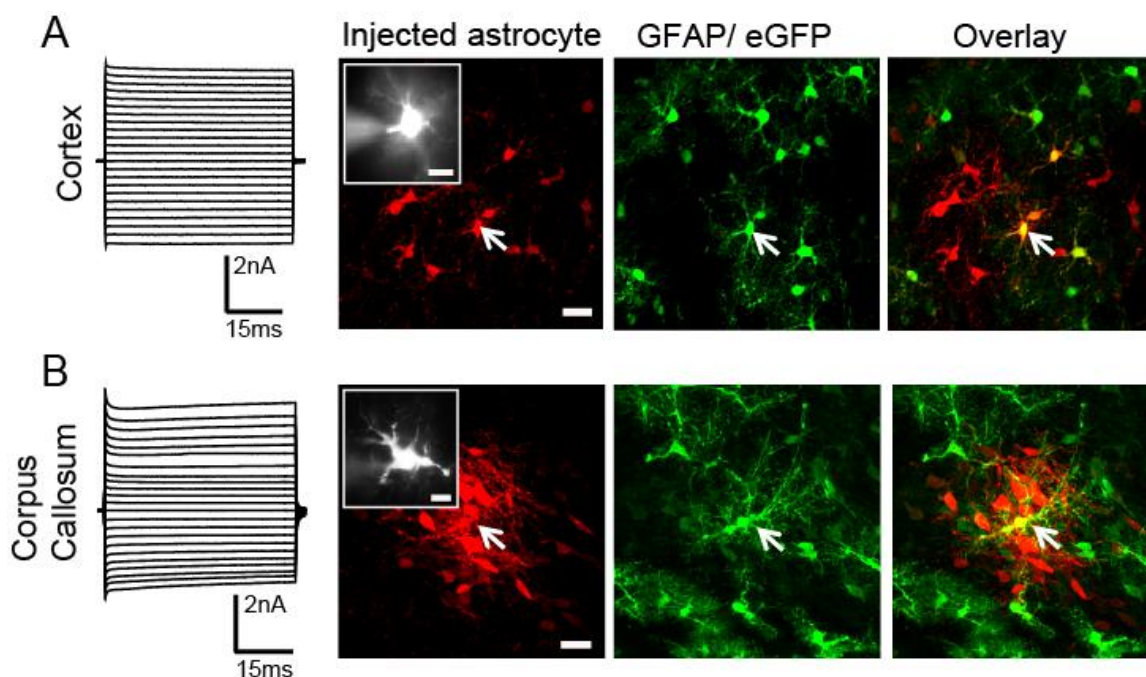


**Figure 14: Astrocyte dye-coupling in the neocortex and corpus callosum of *hGFAP/eGFP* mice.**

First column shows the corresponding passive membrane current of an astrocyte in the neocortex and corpus callosum, recorded in response to de- and hyperpolarizing steps (+50 to -170 mV for 50 ms and 10 mV increments). The scale bar size is 20 μm and in the inset 10 μm. In the second column the spread of the tracer biocytin is labelled with streptavidin-Cy3. Biocytin diffused into  $102 \pm 25$  cells ( $n = 8$ , p30) in the neocortex and to a lesser extent in the corpus callosum, namely on average only  $28 \pm 4$  cells were biocytin filled ( $n = 5$ , p15). Arrows indicate the initially patched astrocyte.

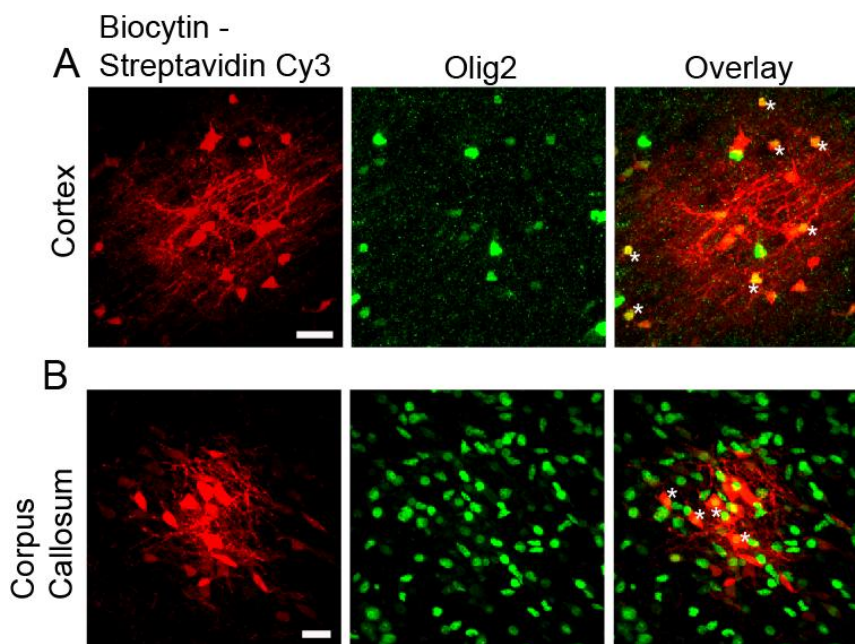


**Figure 15: Immunostaining of gap junctional networks with Olig2 in the neocortex and corpus callosum of *hGFAP/eGFP* mice.**

First column shows biocytin spread, conjugated with streptavidin-Cy3 (A = neocortex, B = corpus callosum); Second column: staining with the oligodendrocyte lineage marker Olig2; Third column: overlay of biocytin filled cells and Olig2 staining; Most of the coupled cells were Olig2+ in the neocortex,  $60 \pm 15\%$ , ( $n = 8$ ) while  $44 \pm 15\%$  were Olig2+ in the corpus callosum ( $n = 5$ ). Biocytin filled cells that were also Olig2+ are indicated by a star. Scale bar:  $20 \mu\text{m}$ .

While in the hippocampus the Olig2 marker labels a distinct population of cells (Griemsmann *et al.*, 2014) the overlay of Olig2 and GFAP/eGFP+ cells derived from cell counting in the networks in the neocortex (the GJNs consist of  $16 \pm 2\%$  GFAP-eGFP+/Olig2+ cells) and in the corpus callosum ( $11 \pm 6\%$  GFAP-eGFP+/Olig2+ cells), revealed that Olig2 is not a cell type-specific marker in *hGFAP/eGFP* mice. Since my quantification of GFAP/eGFP-positive astrocytes in the neocortex and corpus callosum revealed overlap with the Olig2 marker I used the reporter mouse *Cx43ki/ECFP* in which ECFP is expressed by astrocytes but not by NG2 cells (Degen *et al.*, 2012). Using acute coronal brain slices, fixed and subsequently labeled with Olig2 revealed that in the neocortex 20% of the ECFP+ cells expressed Olig2 ( $3240 \pm 879$  ECFP+/Olig2+ cells/ $\text{mm}^3$  from a total of  $15305 \pm 1126$  ECFP+ cells/ $\text{mm}^3$ ) while I could not find any double-positive cells in the corpus callosum. My findings indicate an intermediate glial cell type in the neocortex that coexpressed astrocytic Cx43 and oligodendrocytic Olig2 genes (Griemsmann *et al.* 2014). Furthermore, NG2 cells never participated in the networks

formed in the neocortex of *hGFAP/eGFP* mice ( $0$  of  $143 \pm 14$ ,  $n = 6$ ) (Figure 17). This marker has not been used for my dye-filling experiments in the corpus callosum although Maglione *et al.* 2010 showed that NG2 cells are part of the panglial network when injecting oligodendrocytes in the corpus callosum of *NG2-EYFP* heterozygous animals. These animals allow easy identification of NG2 cells (Karram *et al.*, 2008).

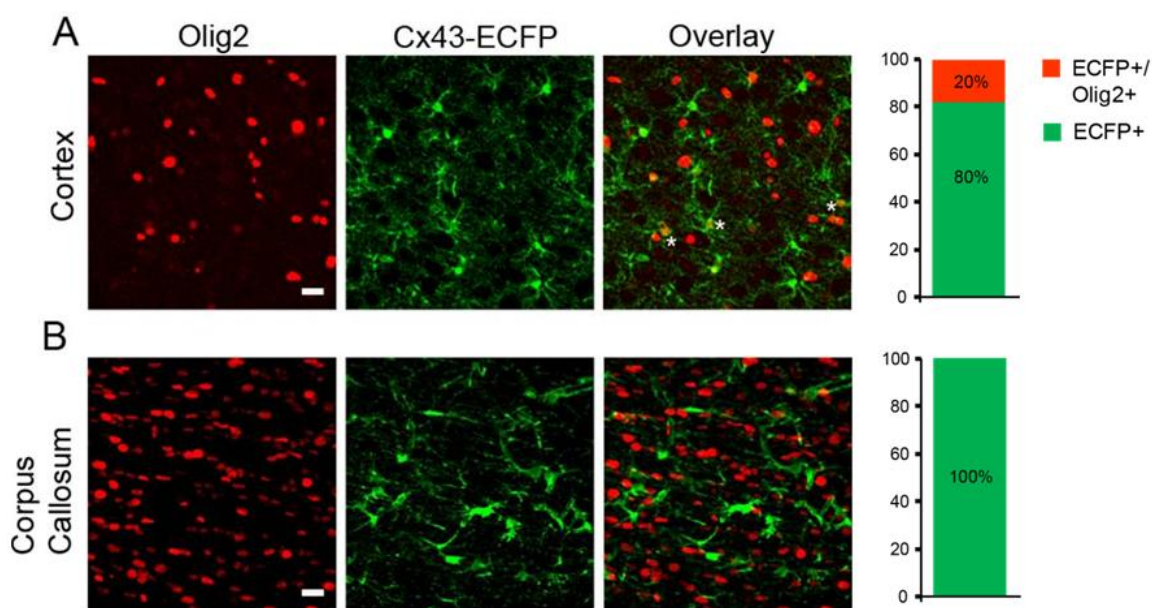


**Figure 16: Cx43-ECFP+ cells expressing Olig2, a transcription factor expressed by both precursor and mature oligodendrocytes.**

Immunostaining for Olig2 in the neocortex and corpus callosum of heterozygous *Cx43<sup>ECFP+</sup>* mice. The overlay image in the third column shows a colocalization of ECFP and Olig2 staining in the neocortex, indicated by stars (A), while in the corpus callosum (B) none of the ECFP positive cells revealed Olig2 expression. Scale bar: 20  $\mu$ m. Graphs indicate that in the neocortex 20% of the cells are ECFP+/Olig2+, while in the corpus callosum none of the cells are double-positive.

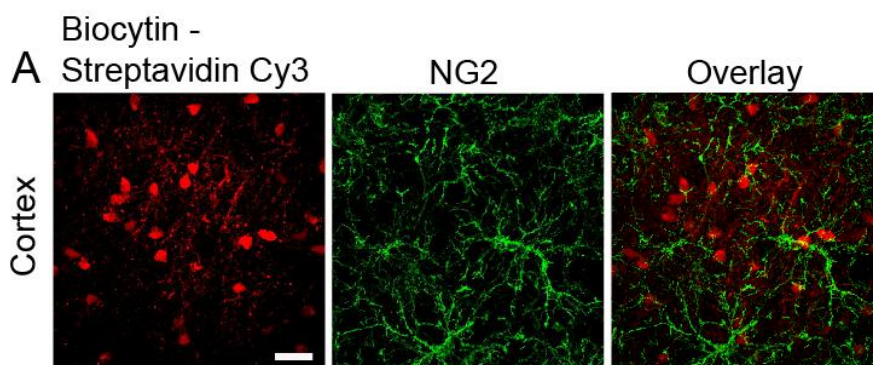


**Figure 17: NG2 cell staining in biocytin networks in the neocortex of *hGFAP/eGFP* mice.**

First picture shows biocytin filled cells which are labelled with streptavidin-Cy3, scale bar: 20  $\mu$ m. Second picture shows the NG2 marker and in the last picture the overlay of both channels is given which shows no overlap of biocytin and NG2 ( $n = 6$ ).

### 3.2 Does the panglial network provide energy for axons?

To study metabolic coupling in the CNS acute brain slices of either wildtype or *hGfap-RFP* mice (astrocytes expressing the red fluorescent protein under the hGFAP-promoter, Hirrlinger *et al.* 2005) were used. A single astrocyte or oligodendrocyte was dialysed via the whole-cell patch-clamp technique with the glucose derivative 2NBDG and the GJ tracer biocytin. Astrocytes were distinguished by their RFP expression and their typical passive membrane current. Oligodendrocytes, in contrast, were identified by their morphology, the presence of voltage independent membrane currents with some decay during voltage steps, sometimes large symmetrical tail currents and moreover by subsequent immunostaining with the oligodendrocyte marker CNPase. The spread of 2NBDG into the coupled cellular partners could be shortly imaged in the living slice but after fixation 2NBDG was only visible in the patched/injected cell. In the corpus callosum, ten astrocytes were injected with 2NBDG. Two oligodendrocytes out of a total of twenty 2NBDG injections could be further analyzed. My experiments revealed that 80% of the 2NBDG injected astrocytes were 2NBDG coupled (8 out of 10). The two injected oligodendrocytes showed 2NBDG spread and could afterwards be validated by expression of CNPase (Figure 19 and 20).

2NBDG dye-transfer experiments were combined with biocytin injection. Subsequent labeling with streptavidin Cy3 revealed that not all 2NBDG coupled cells were also biocytin coupled. Figure 18 shows representative images of a 2NBDG injected astrocyte in an *hGfap-RFP* mouse. The astrocyte was first identified by its RFP expression (Figure 18 A, injected cell indicated by arrow) and then injected via the whole-cell patch-clamp technique with 2NBDG and the gap junctional tracer biocytin. Furthermore, a series of depolarizing and hyperpolarizing voltage steps at a holding potential of -70 mV revealed the typical passive membrane current of astrocytes (Figure 18 E). The overlap of the RFP fluorescence and 2NBDG spread to adjacent cells can be seen in figure 18 C. 2NBDG dialyzed the injected astrocyte and diffused into an adjacent oligodendrocyte (recognizable by its morphology (asterisk) which was later on validated by immunostaining (I&J, indicated by asterisk)) and also into an astrocyte (Figure 18 C, indicated by a star), close to the dye filled oligodendrocyte. However, the astrocyte that was located right next to the injected cell was neither 2NBDG coupled nor positive for biocytin (Figure 18 F&J). Figure 18 D shows an overview of the 2NBDG spread after removal of the

patch-pipette, taken with a 20x objective. This image demonstrates that 2NBDG spreads to several other cells in the corpus callosum. To be able to distinguish the exact number of 2NBDG coupled cells, a setup microscope with a better resolution and advanced features to take images in several focal planes would be an advantage.

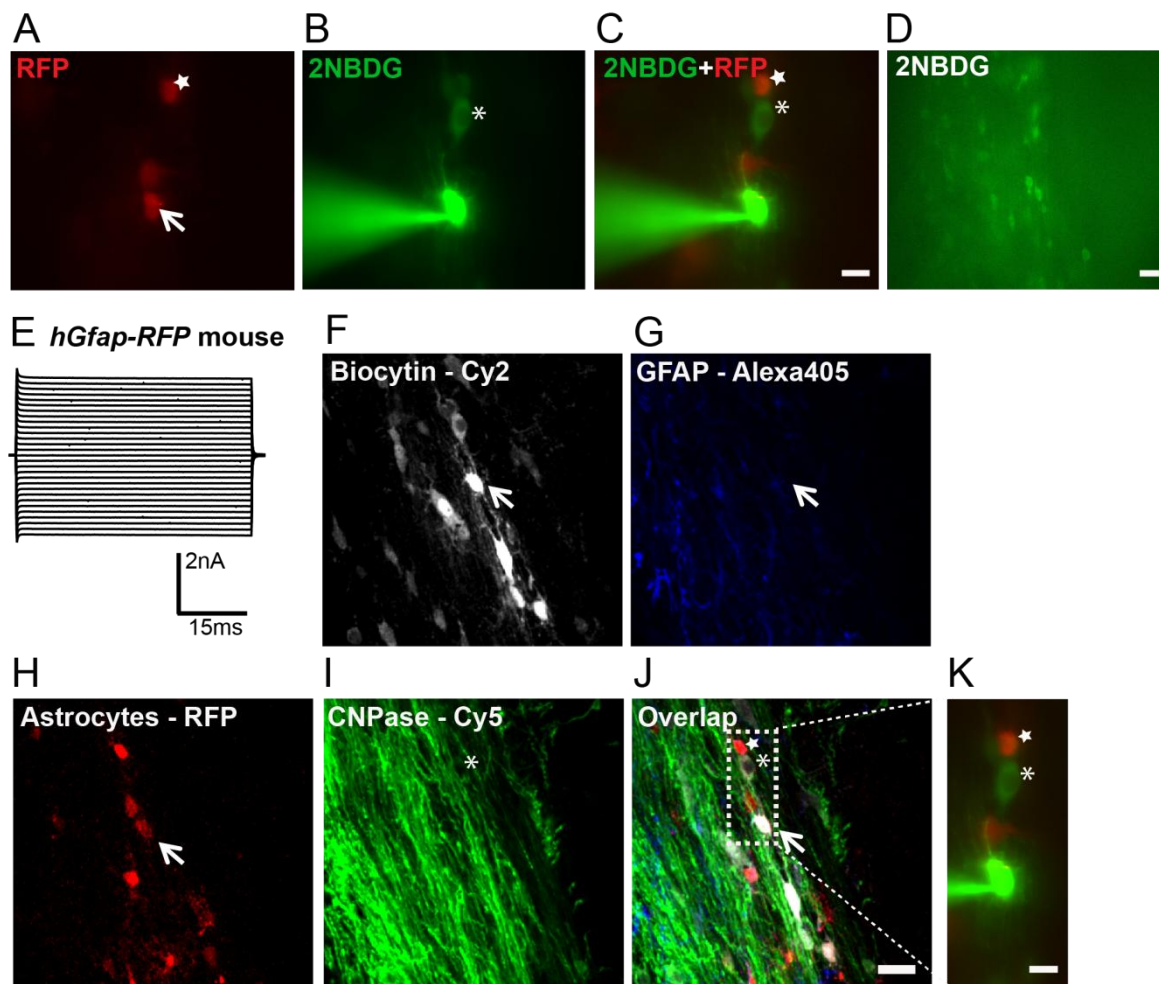
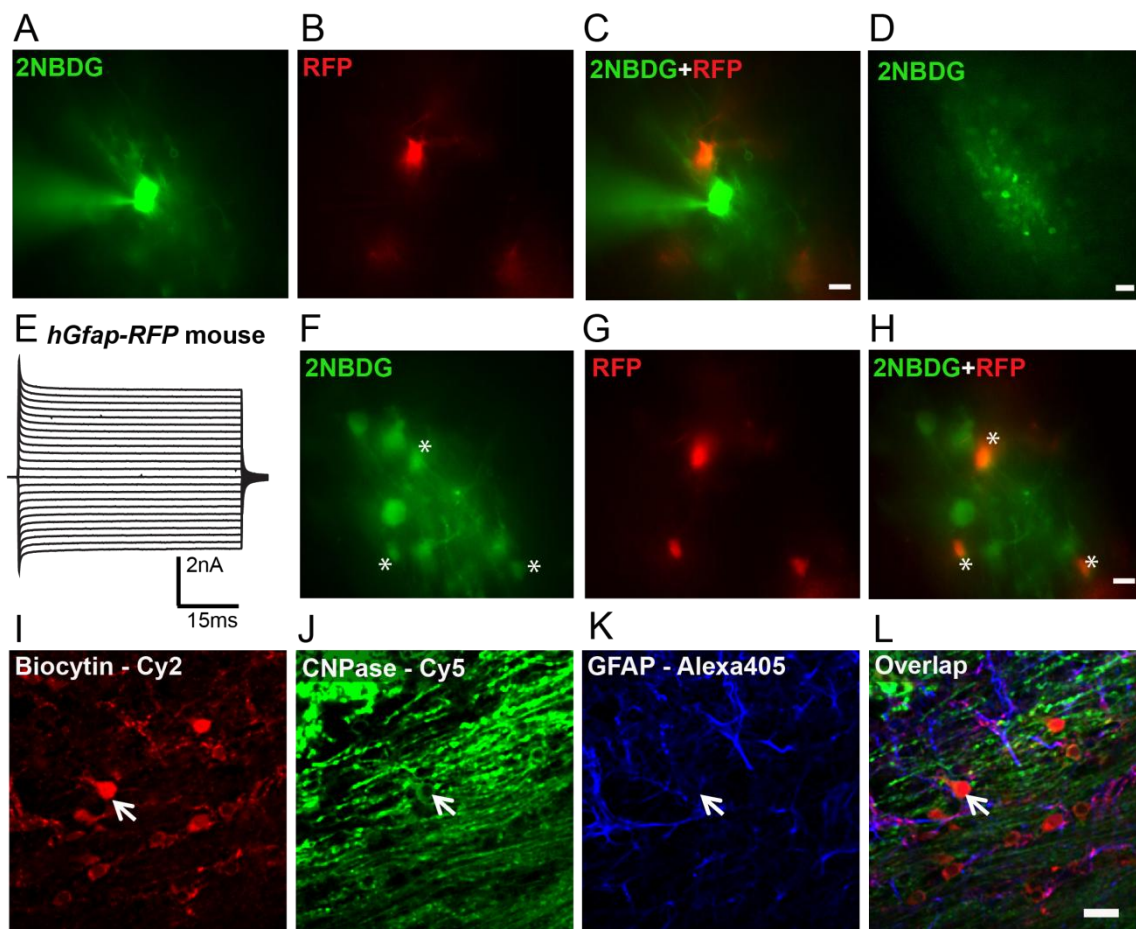


**Figure 18: Astrocytes supply axons with metabolites via a panglial network in the corpus callosum.**

A) Astrocyte, prior identified by its RFP fluorescence, is indicated by arrow. B) Astrocyte was dialyzed with standard internal solution containing 2NBDG (5 mg/ml) and biocytin (2 mg/ml) for 20 min. C) Overlap of RFP fluorescent astrocytes and 2NBDG spread (Scale bar: 10 $\mu$ m). D) Overview of 2NBDG spread after removal of the patch-pipette showing spread to several adjacent cells (Scale bar: 20  $\mu$ m). E) Typical current profile of an astrocyte clamped at -70 mV and currents recorded in response to de- and hyperpolarizing voltage steps ranging from +50 mV to -170 mV for 50 ms each and with 10 mV increments. F-J) Confocal images of dialyzed astrocyte and its coupled cells, revealed with streptavidin-Cy2 labeling (F); marker for GFAP expression in astrocytes, cannot distinguish GFAP staining in injected astrocyte (G); the intrinsic red fluorescence of astrocytes under the hGFAP promoter in GRFU mice (Hirrlinger *et al.*, 2005); (H) marker for CNPase expression in oligodendrocytes, asterisk indicates one oligodendrocyte that was 2NBDG+ and biocytin coupled to astrocyte as seen under setup images (C); (I) and J) Overlap of

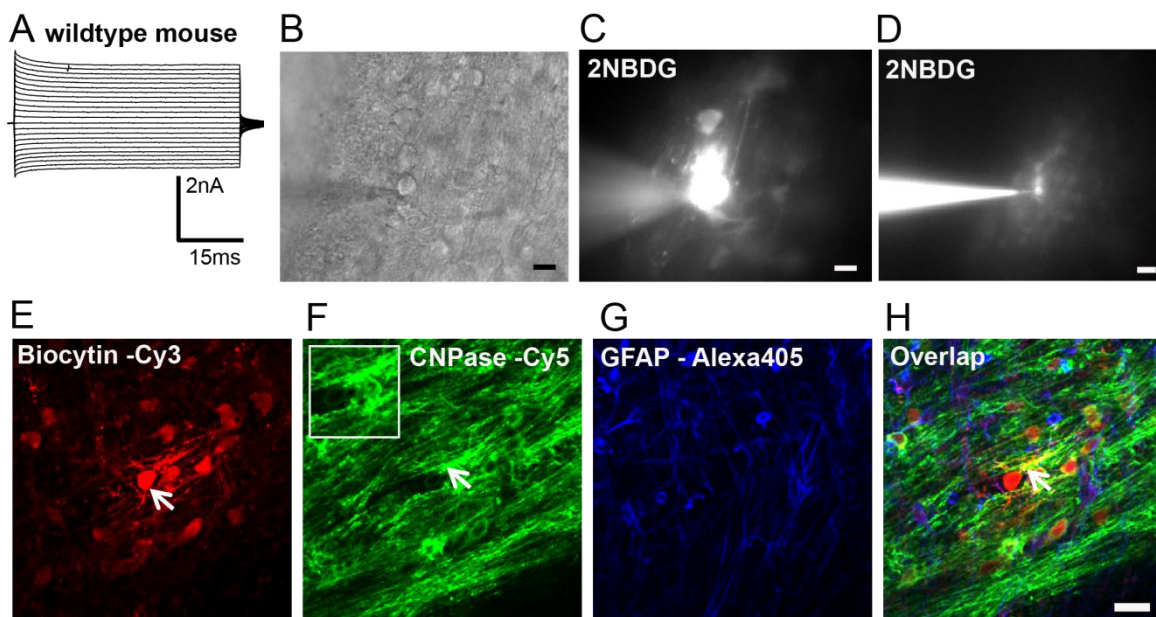
the biocytin coupled cells (grey), RFP fluorescent astrocytes (red), CNPase expression by oligodendrocytes (green) and GFAP expression of astrocytes (blue) (Scale bar: 20  $\mu\text{m}$ ). The arrows indicate the injected astrocyte and the dashed square is shown as a blow up in (K) to show the retrieval of the initially filled cell which was not always possible (star is an astrocyte which was 2NBDG and weakly biocytin coupled to injected astrocyte).

Figure 19 and 20 demonstrate the two examples of an injected oligodendrocyte which showed 2NBDG spread and could afterwards be validated by expression of CNPase. Figure 19 E and 20 A show the typical voltage independent membrane currents with some decay of a coupled oligodendrocyte in the corpus callosum after de- and hyperpolarized voltage steps (Maglione *et al.*, 2010) in a wildtype mouse and *hGfap/RFP* mouse, respectively. Only one cell per slice was dialyzed and oligodendrocytes were furthermore recognized by their slightly oval shaped somata which are often arranged in a pearl-necklace-like structure (Figure 20 B). After 20 min dialysis with the intracellular solution containing 2NBDG and biocytin, 2NBDG spread into the processes oriented along the parallel fibres and revealed little circles that could only be recognized when injecting an oligodendrocyte but not an astrocyte (Figure 19 A and 20 C). From the first overlap image taken with the setup microscope (Figure 19 C) it appears as if the 2NBDG does not spread into adjacent red fluorescent astrocytes but into another focal plane of the same injected oligodendrocyte. Moving to another focal plane (Figure 19 H) revealed that three astrocytes were filled with 2NBDG and therefore metabolically coupled to the oligodendrocyte (Figure 19 H, 2NBDG-positive astrocytes are indicated by an asterisk). The immunostaining for both experiments confirmed that the initial injected cell was CNPase-positive and therefore an oligodendrocyte (Figure 19 J and 20 F). Moreover, the biocytin labeling with Cy2/Cy3-conjugated streptavidin showed spread of the gap junctional tracer (Figure 19 I, 20 E). The biocytin network (17 cells) in the wildtype mouse (Figure 20) consisted of 13 CNPase+ cells, while 4 cells were negative for CNPase as well as for the astrocytic marker GFAP.



**Figure 19: Oligodendrocytes supply axons with metabolites via a panglial network in the corpus callosum of an *hGfap/RFP* mouse.**

A) The oligodendrocyte was recognized by its oval shaped somata and dialyzed with standard internal solution containing 2NBDG (5 mg/ml) and biocytin (2 mg/ml) for 20 min. B) RFP-fluorescent astrocytes in the same patch area. C) Overlap of RFP fluorescent astrocytes and 2NBDG spread (Scale bar: 10 $\mu$ m). D) Overview of 2NBDG spread after removal of the patch-pipette showing spread to several adjacent cells (Scale bar: 20  $\mu$ m). E) Current profile of an oligodendrocyte clamped at -70 mV and currents recorded in response to de- and hyperpolarizing voltage steps ranging from +50 mV to -170 mV for 50 ms each and with 10 mV increments. F-G) Other focal plane of 2NBDG spread under setup microscope showed that three astrocytes are positive for 2NBDG, indicated by an asterisk. J-L) Confocal images of dialyzed oligodendrocyte and its biocytin coupled cells, revealed with streptavidin-Cy2 labeling (I); marker for CNPase expression in oligodendrocytes which shows that the injected oligodendrocyte is CNPase-positiv (J); GFAP-expression of astrocytes (K); L) Overlap of the biocytin coupled cells (red); CNPase expression by oligodendrocytes (green) and GFAP expression of astrocytes (blue) (Scale bar: 20  $\mu$ m)



**Figure 20: Oligodendrocytes supply axons with metabolites via gap junctional network in the corpus callosum of a wildtype mouse.**

A) Current profile of an oligodendrocyte clamped at  $-70$  mV and currents recorded in response to de- and hyperpolarizing voltage steps as described above. B) Oligodendrocyte was recognized by its oval shaped somata and dialyzed with standard internal solution containing (C) 2NBDG (5 mg/ml) and biocytin (2 mg/ml) for 20 min (Scale bar:  $10\ \mu\text{m}$ ). D) Overview of 2NBDG spread showed coupling to several adjacent cells (Scale bar:  $20\ \mu\text{m}$ ). E-H) Confocal images of dialyzed oligodendrocyte (arrow) and its formed network of biocytin filled cells (E); marker for CNPase expression in oligodendrocytes shows that injected oligodendrocyte and its processes are CNPase-positiv, indicated by arrow, inset is a magnification of the injected oligodendrocyte (F); GFAP-expression of astrocytes (G); H) Overlap of the biocytin coupled cells (red); CNPase expression by oligodendrocytes (green) and GFAP expression of astrocytes (blue) (Scale bar:  $20\ \mu\text{m}$ ), arrows indicate patched oligodendrocyte.

### **3.3 Pair recordings of oligodendrocytes in the mouse white matter - corpus callosum**

#### **3.3.1 Gap junctional coupling between oligodendrocytes is low and shows no voltage dependence**

To study the current voltage relation and junctional conductance between oligodendrocytes in the corpus callosum, whole-cell pair recordings were performed in slices from postnatal 16 to 23 day old *Plp-GFP* animals. For this series of experiments (N = 10 pair recordings), cells were selected within a focal plane and with a distance of less than 30  $\mu\text{m}$ . I analysed the junctional conductance and its voltage dependence. Figure 21 shows a representative recording from two oligodendrocytes. To evaluate the current-voltage relationship of the junctional conductance between these pairs of cells, one cell, designated cell 1 (Figure 21 A1, B1) was clamped from a holding potential of -70 mV to a series of depolarizing and hyperpolarizing voltage steps (+50 mV to -170 mV in 10 mV increments for 200 ms, little insets on bottom right of figure 21 B1/C2). The other cell, designated cell 2, was also clamped at -70 mV (Figure 21 A1, B2). The currents in the stimulated cell represent the membrane currents and these were not voltage dependent as shown in the IV-plot. The currents recorded in cell 2 were the currents mediated by the GJs between these two cells. These currents were also not voltage dependent as shown in the IV-plot. Subsequently the same stimulation protocol was applied to cell 2 while cell 1 was clamped at -70 mV. Similar gap junctional currents were recorded in cell 1 indicating that the GJ shows no rectification.

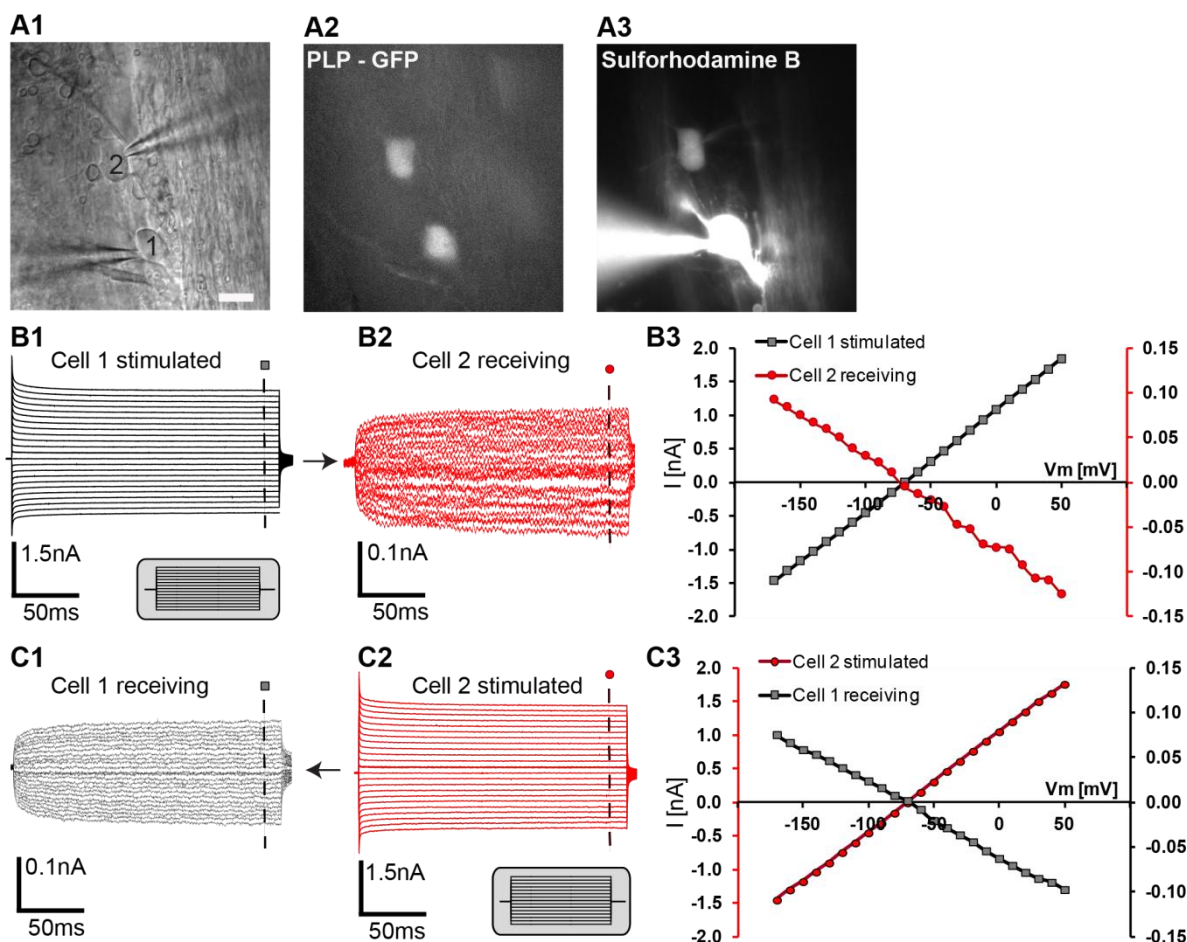


**Figure 21: Pair recording of two oligodendrocytes in the mouse corpus callosum.**

A1) Brightfield image shows two electrodes from a pair recording of oligodendrocyte 1 and oligodendrocyte 2 (Scale bar: 10  $\mu\text{m}$ ). A2) depicts the GFP fluorescence of patched oligodendrocytes, under the PLP promoter (Fuss *et al.*, 2000) and image A3) illustrates the injection of sulforhodamine B into oligodendrocyte 1 which reveals the typical morphology and spread of SR B along parallel processes and furthermore into oligodendrocyte 2. The corresponding current profiles of oligodendrocyte 1 are shown in **B1** and for oligodendrocyte 2 in **C2**. Current profiles were recorded from a holding potential of -70 mV (+50 mV to -170 mV in 10 mV increments for 200 ms, see little inset below current profile). For pair recording, voltage steps are applied in one cell as mentioned above (also termed stimulated cell) and currents are recorded in the stimulated as well as in the receiving cell (B1→B2) and vice versa (C2→C1). **B3** and **C3** present the corresponding IV-plots in absolute values of cell 1 (line with squares) and cell 2 (line with circles). Current responses  $I$  [nA] of the stimulated cell are shown on the left y-axis and transjunctional current of the receiving cell on the right y-axis. The whole cell currents and transjunctional currents of the receiving cells are linear and show no voltage dependence.

Electrical coupling was observed in 90% of the experiments conducted (9 out of 10 experiments). Averaging the gap junctional currents of the receiving cells for all 9 experiments (Figure 22) revealed that the gap junctional conductance is linear with no voltage dependence, as already shown for the representative example above (Figure 21). The junctional conductance directly after forming the whole-cell configuration ranged between 0.24 nS and 1.84 nS and averaged at 0.81 nS and an SEM of  $\pm 0.13$  ( $n = 18$ , details for calculation see chapter 2.6.2). The coupling ratio, which was calculated by dividing the current response of cell 2 by the current of cell 1 at the voltage step of +30 mV, ranged between 0.016 and 0.212, with a mean of 0.067 and an SEM of  $\pm 0.014$ .

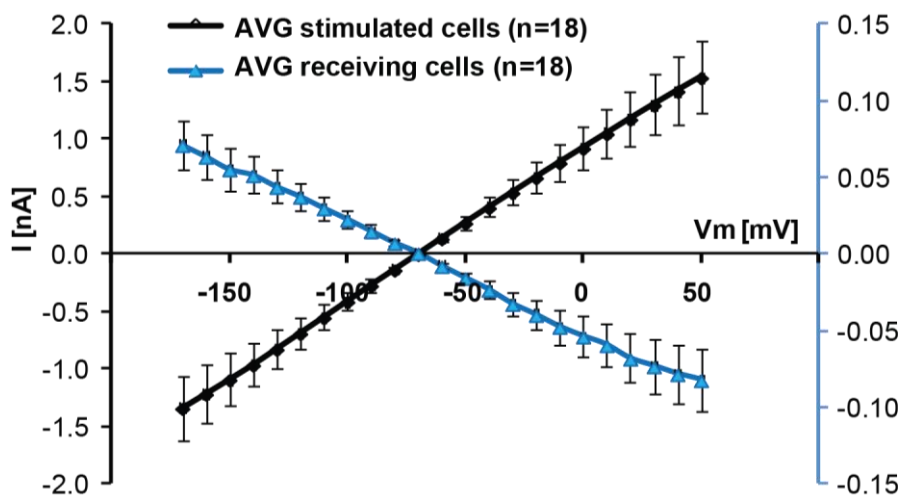


**Figure 22: Average IV-curves of oligodendrocyte pair recordings.**

In 9 out of 10 paired recordings, oligodendrocytes showed electrical coupling. Cells were clamped at -70 mV and voltage steps from +50 mV to -170 mV for 200 ms and in 10 mV increments were applied in the stimulated cell, while the current was measured in the stimulated as well as in the receiving cell. This protocol was applied vice versa, meaning that in an alternating fashion, the stimulated cell is the receiving cell while the receiving cell then is the stimulated cell. All 9 electrical coupled pair recordings of stimulated ( $n = 18$ ) and receiving cells ( $n = 18$ ) showed a linear IV-curve and no voltage dependence. The error bars are given as  $\pm$  SEM.

### 3.3.2 Kainate application does not significantly influence the junctional conductance between oligodendrocyte pairs

Kainate is a ligand for the AMPA- and Kainate ionotropic receptors which are a subtype of the glutamate receptors. These receptors have been shown to increase cytosolic  $\text{Ca}^{2+}$  upon stimulation and thereby reduce the junctional conductance in Bergmann glial cells (Müller et al. 1996). However, it is not yet known whether kainate has a similar effect on the junctional conductance of oligodendrocytes in the corpus callosum. Since oligodendrocytes express AMPA/Kainate receptors, I hypothesized that the junctional conductance could be influenced by the application of kainate. To investigate this, I performed pair recordings of oligodendrocytes and applied 1 mM kainate via the bath solution for 30 seconds and measured the current response in the receiving cell. Figure 23 shows an example of a pair recording over time, to record the junctional conductance. Alternating, either cell 1 or cell 2 received a voltage step of -50 mV, -100 mV, +50 mV and +100 mV every 2 sec, while both cells were clamped at -70 mV (Figure 3 B). A1 and B1 show a section of the current trace over time for cell 1 and cell 2. The blue dashed lines in the current traces mark the current response of the stimulated/receiving cell before (control current) and the dotted lines after application of kainate (peak response after 30 sec application of 1 mM kainate). The magnified squares/cut-outs in A2.1 and B2.1 represent control currents of stimulated cells and the corresponding currents of the receiving cells are given in the blow-ups in A2.2 and B2.2. The currents at peak for the stimulated cell after kainate application are given in A3.1 and B3.1, whereas A3.2 and B3.2 show currents in the receiving cell. In both recordings shown in figure 23 A1/B1, the cells responded with a depolarization upon kainate application which is probably due to the uptake of cytosolic  $\text{Ca}^{2+}$  and moreover seemed to be reversible.

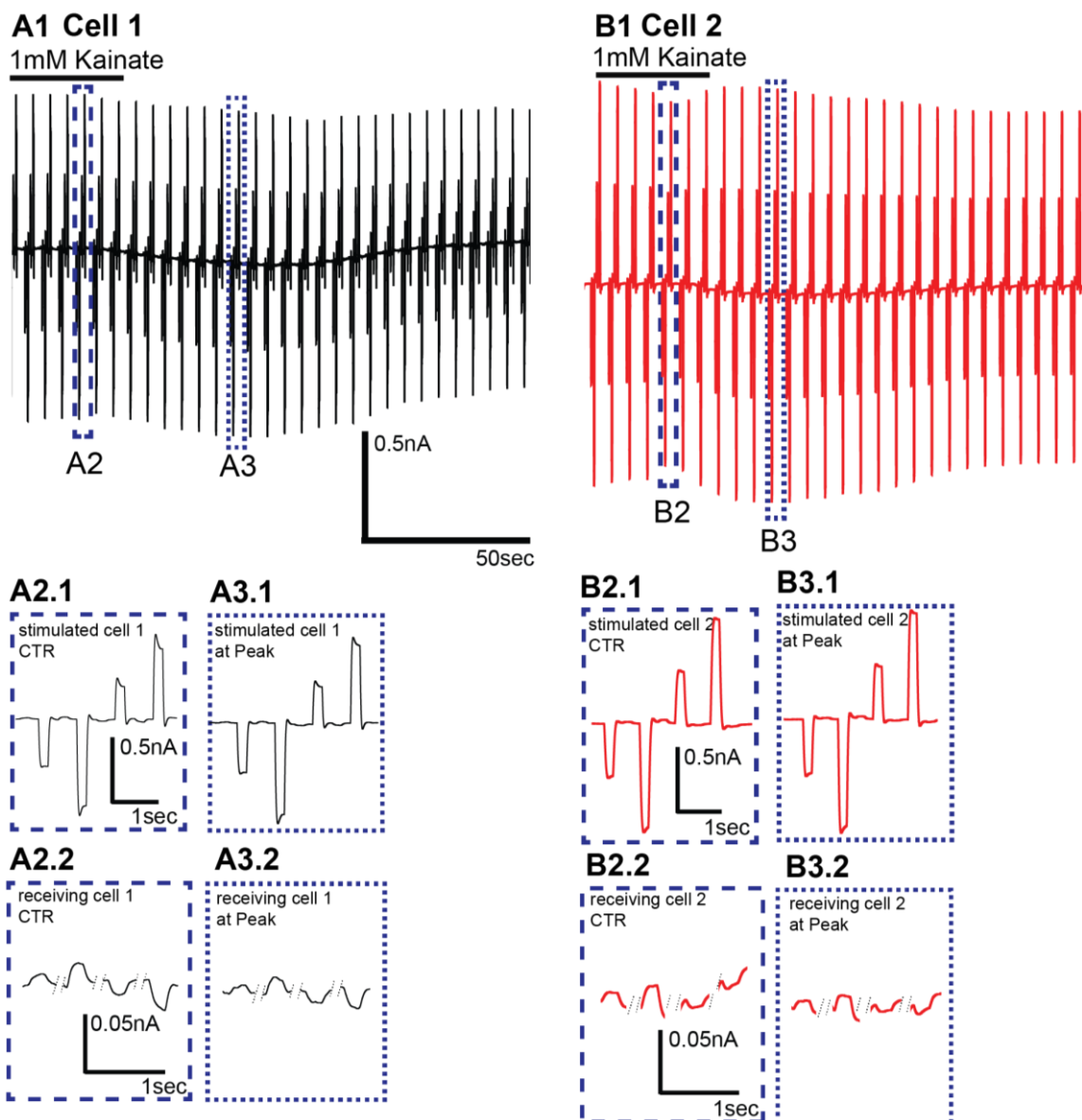


**Figure 23: Current responses of stimulated and receiving cells of a paired recording from oligodendrocytes, over a time course of 150 seconds.**

A1 and B1 show a cut-out (150 s) of the current responses of cell 1 and 2 from a total recording of 8 min. The membrane of each cell was alternating and repetitively clamped with two hyperpolarizing (-50 mV, -100 mV) and two depolarizing voltage steps (+50 mV, +100 mV) (For voltage protocol see figure 12, holding potential of -70 mV). After approximately 100 s of regular ACSF application (cannot be seen in cut-out of current sequence in A1 and B1), 1 mM kainate was applied via the bath perfusion for 30 s (shown as black bar above current sequence in A1 and B1). As kainate wash in was slow, the weak response appeared with a delay. The blue dashed lines in A1 and B1, named A2/B2 are shown as blow ups below. Where A2.1/B2.1 is the response of the stimulated cell at control level and A2.2/B2.2 the response of the receiving cell at control level. The dotted lines in A1 and B2, named A3/B3 are shown below and represent the response of the stimulated and receiving cell after kainate application.

Conductances  $G$  [nS] and junctional conductance  $G_j$  [nS] for each cell were derived from the linear IV-curve between -120 mV to -20 mV, generated by the reverse sequence applied. Comparison of those conductances at control level (taken before and after kainate peak response) with those after kainate application (peak) showed a significant increase in the stimulated cells (Figure 24 A1). When looking at the receiving cells (Figure 24 A2) the conductances were not significantly changed upon kainate application, indicating that kainate does not influence junctional conductance in oligodendrocyte pairs. The data of the stimulated cells show normal distribution and can therefore be displayed as the mean conductance of 10.4 nS with a SEM of  $\pm 1.4$  nS for the control and  $11.4 \pm 1.41$  nS for the peak. Since the data of the receiving cells were not normally distributed, the non-parametric Mann-Whitney-U-Test was applied. The receiving cells showed a median conductance of 0.23 nS (25<sup>th</sup> percentile = 0.128 nS, 75<sup>th</sup> percentile = 0.429 nS;  $n = 10$ ) for the control and 0.25 nS for the kainate peak response (25<sup>th</sup> percentile = 0.147 nS, 75<sup>th</sup> percentile = 0.407 nS/pF;  $n = 10$  cells). Figure 24 B represents conductances of the receiving cells 1 and 2 of all experiments, at the control response and at the peak kainate response. This overview demonstrates that the junctional conductance of oligodendrocyte cell pairs is symmetrical because there is no significant difference between cell 1 and cell 2 at control to kainate response. For each cell pair the normalized junctional conductance ( $G_j$ ) was calculated by dividing the higher value of  $G_j$  by the smaller one. The normalized  $G_j$  gave an average value of 0.88, meaning that the junctional conductance between the cell pairs (5 pairs = 10 cells) only differed to 12 %.

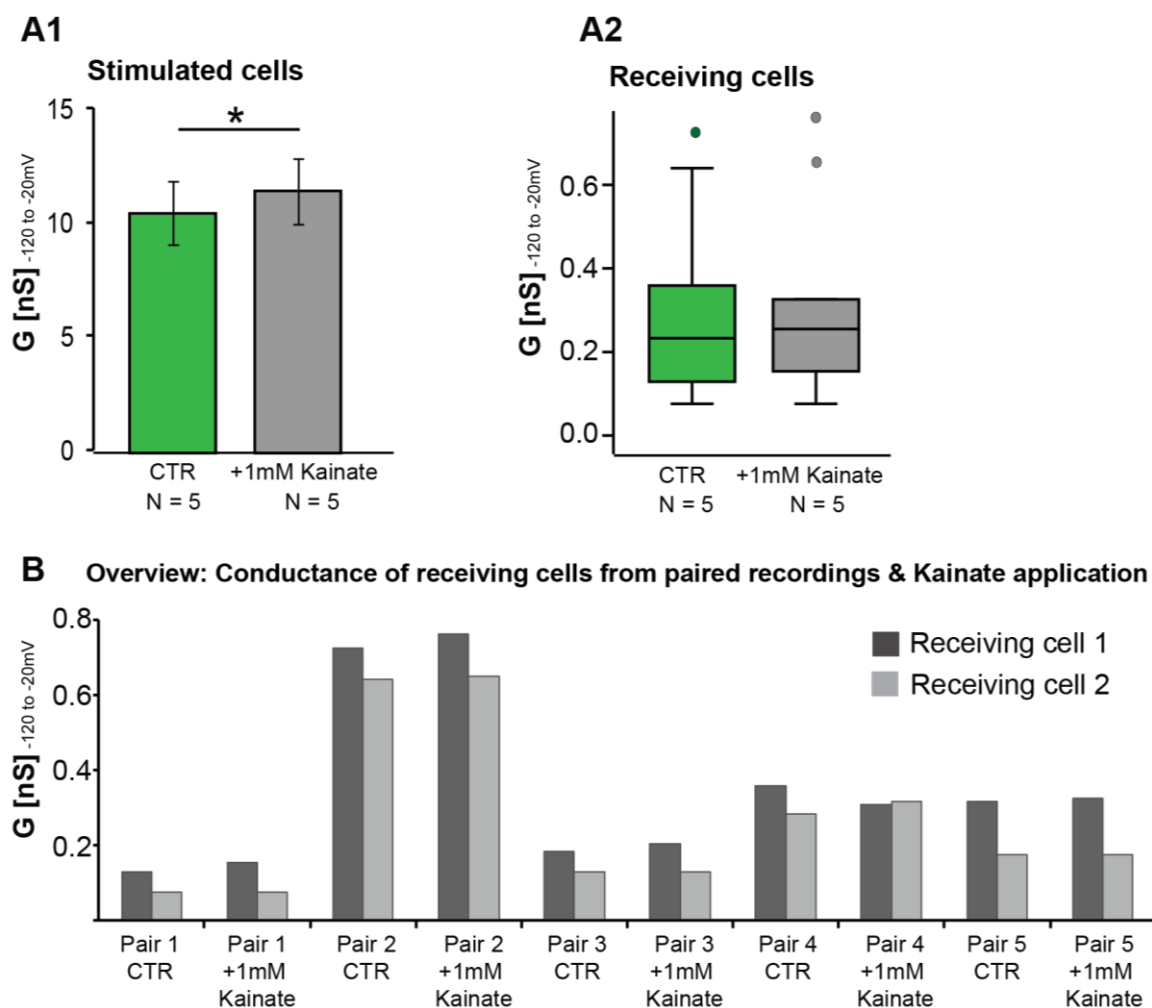


**Figure 24: Conductance of stimulated and receiving cells of oligodendrocyte pair recordings after application of the specific kainate/AMPA receptor ligand kainate.**

Kainate significantly increases the conductance of stimulated cells (A1). The mean conductance at control levels was 10.4 nS with a SEM of  $\pm 1.4$  nS and for the peak response  $11.4 \pm 1.41$  nS. The two paired T-Test was used to determine the significance of  $p = 0.02$  ( $p < 0.05$ ,  $** p < 0.005$ ,  $*** p < 0.001$ ). A2) Kainate did not significantly influence the junctional conductance in the receiving cells (Mann-Whitney-U-Test). Receiving cells: median conductance of 0.23 nS (25<sup>th</sup>percentile = 0.128 nS, 75<sup>th</sup>percentile = 0.429 nS) for the control and 0.25 nS for the kainate peak response (25<sup>th</sup>percentile = 0.147 nS, 75<sup>th</sup>percentile = 0.407 nS/pF). B) Overview of junctional conductance for each receiving cell of a pair recording shows no significant difference between cell 1 and cell 2 neither at control nor after kainate application. This indicates a symmetrical junctional conductance that did not differ more than 12 % after normalization.

### **3.4 Electrophysiological characterization and dye-coupling experiments of microglia under normal physiological conditions as well as pathology-associated microglia and macrophages/monocytes**

Until recently, there were only studies in cultured microglia which addressed the question, mainly by dye-coupling experiments, whether microglia form GJs (Eugenin *et al.*, 2001; Martinez *et al.*, 2002; Dobrenis *et al.*, 2005; Garg *et al.*, 2005; Saez *et al.*, 2013). There was some evidence for coupling *in vitro*, but only a small percentage of the microglia showed coupling, and the networks were small. Last year, a study was published by Wasseff and Scherer, who addressed the question of microglial coupling in *in situ* models, namely in slices from healthy brain, after traumatic brain injury and in an A $\beta$  pathology model (Wasseff and Scherer, 2014). They could not confirm gap junctional dye transfer in these models. At the time of publication by Wasseff and Scherer (2014) dye-coupling experiments were already ongoing in our laboratory that addressed the question whether microglia cells use functional gap junctional communication to participate into the panglial network under normal physiological conditions. I chose to study microglial coupling *in situ* in another pathological model, namely in the glioma context and in the stab wound lesion, since in these pathological models, microglia cells accumulate around the lesion or tumor site and are in close contact to surrounding cells. The following passage will also present a detailed analysis of the electrophysiological properties of microglia and macrophages in the brain tumor and stab wound lesion model as well as in the ischemic stroke. This can provide additional information about the activation status of the immune cells in the different pathological conditions and which could be of interest for the development of new therapeutic approaches.

### 3.4.1 Microglial cells are not part of the panglial network under normal physiological conditions

To study microglial coupling in acute brain slices under normal physiological conditions either the *Cx3cr1<sup>GFP/wt</sup>* mouse (Jung *et al.*, 2000) or the MacGreen mouse (Sasmono *et al.*, 2003) was used. For that purpose the whole-cell patch-clamp technique was combined with dye-coupling experiments. The eGFP-expressing microglia cells were dialyzed with Sulforhodamine 101 (SR101) and biocytin. During dye-filling the cell was characterized by its membrane resting potential and current pattern which offers first implications about the physiological phenotype. Visual control of SR101 under the setup microscope assures cellular access of the dye (Figure 25 inset). After 20 min dialysis the slices were fixed with PFA for 1 h at 4°C and subsequently biocytin was labelled with streptavidin-Cy3. Immunohistological counterstaining was conducted for Iba1 for microglia validation and DAPI for possible coupling to surrounding cells. None of the dye-filled microglia cells ( $n = 20$ ) showed dye-coupling to any other cell under normal physiological conditions, confirming that resting microglia are not part of the panglial network. A representative image of a patched and dye-filled microglia cell in the neocortex is shown in Figure 25A.

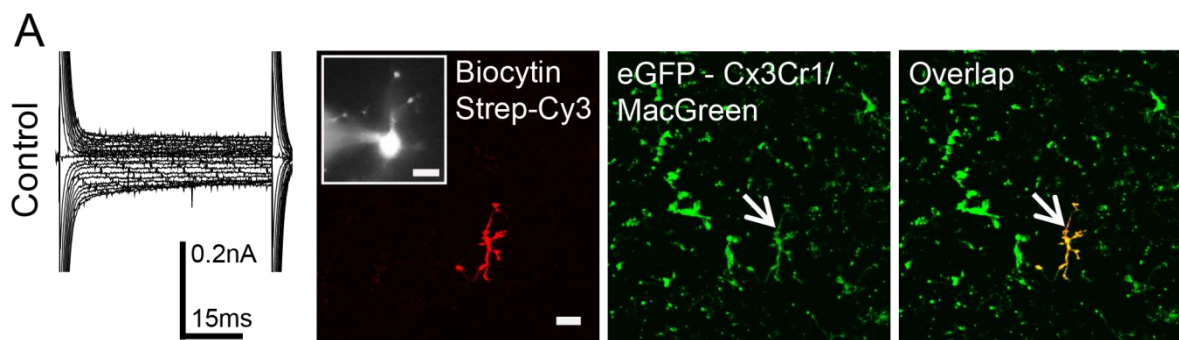


**Figure 25: Lack of gap junctional coupling in microglia under normal physiological conditions.**

Membrane current of a control microglia cell, recorded in response to de- and hyperpolarizing voltage steps from -160 to +50 mV for 50 ms at a holding potential of -70 mV. The second column shows the biocytin staining, the third the eGFP-fluorescence (*Cx3cr1<sup>GFP/wt</sup>* or MacGreen mouse), the overlap is given in the last column (Scale bar: 20  $\mu\text{m}$ ). The inset in the second column is a magnification of the recorded cell dialyzed with SR101 (Scale bar: 10  $\mu\text{m}$ ). Arrow indicates the injected cell.

### 3.4.2 Glioma-associated microglia and macrophages/monocytes express a different membrane current profile

To address the question about microglial coupling in brain pathology, I made use of the *Cx3cr1<sup>GFP/wt</sup> Ccr2<sup>RFP/wt</sup>* mouse line (Saederup *et al.*, 2012). This line allows discrimination between glioma-associated microglia and invading macrophages/monocytes; microglial cells are labeled in green and macrophages/monocytes in both red and green. For these experiments coronal slices were prepared from brains 14-16 days after the inoculation of GL261 glioma cells. Membrane currents of glioma-associated microglia (GAMs) and macrophages/monocytes (GAMPs) were recorded with the whole cell patch-clamp technique. The cells were clamped at -70 mV to a series of depolarizing and hyperpolarizing voltage steps (+50 mV to -160 mV in 10 mV increments for 50 ms). Microglia from unlesioned frontal cortex, striatum, and activated microglia in the stab wound on the contralateral hemisphere of glioma-mouse model served as controls and were recorded as described above. The control tissue lacked RFP-positive cells meaning there were no invading macrophages/monocytes from the periphery. At the stab wound, activated, intrinsic, green fluorescent microglia accumulated while only few RFP-positive macrophages/monocytes were detected. Control microglia in the unlesioned cortex/striatum showed small currents with de- and hyperpolarization and no apparent voltage and time dependence (Figure 26 B, 1<sup>st</sup> column) as already described for resting microglia in the brain stem by Boucsein *et al.* in 2000. GAMs are characterized by inactivating inward rectifying currents with hyperpolarization and small outward currents with depolarization. In contrast, GAMPs showed smaller inward currents with hyperpolarization and slightly larger delayed activating outward currents with depolarization. Finally, stab wound-associated microglia displayed large inward rectifying currents, and only small outward currents (Figure 26B, 4<sup>th</sup> column) as described previously (Seifert *et al.*, 2011). Averaged current voltage curves are given in Figure 26 C. For each group, the mean normalized IV-curves (Current Density [pA/pF]) are displayed in Figure 26 D. The significant increase of the inward current of stab wound-associated microglia is also visible in the average IV-curve in Figure 26 C, last column.

The specific outward conductance was calculated from currents activated at 0 and -20 mV, and the inward conductance from currents activated at -100 and -120 mV.

The conductance was normalized with the cell capacitance and the results are presented as box plots (Figure 27 A). GAMs and GAMPs showed a specific outward conductance with a median of 0.043 nS/pF (25<sup>th</sup>percentile = 0.028nS/pF, 75<sup>th</sup>percentile = 0.054nS/pF; n = 19) and 0.072 nS/pF, respectively (25<sup>th</sup>percentile = 0.053 nS/pF, 75<sup>th</sup>percentile = 0.143 nS/pF; n = 18) (Figure 27 A). Control microglia (MG) displayed a median specific outward conductance of 0.018 nS/pF (25<sup>th</sup>percentile = 0.016 nS/pF, 75<sup>th</sup>percentile = 0.023 nS/pF; n = 29) and stab wound-associated MG a median of 0.026 nS/pF (25<sup>th</sup>percentile = 0.021 nS/pF, 75<sup>th</sup>percentile = 0.03 nS/pF; n = 12) (Figure 27 A). Specific inward conductance of GAMs and GAMPs was significantly smaller (GAMs: median = -0.061 nS/pF, 25<sup>th</sup>percentile = -0.101 nS/pF, 75<sup>th</sup>percentile = -0.035 nS/pF; GAMPs: median = -0.053 nS/pF, 25<sup>th</sup>percentile = -0.106 nS/pF, 75<sup>th</sup>percentile = -0.038 nS/pF) compared to stab wound-associated microglia (median = -0.213 nS/pF, 25<sup>th</sup>percentile = -0.298 nS/pF, 75<sup>th</sup>percentile = -0.191 nS/pF), but was not significantly different from control MG (median = -0.05 nS/pF, 25<sup>th</sup>percentile = -0.064 nS/pF, 75<sup>th</sup>percentile = -0.04 nS/pF) (Figure 27 A).

Taken together, the specific inward conductance  $G$  [nS/pF] of GAMs and GAMPs was not significantly increased and was in a range similar to the control microglia, while GAMs and GAMPs showed a significant increase in the specific outward conductance compared to control microglia. Moreover, the specific outward conductance was significantly higher in GAMPs as compared to GAMs (Figure 27 A).

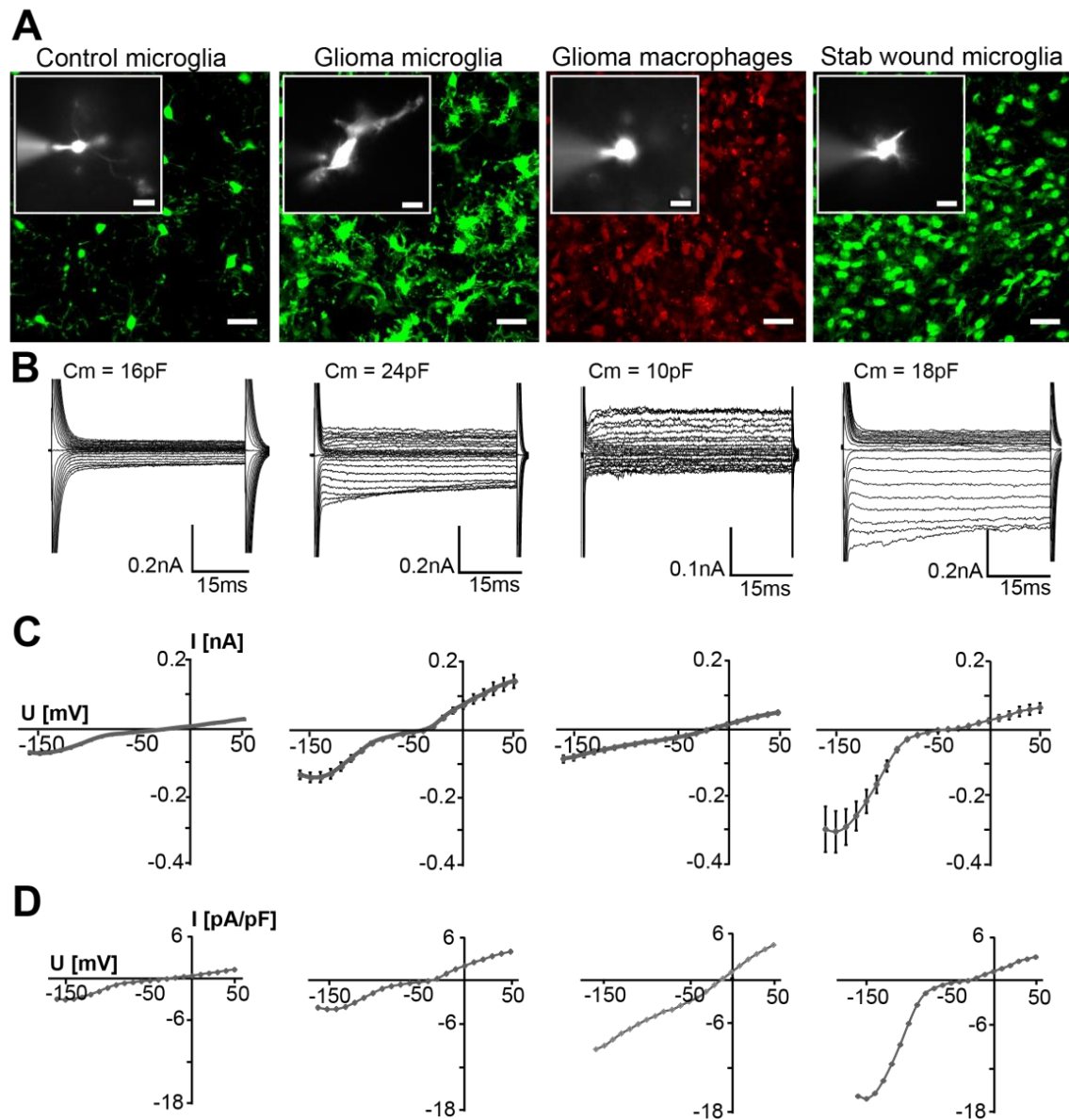


**Figure 26: Morphology and membrane currents of control microglia, GAMS, GAMPs and stab wound-associated microglia.**

(A) Fluorescent images of eGFP and RFP illustrate the typical ramified morphology of control microglia in unlesioned brain, the amoeboid morphology of GAMS, the round morphology of GAMPs and the morphology in stab wound-associated microglia (Scale bar: 20  $\mu\text{m}$ ). Insets depict the corresponding recorded cell dialyzed with SR101 (Scale bar: 10  $\mu\text{m}$ ). The matching membrane current profile, recorded in response to de- and hyperpolarizing voltage steps from  $-160$  to  $+50$  mV for 50 ms and at a holding potential of  $-70$  mV, from each cell are shown in **B**. **C** represents the average-IV-plots from all recordings obtained from control microglia, GAMS, GAMPs and stab wound-associated microglia. **D** displays the mean IV-plots normalized for cell capacitance (current density [pA/pF]) for each group.

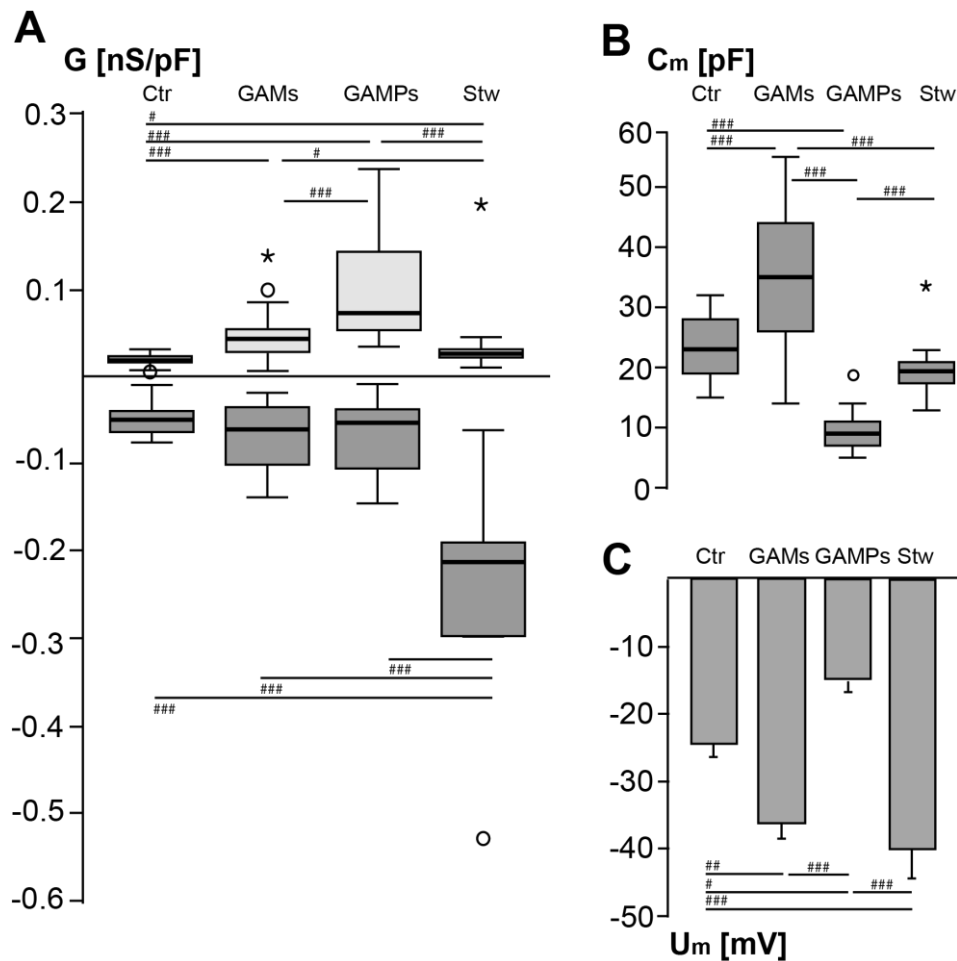


**Figure 27: Specific membrane conductance, membrane capacitance and membrane potential of control microglia, GAMs, GAMPs and stab wound-associated microglia.**

(A) Box plots of outward (light boxes) and inward (dark boxes) conductance normalized to membrane capacitance (G [nS/pF]). Outward conductance was determined between 0 and -20 mV, inward conductance between -100 and -120 mV and averaged for control microglia (Ctr, n = 29), glioma-associated microglia (GAMs, n = 19), glioma-associated macrophages/monocytes (GAMPs, n = 18) and stab wound-associated microglia (Stw, n = 12). Hash marks indicate significance by applying the Mann-Whitney-U-test (#p < 0.05, ##p < 0.005, ###p < 0.001). (B) Box plots of median membrane capacitance (C<sub>m</sub>[pF]). For detailed explanation of calculation please see methods part 2.5.2 (C) Mean membrane potential (U<sub>m</sub>[mV]) for the different cell types. Extreme values are given as asterisks while outliers are presented as circles. Values are given as mean ± SEM.

### 3.4.3 The membrane potential of GAMs is more negative and the membrane area is increased as compared to control microglia

Under normal physiological conditions in the brain microglia cells show a ramified morphological phenotype while GAMs and stab wound-associated microglia display an amoeboid morphology (Figure 26 A). GAMPs are also densely packed but are more roundish and lack almost any processes (Figure 26 A). The membrane area of a cell is correlated to its membrane capacitance (Figure 27 B). The membrane capacitance of GAMs ( $35.42 \pm 2.8$  pF; corresponds to  $3542 \mu\text{m}^2$  assuming a specific membrane capacitance of  $1 \mu\text{F}/\text{cm}^2$ ) was significantly higher as compared to control microglia ( $23.28 \pm 0.96$  pF;  $2328 \mu\text{m}^2$ ), GAMPs ( $9.33 \pm 0.8$  pF;  $933 \mu\text{m}^2$ ) and stab wound-associated microglia ( $19.5 \pm 1.5$  pF;  $1950 \mu\text{m}^2$ ). The membrane capacitance of GAMPs was significantly smaller than that of control microglia (Figure 27 B). This indicates that GAMs have a larger membrane area while GAMPs have a smaller membrane area as compared to control microglia. The membrane potential of GAMs ( $-36.05 \pm 2.27$  mV) and stab wound-associated microglia ( $-39.92 \pm 4.31$  mV) was significantly more negative as compared to control ( $-24.45 \pm 1.88$  mV). GAMPs had a significantly more positive membrane potential ( $-14.61 \pm 1.72$  mV) as compared to GAMs and stab wound-associated microglia (Figure 27 C).

### 3.4.4 Glioma-associated microglia/ macrophages are not coupled by gap junctions

Next, I investigated if gap junctional coupling occurs in microglia/macrophages in the glioma context. To distinguish between GAMs and GAMPs I used the physiological parameter described above, namely the difference in the membrane capacitance. Cells were dialyzed with Sulforhodamine 101 (SR101) and biocytin during whole cell patch-clamp recordings in *Cx3cr1<sup>GFP/wt</sup>* or MacGreen reporter mice (Jung *et al.*, 2000; Sasmono *et al.*, 2003). After recording and dialysis, the slices were fixed with 4% PFA for 1h at 4°C and subsequently labelled with streptavidin-Cy3. Additionally slices were immunohistologically counterstained with the specific microglia marker Iba1 for validation of the cell type and with DAPI for possible coupling to surrounding cells. None of the dye-filled microglia cells in the control tissue (n = 20) showed dye-coupling to any other cell confirming that resting microglia are uncoupled. A representative image of a patched/dye-filled microglial

cell in the cortex is shown in Figure 25. Both within the glioma and in the stab wound area the density of glioma-associated microglia/macrophages is markedly increased and they even make direct cell–cell contacts. GAMs ( $n = 12$ ,  $29.5 \pm 7.25$  pF) and GAMPs ( $n = 5$ ,  $12 \pm 1.5$  pF) were dye-filled and analyzed for dye-coupling (Figure 28 B, C). I never observed any dye-coupling among microglia/macrophages in the glioma microenvironment, nor to any other cell type. Finally, microglial cells in the stab wound area were examined for gap junctional coupling. I never observed any dye-coupling among stab wound microglia ( $n = 6$ , Figure 28 D). As a positive control for this set of experiments, I patched surrounding cells close to the activated microglia, assuming it was an astrocyte or glioma cell and showed that they were biocytin coupled to adjacent cells.

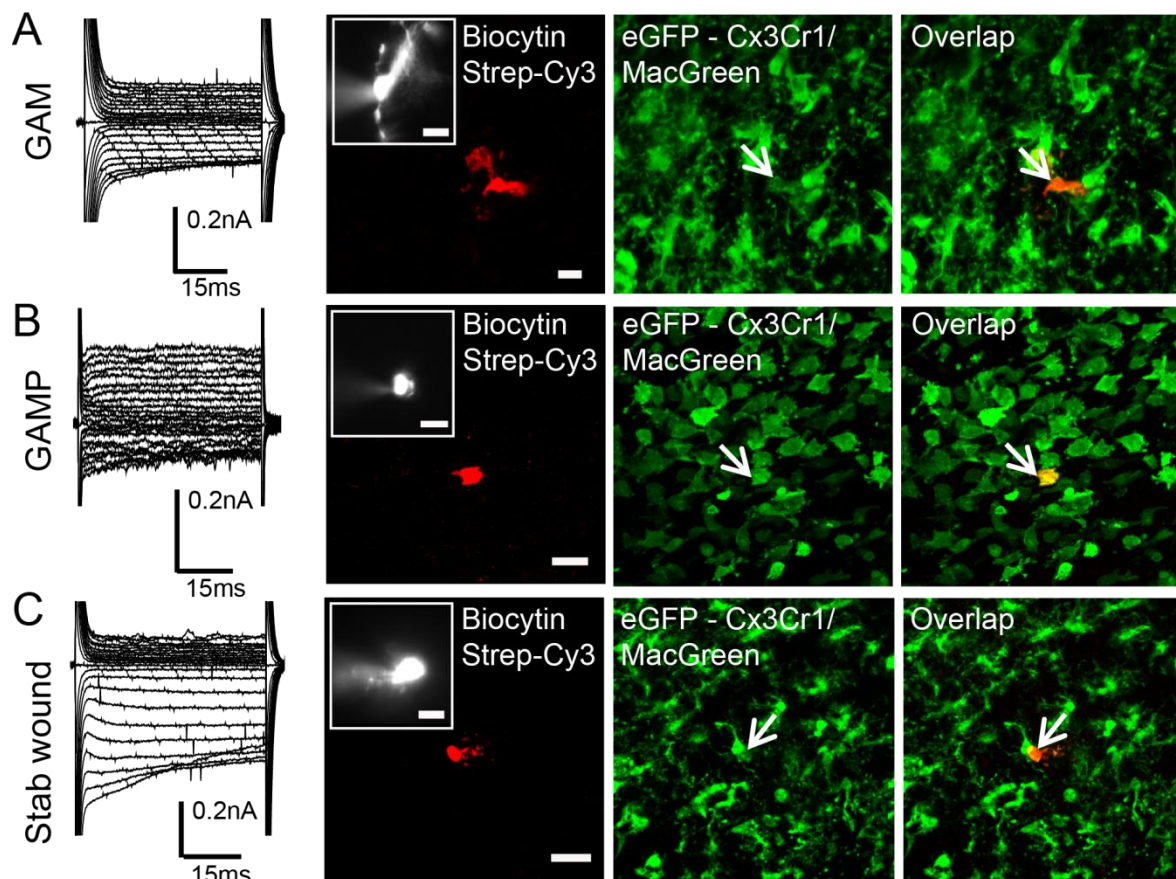


**Figure 28: Lack of coupling of GAMs, GAMPs and stab wound-associated microglia.**

Membrane currents from injected cells, recorded in response to de- and hyperpolarizing voltage steps from  $-160$  to  $+50$  mV for 50 ms at a holding potential of  $-70$  mV. GAM (A), GAMP (B) and a stab wound-associated microglia (C) are shown on the left. The second column shows the biocytin labeled with streptavidin-Cy3, the third the eGFP-fluorescence of either a *Cx3cr1*<sup>GFP/wt</sup> or MacGreen mouse. The overlap is given in the fourth column (Scale bar: 20 μm). The insert in the second

column is a magnification of the recorded cell dialyzed with SR101 (Scale bar: 10  $\mu\text{m}$ ). Arrows indicate the injected cell.

#### **3.4.5 FACS isolated GAMs, GAMPs and control microglia do not express Cx43**

Data from cultured microglia indicate the expression of *Cx43* (Eugenin *et al.*, 2001; Garg *et al.*, 2005). Therefore I compared the *Cx43* expression in GAMs and GAMPs which were isolated from GL261-implanted C57BL/6 mice with control microglia cells isolated from naïve mice. The primers for *Cx43* were designed as described in the methods part 2.11 and validated with sqRT-PCR experiments on total RNA from whole forebrain. sqRT-PCR experiments showed a strong expression of *Cx43* RNA in total brain. Subsequent qRT-PCRs on FACS-isolated GAMs, GAMPs and control microglia, did not reveal any *Cx43* gene expression in microglia/macrophages from the tumor environment nor in control microglia, whereas the whole brain sample which comprises a large population of *Cx43* expressing astrocytes showed a clear signal for *Cx43* (data not shown).

#### **3.4.6 Stroke associated microglia/ macrophages show distinct electrophysiological properties**

In order to characterize electrophysiological properties of activated microglia and invaded macrophages in the stroke tissue, MCAo was induced as described in material and methods. To be able to distinguish activated microglia cells we used a MacGreen transgenic mice that express eGFP-fluorescence under control of the murine CSF-1 receptor promoter (Sasmono *et al.*, 2003). Macrophages that express a tandem dimer red fluorescent protein (tdRFP) were transplanted before induction of ischemia and were thus distinguishable by their red fluorescence (Luche *et al.*, 2007; Gertz *et al.*, 2012). Acute brain slices were prepared from MacGreen transgenic mice 7-9 d after an ischemic insult, as described in the methods paragraph in detail. The whole cell patch-clamp recordings were performed on microglia and macrophages in the stroke area which spanned the striatum. The contralateral side served as control (n = 17). In general, patch-clamp recordings turned out to be difficult in activated microglia and especially macrophages in the stroke area because of increased mobility of the cells, but also due to large necrotic areas and the increased number of dead cells. In contrast, recordings of control microglia in the contralateral hemisphere were almost 100 % suc-

cessful. From a holding potential of -70 mV, currents were recorded from depolarizing and hyperpolarizing voltage steps between +50 mV and -150 mV (for intrinsic microglia -170 mV) in 10 mV increments for 50 ms. Patched cells, that showed a stable seal were dialyzed with Alexa 594 and imaged via a digital camera (Figure 29 A). Control microglia in the contralateral hemisphere showed small currents with no voltage and time dependence (Figure 29 C). Stroke associated microglia (eGFP-positive) cells (n = 33) showed large inactivating inward rectifying currents upon hyperpolarization and small outward currents upon depolarization as described for stab wound-associated microglia in (Seifert *et al.*, 2011). While stroke associated invading macrophages (RFP-positive, n = 13) showed smaller inactivating inward rectifying currents upon hyperpolarization and larger delayed outward currents upon depolarization as already seen in the glioma mouse model in paragraph 3.4.2. Figure 29 C shows the averaged current voltage curves for each group (control microglia, stroke associated microglia and stroke associated macrophages) for a holding potential at -70 mV.

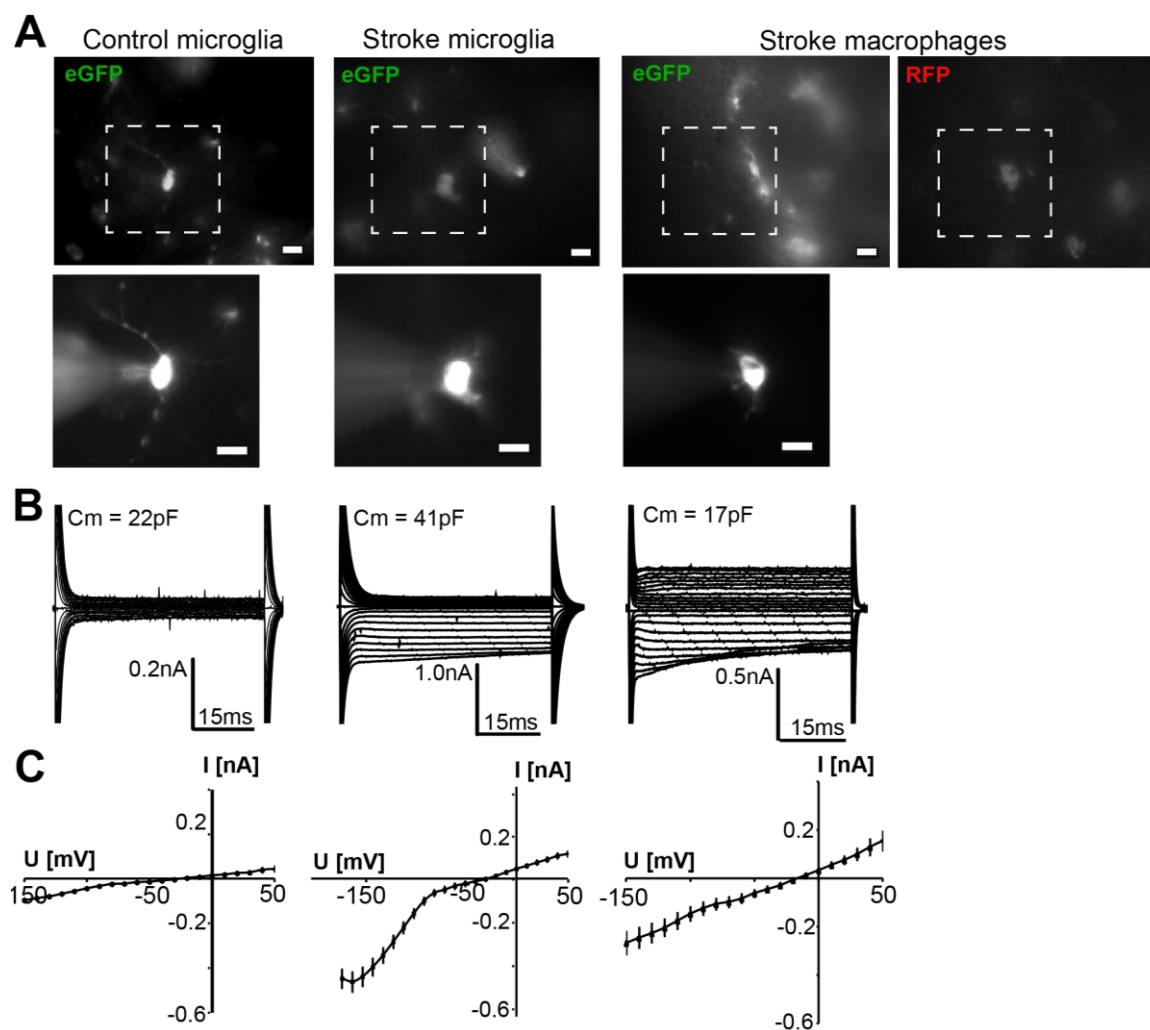


**Figure 29: Comparison of intrinsic microglia and invading macrophages 7 to 9-days after middle cerebral artery occlusion in MacGreen mice.**

A) Fluorescent images of eGFP for microglia or RFP for macrophages display the typical ramified morphology of control microglia on the contra lateral hemisphere, the amoeboid morphology of intrinsic stroke associated microglia and invading stroke associated macrophages; Scale bar: 10  $\mu$ m. The images below show a recorded cell dialyzed with Alexa 594; Scale bar: 10  $\mu$ m. B) Membrane currents from cells shown in (A), recorded in response to de- and hyperpolarizing voltage steps from -150 mV to +50 mV for 50 ms at a holding potential of -70 mV. Macrophages revealed an additional delayed rectifying outward  $K^+$  current compared to intrinsic activated MG. C) I-V plots of average currents from all recordings obtained from control microglia ( $n = 17$ ), intrinsic stroke associated microglia ( $n = 33$ ) and invading stroke associated macrophages ( $n = 13$ ).

The comparison of input membrane resistances ( $R_m$  [ $G\Omega$ ]) showed a significant difference between intrinsic microglia or macrophages vs. control microglia in the contra lateral hemisphere of the stroke animals (Figure 30 A), and the difference between activated microglia and macrophages was small, but significant. Control microglia cells had a median membrane resistance of 2.72  $G\Omega$  (25<sup>th</sup>percentile = 1.25  $G\Omega$ , 75<sup>th</sup>percentile = 3.92  $G\Omega$ ;  $n = 17$ ), the membrane resistance of intrinsic

microglia was only 1.3 G $\Omega$  (25<sup>th</sup>percentile = 0.83 G $\Omega$ , 75<sup>th</sup>percentile = 1.52 G $\Omega$ ; n = 33), and that of invading macrophages 0.7 G $\Omega$  (25<sup>th</sup>percentile = 0.35 G $\Omega$ , 75<sup>th</sup>percentile = 1.22 G $\Omega$ ; n = 13).

The membrane area of a cell is correlated to its membrane capacitance (C<sub>m</sub> [pF]). C<sub>m</sub> was significantly different between intrinsic microglia cells and control cells and intrinsic microglia vs. invading macrophages (Figure 30 B). The control microglia showed a median C<sub>m</sub> of 24 pF (25<sup>th</sup>percentile = 19 pF, 75<sup>th</sup>percentile = 30 pF; n = 17) while activated intrinsic microglia had a significantly higher C<sub>m</sub> of 40 pF (25<sup>th</sup>percentile = 31.5 pF, 75<sup>th</sup>percentile = 48 pF; n = 33). In contrast, invading macrophages showed a significantly lower C<sub>m</sub> of 19 pF (25<sup>th</sup>percentile = 16 pF, 75<sup>th</sup>percentile = 22 pF; n = 13) compared to activated microglia. These results were also comparable to the findings in glioma-associated macrophages where it was shown that these invading cells have a significantly smaller membrane capacitance suggestive for a smaller membrane surface.

Furthermore, the membrane potential differed significantly between intrinsic microglia (median = -30 mV; 25<sup>th</sup>percentile = -49 mV, 75<sup>th</sup>percentile = -15 mV ; n = 33) and control microglia on the contra lateral side (median = -10 mV; 25<sup>th</sup>percentile = -19.5 mV, 75<sup>th</sup>percentile = -5 mV ; n = 17) and invading macrophages (median = -10 mV; 25<sup>th</sup>percentile = -20 mV, 75<sup>th</sup>percentile = -7 mV ; n = 13), respectively. There was no difference between control microglia and macrophages.

Another important characteristic of intrinsic microglia and invading macrophages could be shown by evaluating the specific inward and outward conductance G [nS/pF]. The specific outward conductance was determined from currents activated at 0 and -20 mV, and the inward conductance from currents activated at -100 and -120 mV. The conductances were normalized with the cell capacitance and the results are presented as box plots (Figure 30 D). Intrinsic microglia and invading macrophages showed a significant increase in the specific outward conductance with a median of 0.024 nS/pF (25<sup>th</sup>percentile = 0.017 nS/pF, 75<sup>th</sup>percentile = 0.033 nS/pF; n = 33) and 0.086 nS/pF, respectively (25<sup>th</sup>percentile = 0.044 nS/pF, 75<sup>th</sup>percentile = 0.119 nS/pF; n = 13) as compared to control microglia (median = 0.017 nS/pF, 25<sup>th</sup>percentile = 0.015 nS/pF, 75<sup>th</sup>percentile = 0.019 nS/pF; n = 17).

Additionally, the specific outward conductance was significantly higher in invading macrophages as compared to intrinsic microglia also already seen in glioma-associated macrophages.

Specific inward conductance of intrinsic microglia and invading macrophages was significantly higher (intrinsic microglia: median = -0.14 nS/pF, 25<sup>th</sup> percentile = -0.21 nS/pF, 75<sup>th</sup> percentile = -0.096 nS/pF; invading macrophages: median = -0.106 nS/pF, 25<sup>th</sup> percentile = -0.16 nS/pF, 75<sup>th</sup> percentile = -0.092 nS/pF) compared to control microglia (median = -0.05 nS/pF, 25<sup>th</sup> percentile = -0.06 nS/pF, 75<sup>th</sup> percentile = -0.032 nS/pF). This was in contrast to the glioma environment where the specific inward conductance of microglia and macrophages was similar to control microglia.

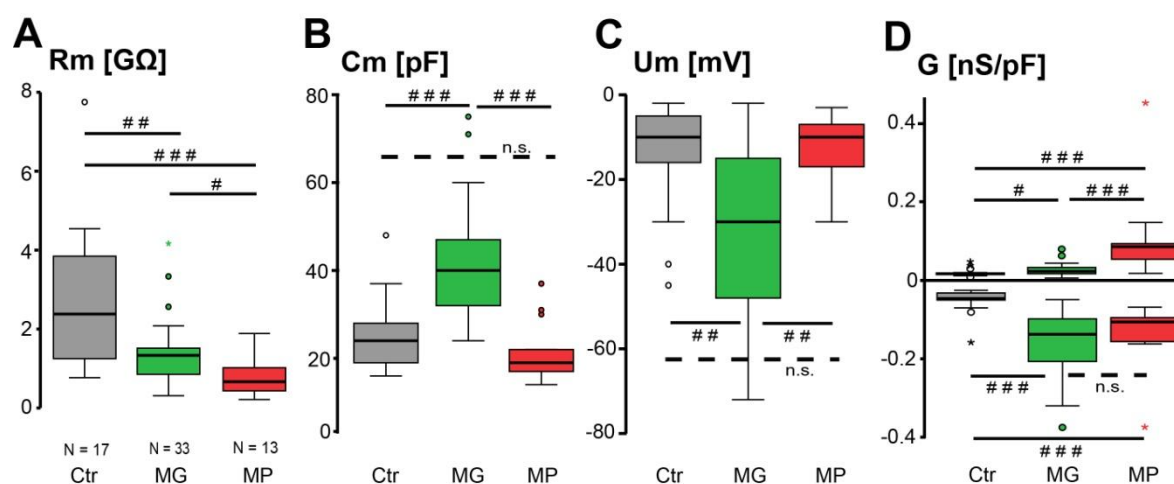


**Figure 30: Membrane resistance [Rm], membrane capacitance [Cm], membrane potential [Um] and specific membrane conductance [G] of stroke associated microglia and macrophages.**

A) Displays the median input membrane resistance, calculated by  $R_m = U/I_{\text{offset}}$ .  $R_m$  revealed a significant difference between intrinsic microglia (MG,  $n = 33$ ) and invading macrophages (MP,  $n = 13$ ) and control microglia cells (Ctr,  $n=17$ ) patched in contra lateral hemisphere of the stroke mice. B) The membrane capacitance ( $C_m$ ) was calculated based on the equation  $C_m = \int I \cdot dt / \Delta U$ , measuring with TIDA software the transient currents evoked in response to a depolarizing +10 mV step from a holding potential of -70 mV (50 ms) and showed a significant difference between intrinsic microglia cells and control cells and intrinsic microglia vs. invading macrophages. C) Median membrane potential ( $U_m$ [mV]) for the different cell types was calculated by using the TIDA software and showed similar differences as already seen in comparison of the  $C_m$ . D) Box plots of outward and inward conductance normalized to membrane capacitance ( $G$  [nS/pF]). Outward conductance was determined between 0 and -20 mV, inward conductance between -100 and -120 mV and averaged for control microglia ( $n = 17$ ), intrinsic stroke associated microglia ( $n = 19$ ) and invading macrophages ( $n = 13$ ). Hash marks indicate significance by applying the Mann-Whitney-U-test (# $p < 0.05$ , ## $p < 0.005$ , ### $p < 0.001$ ).

## 4 Discussion

### 4.1 Astrocytes form panglial networks in the CNS and express a unique antigen profile

The extent of gap junctional coupling between astrocytes differs notably with regard to brain region, size of networks, cellular partners and postnatal age (Wallraff *et al.*, 2004; Haas *et al.*, 2006; Houades *et al.*, 2008; Wang *et al.*, 2008; Maglione *et al.*, 2010; Griemsmann *et al.*, 2014). For example, Haas *et al.* 2006 demonstrated that astrocytes in the grey matter are more extensively coupled than astrocytes in the corpus callosum, but did not study the cellular partners and composition of networks. In 2011, Wasseff and Scherer (Wasseff and Scherer, 2011) found that oligodendrocytes in the neocortex are exclusively coupled to astrocytes and that Cx47, but not Cx32, is required for this heterotypic gap junctional coupling. As a part of a joint project and publication with the research group of Prof. Steinhäuser at the Institute for cellular neurosciences (IZN) in Bonn, I investigated panglial coupling and was able to show that astrocytes in the neocortex are coupled to oligodendrocytes but not to NG2 cells. This demonstrates the heterogeneity of gap junctional networks, because Maglione *et al.* (2010) showed that, in the corpus callosum, NG2 cells are part of the panglial network when injecting an oligodendrocyte with the gap junctional tracer biocytin. Furthermore, I found an intermediate astrocyte cell-type that expressed both Cx43 and Olig2 in the neocortex that was absent in the corpus callosum of *Cx43ki/eCFP* mouse (Griemsmann *et al.*, 2014). On the other hand, injecting an astrocyte in the *hGFAP/eGFP* mouse and quantifying the overlap of GFAP/eGFP+/Olig2+ cells revealed a population of double positive cells in the neocortex as well as in the corpus callosum. This is in accordance with the results of (Cai *et al.*, 2007) demonstrating that during development the oligodendrocytic marker Olig2 is expressed in astrocytes at embryonic stages and downregulated with adulthood. As another interesting aspect, they show that conditional ablation of Olig2 in neocortex and spinal cord leads to a reduced formation of astrocytes in the white matter and that Olig2 function is necessary for astrocyte differentiation in the cerebral white matter. In contrast, astrocytes in the grey matter are still formed with continuous GFAP upregulation. Griemsmann *et al.* showed that knockout of one allele in the *Cx43* mice led to a significant decrease of coupled cells in the hippocampus, but they did not detect

any changes in the network size in the somatosensory cortex or thalamus. My experiments do not provide the information whether Cx30 or Cx43 dominates the gap junctional networks and, therefore, experiments in *Cx43ki/eCFP* (Degen *et al.*, 2012) or *Cx30kiLacZ* animals (in this mouse strain the coding region of the *Gjb6/Cx30* gene is replaced by the reporter gene *LacZ* (Teubner *et al.*, 2003)) have to be performed. Moreover, transcript analysis as shown by Griemsmann *et al.* 2014 for the thalamus and hippocampus is required.

GFAP-eGFP<sup>+</sup>/Olig2<sup>+</sup> cells were found in the corpus callosum of *hGFAP/eGFP* mice, whereas I did not observe Cx43ECFP<sup>+</sup>/Olig2<sup>+</sup> cells in the corpus callosum of *Cx43ki/eCFP* mice. This might be linked to the fact that the quantification of double positive cells in the *hGFAP/eGFP* mouse was done between postnatal day 13-15 while experiments in the *Cx43ki/eCFP* mouse were conducted in older animals (p30). Since Griemsmann *et al.* 2014 showed by western blot analysis that Cx30 and Cx43 expression in the hippocampus was increased 2-fold between p14 and p53 and in the thalamus even 3-fold for Cx30, the upregulation during postnatal development is an important factor to consider. Thus, to gain a clearer picture, one should repeat the gap junctional analysis and cell partner quantification also in adult *hGFAP/eGFP* mice in the corpus callosum. However, due to the advanced myelination in the white matter tract, properly patch clamping the cells in this brain region would be a great challenge.

Taken together, my data shows that astrocytes and oligodendrocytes but not NG2 cells, form panglial networks in the neocortex as well as in the corpus callosum of *hGFAP/eGFP* mice. However, it cannot be ruled out that NG2 cells are part of the network since a co-staining for NG2 was not conducted here, and, as mentioned above, an earlier study (Maglione *et al.* 2010) showed that NG2 cells participate in oligodendrocytic networks in the corpus callosum of *NG2-EYFP* transgenic animals. Hence, these panglial networks may play important roles in information processing, homeostasis of the brain and metabolic support to neurons (Wallraff *et al.*, 2004; Fünfschilling *et al.*, 2012; Pannasch and Rouach, 2013), which will be discussed in the next chapter.

## 4.2 Does the panglial network provide energy for axons?

Several studies have reported the importance of astrocytes as the energy storage elements in the brain (Brown *et al.*, 2005; Brown and Ransom, 2007) and the supplier of metabolites to neurons in the hippocampus (Roach *et al.* 2008). Recent findings by Lee *et al.* 2015 demonstrated that oligodendrocytes in the white matter release lactate, a known property of grey matter astrocytes. Lactate, beneath glucose, has been suggested as one principal metabolite to support axons and neurons. While lactate is shuttled via monocarboxylate transporters (MCT1, expressed in oligodendrocytes) and supports mitochondrial energy metabolism, oligodendrocytes and astrocytes are panglial coupled and serve as spatial potassium buffers, ensure proper ionic homeostasis and are likely the primary source for glucose for axonal energy metabolism (Menichella *et al.*, 2006; Rash, 2010; Saab *et al.*, 2013).

In this work, I showed for the first time that the glucose derivative 2NBDG, when injected either into an astrocyte or an oligodendrocyte, spreads to surrounding cells in the corpus callosum, thus using the gap junctional pathway and the panglial network. Moreover, when injecting an oligodendrocyte with 2NBDG it spread into the processes oriented along the parallel fibres, potentially providing a direct glucose support. Thus not only astrocytes which contact blood vessels with their endfeet supply axons with metabolites but also oligodendrocytes which are in close contact to neuronal elements, may serve as a metabolite provider.

The immediate imaging of 2NBDG showed spreading from an injected oligodendrocyte to adjacent astrocytes and vice versa. This also implies that metabolic support with glucose via the gap junctional pathway can be bidirectional between oligodendrocytes and astrocytes in the corpus callosum. Such bidirectional gap junctional communication has been shown by Maglione *et al.* in 2010 with the tracer biocytin and therefore supports the possible panglial-metabolic coupling in the corpus callosum. To be certain that this energy support is GJ mediated I would have to repeat the experiments by using a GJ blocker, e.g. carbenoxolone (CBX). CBX was used in the study by Rouach *et al.* in 2008. They showed that 2NBDG interastrocytic trafficking is mediated by GJs because it is abolished by CBX. Furthermore, they conducted paired recordings of field excitatory postsynaptic potentials (fEPSPs) in neurons evoked by Schaffer collaterals stimulations. Simultaneous an astrocyte was dialysed with a higher concentration

of glucose or lactate and Rouach *et al.* could show that during exogenous glucose deprivation (EGD), astroglial metabolic networks can inhibit depression of fEPSPs. When this experiment was performed in Cx43/Cx30 double-knockout mice (the main connexins expressed by astrocytes), the depression of fEPSPs due to EGD was maintained.

My data do not provide information whether glial metabolic coupling in the corpus callosum has a beneficial effect and might be able to compensate the lack of glucose during ischemia and supply faster energy metabolites for axonal function.

Consequently my master student Niklas Meyer investigated the ability of coupled oligodendrocytes in the corpus callosum of adult *Plp-GFP* mice (Fuss *et al.* 2005) to support and maintain compound action potential (CAP) propagation via axons through glucose supply via GJs. He used the method of exogenous glucose deprivation (EGD) which has been employed together with CAP experiments before in the optic nerve (Wender *et al.*, 2000) or in the hippocampus as mentioned above (Rouach *et al.* 2008). Prior to EGD, an oligodendrocyte was patched and dialyzed via patch- pipette (for 20 min) with standard intracellular solution containing twice the usual concentration of glucose (20 mM). After a 90 min stimulation protocol with a 55 min EGD starting after 5 min, he could show that the CAPs were partially maintained and a higher recovery of CAPs after reapplication of regular ACSF was achieved (Figure 31, kindly provided by Niklas Meyer).

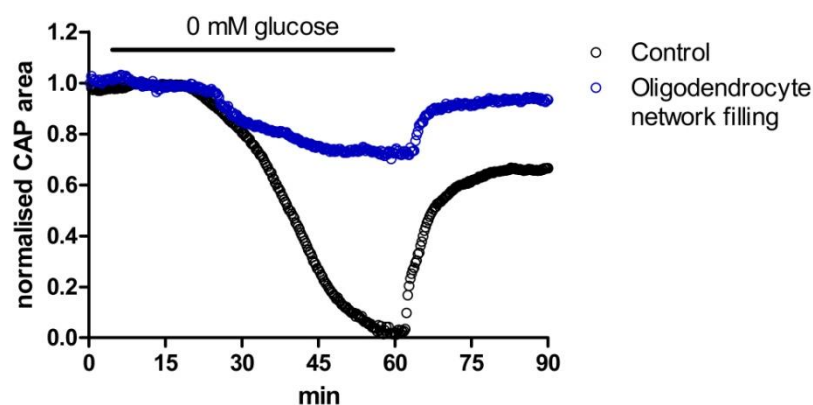


**Figure 31: Averaged EGD results under control conditions and previous oligodendrocyte network filling.**

Glucose- free ACSF was applied after 5 min. After 60 min reapplication of regular ACSF. Measurements during control conditions are shown as black hollow circles and blue circles display prior oligodendrocyte filling. CAP decline was significantly smaller in prior oligodendrocyte filling as compared to control condition.

These findings are in line with studies of Rouach *et al.* 2008 showing that glucose-filled astrocyte networks sustain fEPSPs during EGD experiments in the mouse hippocampus. Although our findings are still rather preliminary, they indicate the importance of glial gap junctional networks for energy supply of the neuronal compartments. Further experiments have to be conducted to verify my previous findings that the panglial network serves as an energy route for axons, and to investigate which connexins are crucial. For example, it should be tested in Cx30, Cx43, Cx47 and Cx32 single knockout mice as well as Cx30/Cx47 and Cx32/Cx47 double knockout mice, whether abolished astrocyte/oligodendrocyte or oligodendrocyte/oligodendrocyte coupling has an effect on the glucose derivative 2NBDG-spread as well as on CAPs and their recovery phase in the corpus callosum upon EGD.

Another interesting observation that should be followed up on is that 2NBDG and the GJ tracer biocytin do not necessarily spread to the same cells. Does this hint to GJ selectivity, namely that different connexins are responsible for the transfer of 2NBDG and of biocytin?

2NBDG can be easily imaged in the living slice, but unfortunately its spread into adjacent cells is no longer visible after fixation and subsequent immunostaining, but only in the patched and dialyzed cell. Using a microscope with a higher resolution and programmable focal plane as used for confocal microscopes would provide a major advantage for my metabolic coupling study, because it would allow an exact analysis of the number of 2NBDG coupled cells in the living slice.

### **4.3 Oligodendrocytes are electrically coupled in the corpus callosum and display voltage independent gap junctional conductance which could not be inhibited by kainate**

Previous electrophysiological studies have focused on mammalian cells transfected with altered combination of connexins and have identified that Cx47 and Cx32 can mediate electrical coupling (Elfgang *et al.*, 1995; Teubner *et al.*, 2001).

Findings by Kettenmann and Ransom (Kettenmann and Ransom, 1988) suggest that oligodendrocytes provide weak electrical coupling with an average coupling ratio of  $0.11 \pm 0.1$  and non-rectifying currents. An earlier study in murine corpus callosum slices characterized the currents of oligodendrocytes with the patch-clamp technique and showed whole-cell neurotransmitter-activated currents upon glutamate and kainate bath application (Berger *et al.* 1992).

In this study I showed for the first time in acute mouse brain slices that oligodendrocytes in the white matter corpus callosum are electrically coupled and display a linear, voltage independent junctional conductance, which was not influenced by the GJ modulator kainate.

The lower coupling ratio in my experiments (mean of  $0.067 \pm 0.014$ ) compared to the findings of Kettenmann and Ransom in 1988 could be due to the fact that oligodendrocytes in the corpus callosum are coupled to adjacent cells and that the junctional current generated in the stimulated cell is passed through other additional GJs in the syncytium, or that one or more cells are interspersed between the two recorded cells. A paper by Müller *et al.* (1996) studied the electrical coupling among Bergmann glial cells in acute brain slices of mouse cerebellum and demonstrated a similar electrical coupling ratio of  $0.032 \pm 0.022$  as well as a linear and voltage independent junctional conductance. Linear and voltage independent junctional conductances were also shown by Meme *et al.* (2009) for hippocampal astrocytes in rat brain slices. In contrast to other studies, I was not able to demonstrate that kainate/AMPA receptor activation leads to a block of junctional conductance in oligodendrocytes. This could be due to the weaker electrical coupling among oligodendrocytes in general or to a lower  $\text{Ca}^{2+}$  permeability of oligodendrocyte kainate/AMPA receptor in the corpus callosum;  $\text{Ca}^{2+}$  has been shown to be one of the main regulatory factors of gap junctional permeability in the Bergmann glial cells (Müller *et al.*, 1992). Furthermore, astrocytes are also abundantly present in this white matter tract and presumably take up the bulk of applied neuro-

transmitters. These results suggest that the (weak) electrical coupling among oligodendrocytes and maybe also to neighbouring astrocytes (it is known that oligodendrocytes are also dye-coupled to astrocytes in the mouse corpus callosum (Maglione *et al.* 2010)), represents another communication pathway mediating the spread of small molecules, such as ions and metabolites. Hence, electrical coupling could be an alternative pathway and could play an important role under normal physiological conditions as well as in pathological conditions when dye-coupling is aberrant.

Since the electrical coupling among oligodendrocytes in the mouse corpus callosum was low compared to oligodendrocytes *in vitro* or to pairs of astrocytes *in situ*, further studies should be conducted to shed more light on this complex communication pathway. This can be done, for example, by application of the potassium channel blockers  $Ba^{2+}$  or  $Cs^+$ , which increase the coupling ratio in astrocytes and oligodendrocyte pairs by increasing the effective length constant of the membrane without any direct effect on junctional resistance (Kettenmann and Ransom, 1988). Kettenmann and Ransom showed oligodendrocyte pairs that were not or only weakly electrically coupled, increased coupling upon  $BaCl_2$  or  $CsCl$  bath application. Possibly, in my experiments this (depolarization and increase of the input resistance) may help to better study the influence of the gap junctional modulator kainate. In addition, gap junctional blockers like carbenoxolone or halothane could be applied to provide evidence of the involvement of GJs and underline the importance of junctional conductance mediated by GJs.

Another interesting aspect of gap junctional communication are the panglial networks that are formed among oligodendrocytes and astrocytes. As these networks are also formed in the corpus callosum via heterotypic GJs it is most likely that they show an asymmetrical junctional conductance. Studies on hippocampal astrocytes showed that activation of endothelin receptors (Blomstrand *et al.* 2004) decreases junctional conductance. Endothelin might exert a similar effect on the oligodendrocyte - astrocyte junctional conductance. Finally, the coupling ratio and its modulation could be investigated in pathologies such as stroke or leukodystrophies. For example, Wang *et al.*, 2008, showed that dye-coupling among astrocytes was decreased under ischemic conditions. Another study used an *in vitro* Pelizaeus-Merzbacher-like disease model and showed that four out of six mutants were not electrically coupled via the Cx47/Cx47 and Cx47/Cx43 GJ channels,

suggesting that destruction of the glial network might contribute to the outcome of the disease (Kim et al., 2013). In conclusion, my findings provide the first characterization of electrical coupling in an important white matter tract of the brain - the corpus callosum. However, additional experiments need to be performed to fully understand the electrical coupling among oligodendrocytes and astrocytes and its implications for white matter diseases.

#### **4.4 Glioma-associated microglia and macrophages/monocytes display distinct electrophysiological properties and do not communicate via gap junctions**

Microglial cells and macrophages/monocytes *in vitro* express a distinct pattern of K<sup>+</sup>-channels (Kettenmann *et al.*, 1990; Kettenmann *et al.*, 2011) that can be functionally linked to their activation state. Inward rectifiers are present in cultured cells without additional stimulation. They play a role in the maintenance of the negative resting membrane potential and control of proliferation (Kettenmann *et al.*, 1990; Kettenmann *et al.*, 2011). Outward potassium conductances are expressed in cultured microglia after inflammatory stimulation with lipopolysaccharide (LPS) or interferon- $\gamma$  (IFN- $\gamma$ ) and are functionally linked to the induction of certain activation parameters, like secretion of inflammatory cytokines, reactive oxygen species or proliferation (Newell and Schlichter, 2005; Pannasch *et al.*, 2006). *In situ* patch-clamp recordings revealed three types of current profiles expressed by microglia that correlated to their state of activation.

Microglia in the healthy brain show small currents without time or voltage dependence (Boucsein *et al.*, 2000). In an early stage of activation, e.g. 12 h after facial nerve axotomy in the facial nucleus, they express inward rectifying currents and no significant outward conductance and thus can be compared to cultured microglial cells that did not receive inflammatory stimuli. 24 h after axotomy, microglia *in situ* express additional outward rectifying currents upon depolarization, comparable to the pattern found in LPS- or IFN- $\gamma$ -activated microglia *in vitro*. Prominent inward and outward currents were also found in microglia in stroke tissue 48 h after middle artery occlusion (MCAo) (Lyons *et al.*, 2000) or 24 h after a stab wound (Seifert *et al.*, 2011).

My results show that glioma-associated microglia express a current pattern that resembles the early stage of activation as seen 12 h after lesion in the facial nu-

cleus, or the unstimulated microglia *in vitro*. Thus, the characteristic current pattern implies that microglia in the tumor microenvironment remain in an “intermediate down-regulated” activation state suggestive of immune-suppression by the glioma cells. A microarray gene expression analysis of the activation state of glioma-associated microglia and macrophages, performed in our lab, revealed similar results. This study showed that glioma-associated microglia can not be described with one single activation state, they rather display a mixture of known phenotypes which points to an “intermediate” state as well (Szulzewsky *et al.*, 2015)

Using *Cx3cr1<sup>GFP/wt</sup>/Ccr2<sup>RFP/wt</sup>* mice, I could distinguish between intrinsic microglia and invading macrophages/monocytes. The macrophages/monocytes had a current profile which was clearly distinct from microglia. They expressed a higher density of the outward rectifier currents and a significantly lower membrane capacitance reflecting a smaller cell membrane area.

There is previous evidence for microglial coupling from *in vitro* studies. Dobrenis *et al.* (2005) showed a gradual transfer of lucifer yellow and thus functional coupling of microglia to neurons in co-cultures. However, the percentage of coupled cells was low (<5%) and the networks were very small. Another *in vitro* study by Eugenin *et al.* in 2001 reports that microglia increase their frequency of dye coupling upon application of LPS and IFN- $\gamma$  or IFN- $\gamma$  plus tumor necrosis factor alpha (TNF- $\alpha$ ). However, stimulation with only one substance did not increase the incidence of dye coupling. Cx43 is the connexin isoform that is most abundantly expressed by cells of the immune system (Oviedo-Orta and Howard Evans, 2004) and has been detected in cultured microglia (Eugenin *et al.*, 2001; Garg *et al.*, 2005). Finally, GJ plaques at opposing cell membranes were described for cultured microglial cells (Garg *et al.*, 2005). In this publication the authors report that peptidoglycan (PGN, cell wall product of *Staphylococcus aureus*) increases Cx43 expression in microglia and lucifer yellow microinjection reveals dye coupling which was blocked by 18- $\alpha$ -glycyrrhetic acid, another frequently used GJ blocker. Also for this study, the percentage of coupled cells was low and the representative image only shows one adjacent cell that is dye coupled to the initial microinjected cell.

Recently Wasseff and Scherer (Wasseff and Scherer, 2014) reported the lack of GJ coupling both in resting microglia and in activated microglia after brain injury and in a model of Alzheimer’s disease. Moreover they conducted

immunohistochemical stainings for Cx43 and could not find Cx43 GJ plaques between microglia or an upregulation of Cx43 at the stab wound site as stated by Eugenin *et al.* 2001. Nevertheless, they did find an upregulation of Cx43 in surrounding uninjured cortex.

With my study I provide evidence that microglia and macrophages/monocytes do not communicate via GJs in a glioma mouse model, and furthermore confirm the previous observations for resting microglia and activated microglia in traumatic injury (Wasseff and Scherer, 2014). Consistent with the lack of functional GJ communication, Cx43 expression could not be detected in acutely FACS-isolated microglia or macrophages from the glioma tissue with a highly sensitive qRT-PCR approach. In conclusion, the dye-coupling studies in acute slices of unlesioned brain and in the glioma and stroke pathological models do not provide any evidence for functional GJ communication of microglia/brain macrophages, neither among each other nor with other cells of the brain. Thus, brain immune cells are not part of the glial syncytium.

#### **4.5 Stroke-associated microglia and macrophages/monocytes display distinct electrophysiological properties**

As demonstrated in the study by Lyons *et al.* 2000, microglia and macrophages in the stroke area 48h after induction of stroke by MCAo display a membrane current pattern resembling those of activated microglia *in vitro* or after FNA.

By comparison of intrinsic microglia and macrophages that invaded into the stroke area I could show that these cells are different from each other in regard of their membrane current profiles and their membrane capacitance as well as their specific outward conductance. Additionally, I provide evidence for the first time that the outward current of invading macrophages is maintained 7-9 d after stroke induction suggesting the these cells remain activated beyond the previously shown 48 h time frame (Lyons *et al.*, 2000).

The activated, invading tdRFP fluorescent macrophages revealed an additional delayed rectifying outward K<sup>+</sup> current which was also observed by Lyons *et al.* (2000), 6h and 48h after MCAo and might be indicative for a higher activation state. This current profile is also typical for LPS-activated microglia *in vitro* (Norenberg *et al.*, 1994) and is seen in activated microglia *in situ* after facial nerve axotomy (Boucsein *et al.*, 2000).

For the stroke-model used in this study one has to take into account that maybe not all cells are depleted in the bone marrow after radiation, therefore it could be possible that a small subpopulation of invading macrophages are also eGFP<sup>+</sup> (although I tried to differentiate macrophages from microglia via their significantly lower membrane capacitance). To validate the previous data it would be advantageous to use the *Cx3Cr1*<sup>GFP/wt</sup>*x**Ccr2*<sup>RFP/wt</sup> mouse (Saederup *et al.*, 2012) because the *CCR2* gene is expressed by blood monocytes and is replaced in one allele by a monomeric RFP (red fluorescent protein) reporter gene (*Ccr2*<sup>RFP/wt</sup>). This model would allow the visualization of CCR2<sup>+</sup> monocyte-derived macrophages in the stroke area.

Since the main focus was on the electrophysiological characterization of stroke-associated microglia and macrophages, I only conducted a few experiments injecting stroke-associated microglia and macrophages with the gap junctional tracer biocytin. These experiments revealed no dye coupling of microglia or macrophages via GJs (data not presented in results since number of experiments is too low) and were in line with previous studies showing the lack of gap junctional coupling in other pathologies (Wasseff and Scherer, 2014).

In conclusion, all *in situ* studies so far did not detect any functional coupling via GJs of microglia cells, neither under pathological conditions nor in the normal functioning brain. In a further investigation, dye-coupling experiments could be performed in other pathological models, for instance the FNA model which has already been intensively characterized (Kreutzberg, 1996; Boucsein *et al.*, 2000). In this model, the microglia density after axotomy is very high due to massive proliferation. Thus, it might be possible that activated microglia form gap junctional networks in this model. As microglia cells are highly active in synaptic stripping of the axotomized motoneurons of the facial nucleus and closely interact with the neurons, there may also be heterocellular coupling between microglia and neurons. Moreover, additional analysis of expression patterns of other connexins could be conducted, apart from Cx43 that we studied. If functional coupling among microglia cells *in situ* cannot be found, the expression of connexins could also indicate the presence of functional hemichannels in microglia cells. Recently, Orellana *et al.* (Orellana *et al.*, 2012) showed the upregulation and expression of Cx43 and hemichannels after A $\beta$  stimulation *in vitro*. Hence, one could use a comparable

activation model (e.g. LPS activation) to see similar effects of connexin expression and hemichannel function. Altogether, in my work I have shown that microglia do not express Cx43 *in vivo* and do not form GJ neither in the normal brain, nor in the glioma and stroke mouse models. Furthermore, resident microglia and infiltrating macrophages display distinctive electrophysiological characteristics in the context of both pathological models.

## 5 Summary

Glial cells play an important role during development and are essential for proper function of the central nervous system (CNS) and aberrant glial function has been described in all CNS pathologies. Astrocytes and oligodendrocytes are coupled via gap junctions (GJ), which allow exchange of ions, signalling molecules, metabolites, and form panglial networks of various size and composition in the different brain areas. NG2 cells, a type of glial precursors, can also participate in these networks. However, not much is yet known about whether microglia, the immune cells of the brain, participate in GJ coupling. GJs are formed by connexins (Cx). Astrocytes express Cx30 and Cx43 and oligodendrocytes express Cx32 and Cx47. Whether or not microglia express any Cxs is still controversial.

In my doctoral thesis I studied glial gap junctional communication among astrocytes, oligodendrocytes and NG2 cells in different brain areas. I characterized oligodendrocytic electrical coupling and investigated whether panglial networks in the corpus callosum are used for glucose transport to axons. I furthermore asked if microglial cells form functional GJs in physiology and pathology, and characterized their electrophysiological properties change in pathology. To study these questions, I used the whole-cell patch-clamp technique combined with dye-filling to trace the glial networks in murine acute brain slices, followed by immunostaining for cell-type specific markers, allowing the characterization of the panglial network. Identification of cell types during experiments was achieved by using transgenic mouse models with fluorescently labeled glia. Electrical coupling of glial cell pairs and biophysical properties were characterized by paired recordings.

My results show that astrocytes and oligodendrocytes form panglial networks in both the neocortex and in the corpus callosum, while the networks in the neocortex are larger and NG2 cells only participate in the networks in the corpus callosum. Furthermore, I found an intermediate astrocyte cell-type that expressed both *Cx43* and *Olig2*, which was present in the neocortex, but not in the corpus callosum.

Astrocytes act as energy storage elements and supply neurons with glucose via GJ. By dialysing glial cells with the glucose derivative 2NBDG, I studied their metabolic coupling. Astrocytes in the corpus callosum were metabolically coupled to oligodendrocytes. When injected into oligodendrocytes, 2NBDG spread into adja-

cent astrocytes and into the processes oriented along the myelinated axons, suggesting that this pathway may serve as a route for energy supply to axons.

Oligodendrocytes in the corpus callosum are not only dye- and metabolically coupled to astrocytes, but are also electrically coupled to one another, which is essential for a stable intracellular and extracellular ionic homeostasis. Using paired recordings, I found that coupled oligodendrocytes have a linear, voltage independent, junctional conductance which could not be influenced by the GJ modulator kainate.

Microglial cells, the resident immune cells of the CNS, respond to brain pathology with rapid phenotypical and functional changes, accompanied by alteration of their membrane current pattern. I studied coupling and membrane currents in glioma-associated microglia and macrophages/monocytes as well as stroke-associated microglia/macrophages in the MCAo model and compared these to control and stab wound-associated microglia. The current profile of microglia showed inward rectifying currents reminiscent of an intermediate activation state when compared to other disease models or cell culture. Glioma- and stroke-associated macrophages/monocytes showed a higher specific outward conductance and a significantly lower capacitance indicative of a smaller membrane area than microglia. In none of the models studied, dye-coupling of microglia/macrophages via GJs was observed. Consistently with these observations, no Cx43 expression was found when performing qRT-PCRs in freshly isolated microglia and macrophages.

Proper GJ coupling is a prerequisite for normal brain function. In this work, I provide new evidence that GJ coupling among glial cells in different areas of the CNS is highly heterogeneous in regard of function, cell types participating, and size of the networks.

## 6 Zusammenfassung

Glia-Zellen spielen nicht nur eine wichtige Rolle während der Entwicklung sondern auch für viele essentielle Funktionen des Zentralen Nervensystems (ZNS). Fehlfunktionen der verschiedenen Glia-Zelltypen spielen bei verschiedenen Pathologien des ZNS eine wichtige Rolle. Astrozyten und Oligodendrozyten sind über Gap Junction (GJ) Proteine miteinander verbunden. Diese GJs ermöglichen den Austausch von Ionen, Signalmolekülen, Metaboliten und formen pangliale Netzwerke, welche sich in ihrer Größe und Zusammensetzung in verschiedenen Gehirnarealen unterscheiden können. NG2-Zellen, eine Art Glia-Vorläuferzelle, können auch Teil dieser panglialen Netzwerke sein. Hingegen weiß man bisher nicht, ob Mikrogliazellen - die Immunzellen des Gehirns - an der GJ Kopplung beteiligt sind. Auf molekularer Ebene setzen sich GJs aus Connexin (Cx)-Untereinheiten zusammen. Astrozyten exprimieren Cx30 und Cx43 und Oligodendrozyten Cx32 und Cx47. Die Expression von Connexinen und Formierung von GJs in Mikrogliazellen ist hingegen noch umstritten.

In meiner Doktorarbeit habe ich die gliale GJ-Kommunikation zwischen Astrozyten, Oligodendrozyten und NG2-Zellen in verschiedenen Gehirnarealen untersucht. Desweiteren habe ich die elektrische Kopplung zwischen Oligodendrozyten charakterisiert und untersucht, ob sich das murine Gehirn die panglialen Netzwerke für den Glukose-Transport zu den Axonen im Corpus Callosum zu Nutze macht. Darüber hinaus stellte ich die Frage, ob Mikrogliazellen unter normalen physiologischen oder pathologischen Bedingungen funktionelle GJs bilden, und wie sich die elektrophysiologischen Eigenschaften der Mikrogliazellen unter diesen Bedingungen verändern.

Hierfür verwendete ich die Ganzzell-Patch-Clamp Technik an Gliazellen in akut isolierten Gehirnschnitten der Maus. Mit Hilfe dieser Methode wurde über die Patch-Pipette eine Glia-Zelle mit einem GJ-Tracer injiziert, welcher bei GJ-gekoppelten Zellen in benachbarte Zellen diffundierte. Im Anschluss wurden diese Hirnschnitte fixiert und mit zelltypspezifischen Markern immunhistologisch gefärbt, was eine Auswertung der einzelnen Zellen im panglialen Netzwerk ermöglichte. Durch die Verwendung von transgenen Mausmodellen mit fluoreszenzmarkierten Glia-Zellen konnte ich die initial gefüllte Zelle identifizieren. Die elektrische

Kopplung von Glia-Zellpaaren und deren biophysikalischen Eigenschaften wurden mittels Paar-Aufnahmen/Pair recordings charakterisiert.

Meine Ergebnisse zeigen, dass Astrozyten und Oligodendrozyten pangliale Netzwerke im Neocortex als auch im Corpus callosum ausbilden, die Netzwerke im Neocortex größer sind als im Corpus callosum und NG2-Zellen nur in den Netzwerken des Corpus callosum vorkommen. Zusätzlich habe ich eine intermediäre Astrozyten-Zellart im Neocortex, jedoch nicht im Corpus Callosum charakterisieren können, welche sowohl *Cx43* als auch *Olig2* exprimiert.

Astrozyten wirken als Energiespeicher und versorgen Neurone mit Metaboliten, wobei sie den Transport von Glukose über GJ-Netzwerke nutzen, wie z.B. im Hippocampus gezeigt. Hier untersuchte ich die metabolische Kopplung zwischen Glia-Zellen im Corpus Callosum mit Hilfe eines grün-fluoreszenten Glucosederivats 2NBDG und der Ganzzell-Patch-Clamp Technik. Die Experimente zeigten, dass Astrozyten im Corpus Callosum metabolisch zu Oligodendrozyten gekoppelt sind, als auch umgekehrt. Die Injektion von Oligodendrozyten zeigte eine zusätzlich Verteilung des Glucosederivats in anliegende Fortsätze, entlang der markhaltigen Axone, was eine direkte axonale Energieversorgung durch die Oligodendrozyten suggeriert. Oligodendrozyten im Corpus Callosum sind nicht nur Farbstoff- und metabolisch gekoppelt zu Astrozyten, sondern auch elektrisch. Die elektrische Kopplung ist essentiell für ein stabiles intrazelluläres als auch extrazelluläres Ionen-Gleichgewicht. Die Paar-Aufnahmen von Oligodendrozyten haben gezeigt, dass die junctionale Leitfähigkeit linear und spannungsunabhängig ist. Ferner zeigt die Verabreichung des GJ-Modulator Kainate keinen Einfluss auf diese Leitfähigkeit.

Mikrogliazellen, die Immunzellen des ZNSs, reagieren umgehend auf Pathologien mit phänotypischen und funktionellen Veränderungen als auch mit Veränderung ihrer Membranstromprofile. Hier wurden die GJ-Kopplung und die Membranströme von Mikrogliazellen und invadierenden Makrophagen/Monocyten im Glioma- und Schlaganfall/Ischämie-Modell untersucht und mit Kontroll-Mikrogliazellen und stichwunden-assoziierten Mikrogliazellen verglichen. Das Stromprofil von Mikrogliazellen zeigte einwärts-gleichgerichtete Ströme, was auf einen intermediären Aktivierungszustand, im Vergleich zu anderen Pathologien oder Zellkulturen hinweist. Glioma- und Schlaganfall-assoziierte Makrophagen/Monocyten besitzen eine höhere, nach außen gerichtete, spezifische Leitfähigkeit und eine deutlich

geringere Kapazität als Mikrogliazellen, bezeichnend für eine kleinere Membranoberfläche. In keinem der untersuchten Modelle war eine Farbstoffkopplung von Mikroglia/ Makrophagen durch GJs nachweisbar. Diese Beobachtungen wurden zusätzlich gestützt durch die fehlende Cx43-Expression, in frisch isolierten Mikroglia und Makrophagen in qRT-PCR Untersuchungen.

Die ordnungsgemäße GJ-Kopplung ist eine Voraussetzung für normale Gehirnfunktionen. Die Ergebnisse meiner Arbeit liefern neue Erkenntnisse, dass die GJ-Kopplung zwischen Glia-Zellen in verschiedenen Hirnarealen des ZNSs hinsichtlich der Funktionen der beteiligten Glia-Zellarten als auch der Größe der Netzwerke eine große Heterogenität aufweisen.

## **7 Eidesstattliche Erklärung**

Hiermit erkläre ich, Nadine Richter, dass ich die vorliegende Dissertation mit dem Titel "Properties of gap junctional coupling among glial cells in the central nervous system" selbständig verfasst habe und keine weiteren Hilfsmittel als die angegebenen verwendet habe.

Des Weiteren erkläre ich, dass die vorliegende Arbeit nie in dieser oder einer anderen Form Gegenstand eines früheren Promotionsverfahrens war.

Nadine Richter

Berlin, den 01.05.2015

## 8 References

- Abrams, C. K. and Freidin, M.** (2014) GJB1-associated X-linked Charcot-Marie-Tooth disease, a disorder affecting the central and peripheral nervous systems. *Cell Tissue Res*. doi:10.1007/s00441-014-2014-6.
- Allen, N. J. and Barres, B. A.** (2009) Neuroscience: Glia - more than just brain glue. *Nature* **457**, 675-677. doi:10.1038/457675a.
- Azevedo, F. A., Carvalho, L. R., Grinberg, L. T., Farfel, J. M., Ferretti, R. E., Leite, R. E., Jacob Filho, W., Lent, R. and Herculano-Houzel, S.** (2009) Equal numbers of neuronal and nonneuronal cells make the human brain an isometrically scaled-up primate brain. *J Comp Neurol* **513**, 532-541. doi:10.1002/cne.21974.
- Barres, B. A.** (2008) The mystery and magic of glia: a perspective on their roles in health and disease. *Neuron* **60**, 430-440. doi:10.1016/j.neuron.2008.10.013.
- Baumann, N. and Pham-Dinh, D.** (2001) Biology of oligodendrocyte and myelin in the mammalian central nervous system. *Physiol Rev* **81**, 871-927.
- Berger, T., Muller, T. and Kettenmann, H.** (1995) Developmental regulation of ion channels and receptors on glial cells. *Perspect Dev Neurobiol* **2**, 347-356.
- Berger, T., Schnitzer, J. and Kettenmann, H.** (1991) Developmental changes in the membrane current pattern, K<sup>+</sup> buffer capacity, and morphology of glial cells in the corpus callosum slice. *J Neurosci* **11**, 3008-3024.
- Berger, T., Walz, W., Schnitzer, J. and Kettenmann, H.** (1992) GABA- and glutamate-activated currents in glial cells of the mouse corpus callosum slice. *J Neurosci Res* **31**, 21-27. doi:10.1002/jnr.490310104.
- Bergles, D. E., Roberts, J. D., Somogyi, P. and Jahr, C. E.** (2000) Glutamatergic synapses on oligodendrocyte precursor cells in the hippocampus. *Nature* **405**, 187-191. doi:10.1038/35012083.
- Blomstrand, F., Venance, L., Siren, A. L., Ezan, P., Hanse, E., Glowinski, J., Ehrenreich, H. and Giaume, C.** (2004) Endothelins regulate astrocyte gap junctions in rat hippocampal slices. *Eur J Neurosci* **19**, 1005-1015.
- Boucsein, C., Kettenmann, H. and Nolte, C.** (2000) Electrophysiological properties of microglial cells in normal and pathologic rat brain slices. *Eur J Neurosci* **12**, 2049-2058.
- Bowman, C. L. and Kimelberg, H. K.** (1984) Excitatory amino acids directly depolarize rat brain astrocytes in primary culture. *Nature* **311**, 656-659.
- Brown, A. M. and Ransom, B. R.** (2007) Astrocyte glycogen and brain energy metabolism. *Glia* **55**, 1263-1271. doi:10.1002/glia.20557.
- Brown, A. M., Sickmann, H. M., Fosgerau, K., Lund, T. M., Schousboe, A., Waagepetersen, H. S. and Ransom, B. R.** (2005) Astrocyte glycogen metabolism is required for neural activity during aglycemia or intense stimulation in mouse white matter. *J Neurosci Res* **79**, 74-80. doi:10.1002/jnr.20335.
- Bruzzone, R., White, T. W. and Paul, D. L.** (1996) Connections with connexins: the molecular basis of direct intercellular signaling. *Eur J Biochem* **238**, 1-27.
- Butt, A. M.** (2013) *Neuroglia - Structure and function of oligodendrocytes*. Oxford University Press.
- Cahoy, J. D., Emery, B., Kaushal, A., Foo, L. C., Zamanian, J. L., Christopherson, K. S., Xing, Y., Lubischer, J. L., Krieg, P. A., Krupenko, S. A., Thompson, W. J. and Barres, B. A.** (2008) A transcriptome database for astrocytes, neurons, and

- oligodendrocytes: a new resource for understanding brain development and function. *J Neurosci* **28**, 264-278. doi:10.1523/JNEUROSCI.4178-07.2008.
- Cai, J., Chen, Y., Cai, W. H., Hurlock, E. C., Wu, H., Kernie, S. G., Parada, L. F. and Lu, Q. R.** (2007) A crucial role for Olig2 in white matter astrocyte development. *Development* **134**, 1887-1899. doi:10.1242/dev.02847.
- Campbell, K. and Gotz, M.** (2002) Radial glia: multi-purpose cells for vertebrate brain development. *Trends Neurosci* **25**, 235-238.
- Charles, N. A., Holland, E. C., Gilbertson, R., Glass, R. and Kettenmann, H.** (2011) The brain tumor microenvironment. *Glia* **59**, 1169-1180. doi:10.1002/glia.21136.
- Degen, J., Dublin, P., Zhang, J., Dobrowolski, R., Jokwitz, M., Karram, K., Trotter, J., Jabs, R., Willecke, K., Steinhäuser, C. and Theis, M.** (2012) Dual reporter approaches for identification of Cre efficacy and astrocyte heterogeneity. *FASEB J* **26**, 4576-4583. doi:10.1096/fj.12-207183.
- Del Rio-Hortega, P.** (1920) La microglia y su transformación en células an basocito y cuerpos granulo-adiposos. *Trab. Lab. Invest. Biol. Madrid*, 37-82.
- Dobrenis, K., Chang, H. Y., Pina-Benabou, M. H., Woodroffe, A., Lee, S. C., Rozental, R., Spray, D. C. and Scemes, E.** (2005) Human and mouse microglia express connexin36, and functional gap junctions are formed between rodent microglia and neurons. *J Neurosci Res* **82**, 306-315. doi:10.1002/jnr.20650.
- Donnan, G. A., Fisher, M., Macleod, M. and Davis, S. M.** (2008) Stroke. *Lancet* **371**, 1612-1623. doi:10.1016/S0140-6736(08)60694-7.
- Elfang, C., Eckert, R., Lichtenberg-Frate, H., Butterweck, A., Traub, O., Klein, R. A., Hulser, D. F. and Willecke, K.** (1995) Specific permeability and selective formation of gap junction channels in connexin-transfected HeLa cells. *J Cell Biol* **129**, 805-817.
- Eugenin, E. A., Babilio, D., Saez, J. C., Orellana, J. A., Raine, C. S., Bukauskas, F., Bennett, M. V. and Berman, J. W.** (2012) The role of gap junction channels during physiologic and pathologic conditions of the human central nervous system. *J Neuroimmune Pharmacol* **7**, 499-518. doi:10.1007/s11481-012-9352-5.
- Eugenin, E. A., Eckardt, D., Theis, M., Willecke, K., Bennett, M. V. and Saez, J. C.** (2001) Microglia at brain stab wounds express connexin 43 and in vitro form functional gap junctions after treatment with interferon-gamma and tumor necrosis factor-alpha. *Proc Natl Acad Sci U S A* **98**, 4190-4195. doi:10.1073/pnas.051634298  
051634298 [pii].
- Fünfschilling, U., Supplie, L. M., Mahad, D., Boretius, S., Saab, A. S., Edgar, J., Brinkmann, B. G., Kassmann, C. M., Tzvetanova, I. D., Mobius, W., Diaz, F., Meijer, D., Suter, U., Hamprecht, B., Sereda, M. W., Moraes, C. T., Frahm, J., Goebbels, S. and Nave, K. A.** (2012) Glycolytic oligodendrocytes maintain myelin and long-term axonal integrity. *Nature* **485**, 517-521. doi:10.1038/nature11007.
- Fuss, B., Mallon, B., Phan, T., Ohlemeyer, C., Kirchhoff, F., Nishiyama, A. and Macklin, W. B.** (2000) Purification and analysis of in vivo-differentiated oligodendrocytes expressing the green fluorescent protein. *Dev Biol* **218**, 259-274. doi:10.1006/dbio.1999.9574.
- Gabrusiewicz, K., Ellert-Miklaszewska, A., Lipko, M., Sielska, M., Frankowska, M. and Kaminska, B.** (2011) Characteristics of the alternative phenotype of microglia/macrophages and its modulation in experimental gliomas. *PLoS One* **6**, e23902. doi:10.1371/journal.pone.0023902.

- Garg, S., Md Syed, M. and Kielian, T.** (2005) Staphylococcus aureus-derived peptidoglycan induces Cx43 expression and functional gap junction intercellular communication in microglia. *J Neurochem* **95**, 475-483. doi:JNC3384 [pii]10.1111/j.1471-4159.2005.03384.x.
- Gertz, K., Kronenberg, G., Kalin, R. E., Baldinger, T., Werner, C., Balkaya, M., Eom, G. D., Hellmann-Regen, J., Krober, J., Miller, K. R., Lindauer, U., Laufs, U., Dirnagl, U., Heppner, F. L. and Endres, M.** (2012) Essential role of interleukin-6 in post-stroke angiogenesis. *Brain* **135**, 1964-1980. doi:10.1093/brain/aws075.
- Ginhoux, F., Greter, M., Leboeuf, M., Nandi, S., See, P., Gokhan, S., Mehler, M. F., Conway, S. J., Ng, L. G., Stanley, E. R., Samokhvalov, I. M. and Merad, M.** (2010) Fate mapping analysis reveals that adult microglia derive from primitive macrophages. *Science* **330**, 841-845. doi:10.1126/science.1194637.
- Griemsmann, S., Hoft, S. P., Bedner, P., Zhang, J., von Staden, E., Beinhauer, A., Degen, J., Dublin, P., Cope, D. W., Richter, N., Crunelli, V., Jabs, R., Willecke, K., Theis, M., Seifert, G., Kettenmann, H. and Steinhauser, C.** (2014) Characterization of Panglial Gap Junction Networks in the Thalamus, Neocortex, and Hippocampus Reveals a Unique Population of Glial Cells. *Cereb Cortex*. doi:10.1093/cercor/bhu157.
- Haas, B., Schipke, C. G., Peters, O., Sohl, G., Willecke, K. and Kettenmann, H.** (2006) Activity-dependent ATP-waves in the mouse neocortex are independent from astrocytic calcium waves. *Cereb Cortex* **16**, 237-246. doi:10.1093/cercor/bhi101.
- Haas, S., Brockhaus, J., Verkhratsky, A. and Kettenmann, H.** (1996) ATP-induced membrane currents in amoeboid microglia acutely isolated from mouse brain slices. *Neuroscience* **75**, 257-261. doi:0306452296002709 [pii].
- Hamill, O. P., Marty, A., Neher, E., Sakmann, B. and Sigworth, F. J.** (1981) Improved patch-clamp techniques for high-resolution current recording from cells and cell-free membrane patches. *Pflugers Arch* **391**, 85-100.
- Hanisch, U. K. and Kettenmann, H.** (2007) Microglia: active sensor and versatile effector cells in the normal and pathologic brain. *Nat Neurosci* **10**, 1387-1394. doi:10.1038/nn1997.
- Hirrlinger, P. G., Scheller, A., Braun, C., Quintela-Schneider, M., Fuss, B., Hirrlinger, J. and Kirchhoff, F.** (2005) Expression of reef coral fluorescent proteins in the central nervous system of transgenic mice. *Mol Cell Neurosci* **30**, 291-303. doi:10.1016/j.mcn.2005.08.011.
- Houades, V., Koulakoff, A., Ezan, P., Seif, I. and Giaume, C.** (2008) Gap junction-mediated astrocytic networks in the mouse barrel cortex. *J Neurosci* **28**, 5207-5217. doi:10.1523/JNEUROSCI.5100-07.2008.
- Institute, N.** (2009) Brain Basics: Preventing Stroke. *National Institute of Neurological Disorders and Stroke*.
- Jabs, R., Pivneva, T., Huttmann, K., Wyczynski, A., Nolte, C., Kettenmann, H. and Steinhauser, C.** (2005) Synaptic transmission onto hippocampal glial cells with hGFAP promoter activity. *J Cell Sci* **118**, 3791-3803. doi:10.1242/jcs.02515.
- Jung, S., Aliberti, J., Graemmel, P., Sunshine, M. J., Kreutzberg, G. W., Sher, A. and Littman, D. R.** (2000) Analysis of fractalkine receptor CX(3)CR1 function by targeted deletion and green fluorescent protein reporter gene insertion. *Mol Cell Biol* **20**, 4106-4114.
- Karram, K., Goebbels, S., Schwab, M., Jennissen, K., Seifert, G., Steinhauser, C., Nave, K. A. and Trotter, J.** (2008) NG2-expressing cells in the nervous system

- revealed by the NG2-EYFP-knockin mouse. *Genesis* **46**, 743-757. doi:10.1002/dvg.20440.
- Kerber, M., Reiss, Y., Wickersheim, A., Jugold, M., Kiessling, F., Heil, M., Tchaikovski, V., Waltenberger, J., Shibuya, M., Plate, K. H. and Machein, M. R.** (2008) Flt-1 signaling in macrophages promotes glioma growth in vivo. *Cancer Res* **68**, 7342-7351. doi:10.1158/0008-5472.CAN-07-6241.
- Kettenmann, H., Backus, K. H. and Schachner, M.** (1984a) Aspartate, glutamate and gamma-aminobutyric acid depolarize cultured astrocytes. *Neurosci Lett* **52**, 25-29. doi:0304-3940(84)90345-8 [pii].
- Kettenmann, H., Gilbert, P. and Schachner, M.** (1984b) Depolarization of cultured oligodendrocytes by glutamate and GABA. *Neurosci Lett* **47**, 271-276.
- Kettenmann, H., Hanisch, U. K., Noda, M. and Verkhratsky, A.** (2011) Physiology of microglia. *Physiol Rev* **91**, 461-553. doi:10.1152/physrev.00011.2010.
- Kettenmann, H., Hoppe, D., Gottmann, K., Banati, R. and Kreutzberg, G.** (1990) Cultured microglial cells have a distinct pattern of membrane channels different from peritoneal macrophages. *J Neurosci Res* **26**, 278-287. doi:10.1002/jnr.490260303.
- Kettenmann, H. and Ransom, B. R.** (1988) Electrical coupling between astrocytes and between oligodendrocytes studied in mammalian cell cultures. *Glia* **1**, 64-73. doi:10.1002/glia.440010108.
- Kettenmann, H. and Verkhratsky, A.** (2008) Neuroglia: the 150 years after. *Trends Neurosci* **31**, 653-659. doi:10.1016/j.tins.2008.09.003.
- Kigerl, K. A., Gensel, J. C., Ankeny, D. P., Alexander, J. K., Donnelly, D. J. and Popovich, P. G.** (2009) Identification of two distinct macrophage subsets with divergent effects causing either neurotoxicity or regeneration in the injured mouse spinal cord. *J Neurosci* **29**, 13435-13444. doi:10.1523/JNEUROSCI.3257-09.2009.
- Kreutzberg, G. W.** (1996) Microglia: a sensor for pathological events in the CNS. *Trends Neurosci* **19**, 312-318.
- Kukley, M., Capetillo-Zarate, E. and Dietrich, D.** (2007) Vesicular glutamate release from axons in white matter. *Nat Neurosci* **10**, 311-320. doi:10.1038/nn1850.
- Li, W. and Graeber, M. B.** (2012) The molecular profile of microglia under the influence of glioma. *Neuro Oncol* **14**, 958-978. doi:10.1093/neuonc/nos116.
- Lu, Q. R., Sun, T., Zhu, Z., Ma, N., Garcia, M., Stiles, C. D. and Rowitch, D. H.** (2002) Common developmental requirement for Olig function indicates a motor neuron/oligodendrocyte connection. *Cell* **109**, 75-86.
- Luche, H., Weber, O., Nageswara Rao, T., Blum, C. and Fehling, H. J.** (2007) Faithful activation of an extra-bright red fluorescent protein in "knock-in" Cre-reporter mice ideally suited for lineage tracing studies. *Eur J Immunol* **37**, 43-53. doi:10.1002/eji.200636745.
- Lyons, S. A., Pastor, A., Ohlemeyer, C., Kann, O., Wiegand, F., Prass, K., Knapp, F., Kettenmann, H. and Dirnagl, U.** (2000) Distinct physiologic properties of microglia and blood-borne cells in rat brain slices after permanent middle cerebral artery occlusion. *J Cereb Blood Flow Metab* **20**, 1537-1549. doi:10.1097/00004647-200011000-00003.
- Maglione, M., Tress, O., Haas, B., Karram, K., Trotter, J., Willecke, K. and Kettenmann, H.** (2010) Oligodendrocytes in mouse corpus callosum are coupled via gap junction channels formed by connexin47 and connexin32. *Glia* **58**, 1104-1117. doi:10.1002/glia.20991.

- Mantovani, A., Sica, A., Sozzani, S., Allavena, P., Vecchi, A. and Locati, M.** (2004) The chemokine system in diverse forms of macrophage activation and polarization. *Trends Immunol* **25**, 677-686. doi:10.1016/j.it.2004.09.015.
- Markovic, D. S., Vinnakota, K., Chirasani, S., Synowitz, M., Raguette, H., Stock, K., Sliwa, M., Lehmann, S., Kalin, R., van Rooijen, N., Holmbeck, K., Heppner, F. L., Kiwit, J., Matyash, V., Lehnardt, S., Kaminska, B., Glass, R. and Kettenmann, H.** (2009) Gliomas induce and exploit microglial MT1-MMP expression for tumor expansion. *Proc Natl Acad Sci U S A* **106**, 12530-12535. doi:10.1073/pnas.0804273106.
- Marshall, C. A., Novitsch, B. G. and Goldman, J. E.** (2005) Olig2 directs astrocyte and oligodendrocyte formation in postnatal subventricular zone cells. *J Neurosci* **25**, 7289-7298. doi:10.1523/JNEUROSCI.1924-05.2005.
- Martinez, A. D., Eugenin, E. A., Branes, M. C., Bennett, M. V. and Saez, J. C.** (2002) Identification of second messengers that induce expression of functional gap junctions in microglia cultured from newborn rats. *Brain Res* **943**, 191-201.
- Meme, W., Ezan, P., Venance, L., Glowinski, J. and Giaume, C.** (2004) ATP-induced inhibition of gap junctional communication is enhanced by interleukin-1 beta treatment in cultured astrocytes. *Neuroscience* **126**, 95-104. doi:10.1016/j.neuroscience.2004.03.031.
- Meme, W., Vandecasteele, M., Giaume, C. and Venance, L.** (2009) Electrical coupling between hippocampal astrocytes in rat brain slices. *Neurosci Res* **63**, 236-243. doi:10.1016/j.neures.2008.12.008.
- Menichella, D. M., Majdan, M., Awatramani, R., Goodenough, D. A., Sirkowski, E., Scherer, S. S. and Paul, D. L.** (2006) Genetic and physiological evidence that oligodendrocyte gap junctions contribute to spatial buffering of potassium released during neuronal activity. *J Neurosci* **26**, 10984-10991. doi:10.1523/JNEUROSCI.0304-06.2006.
- Mika, T. and Prochnow, N.** (2012) Functions of connexins and large pore channels on microglial cells: the gates to environment. *Brain Res* **1487**, 16-24. doi:S0006-8993(12)01167-5 [pii]  
10.1016/j.brainres.2012.07.020.
- Müller, T., Möller, T., Berger, T., Schnitzer, J. and Kettenmann, H.** (1992) Calcium entry through kainate receptors and resulting potassium-channel blockade in Bergmann glial cells. *Science* **256**, 1563-1566.
- Müller, T., Möller, T., Neuhaus, J. and Kettenmann, H.** (1996) Electrical coupling among Bergmann glial cells and its modulation by glutamate receptor activation. *Glia* **17**, 274-284. doi:10.1002/(SICI)1098-1136(199608)17:4<274::AID-GLIA2>3.0.CO;2-#.
- Newell, E. W. and Schlichter, L. C.** (2005) Integration of K<sup>+</sup> and Cl<sup>-</sup> currents regulate steady-state and dynamic membrane potentials in cultured rat microglia. *J Physiol* **567**, 869-890. doi:10.1113/jphysiol.2005.092056.
- Nimmerjahn, A., Kirchhoff, F. and Helmchen, F.** (2005) Resting microglial cells are highly dynamic surveillants of brain parenchyma in vivo. *Science* **308**, 1314-1318. doi:1110647 [pii]  
10.1126/science.1110647.
- Nishiyama, A.** (2007) Polydendrocytes: NG2 cells with many roles in development and repair of the CNS. *Neuroscientist* **13**, 62-76. doi:10.1177/1073858406295586.
- Nishiyama, A.** (2013) *Neuroglia - NG2 Cells (Polydendrocytes)*. Oxford University Press.

- Nishiyama, A., Komitova, M., Suzuki, R. and Zhu, X.** (2009) Polydendrocytes (NG2 cells): multifunctional cells with lineage plasticity. *Nat Rev Neurosci* **10**, 9-22. doi:10.1038/nrn2495.
- Nolte, C., Matyash, M., Pivneva, T., Schipke, C. G., Ohlemeyer, C., Hanisch, U. K., Kirchhoff, F. and Kettenmann, H.** (2001) GFAP promoter-controlled EGFP-expressing transgenic mice: a tool to visualize astrocytes and astrogliosis in living brain tissue. *Glia* **33**, 72-86. doi:10.1002/1098-1136(20010101)33:1<72::AID-GLIA1007>3.0.CO;2-A [pii].
- Norenberg, W., Gebicke-Haerter, P. J. and Illes, P.** (1994) Voltage-dependent potassium channels in activated rat microglia. *J Physiol* **475**, 15-32.
- Nualart-Marti, A., Solsona, C. and Fields, R. D.** (2013) Gap junction communication in myelinating glia. *Biochim Biophys Acta* **1828**, 69-78. doi:10.1016/j.bbamem.2012.01.024.
- Olah, M., Raj, D., Brouwer, N., De Haas, A. H., Eggen, B. J., Den Dunnen, W. F., Biber, K. P. and Boddeke, H. W.** (2012) An optimized protocol for the acute isolation of human microglia from autopsy brain samples. *Glia* **60**, 96-111. doi:10.1002/glia.21251.
- Orellana, J. A., Shoji, K. F., Abudara, V., Ezan, P., Amigou, E., Saez, P. J., Jiang, J. X., Naus, C. C., Saez, J. C. and Giaume, C.** (2011) Amyloid beta-induced death in neurons involves glial and neuronal hemichannels. *J Neurosci* **31**, 4962-4977. doi:10.1523/JNEUROSCI.6417-10.2011.
- Orellana, J. A., von Bernhardi, R., Giaume, C. and Saez, J. C.** (2012) Glial hemichannels and their involvement in aging and neurodegenerative diseases. *Rev Neurosci* **23**, 163-177. doi:10.1515/revneuro-2011-0065.
- Orthmann-Murphy, J. L., Abrams, C. K. and Scherer, S. S.** (2008) Gap junctions couple astrocytes and oligodendrocytes. *J Mol Neurosci* **35**, 101-116. doi:10.1007/s12031-007-9027-5.
- Oviedo-Orta, E. and Howard Evans, W.** (2004) Gap junctions and connexin-mediated communication in the immune system. *Biochim Biophys Acta* **1662**, 102-112. doi:10.1016/j.bbamem.2003.10.021.
- Pannasch, U., Farber, K., Nolte, C., Blonski, M., Yan Chiu, S., Messing, A. and Kettenmann, H.** (2006) The potassium channels Kv1.5 and Kv1.3 modulate distinct functions of microglia. *Mol Cell Neurosci* **33**, 401-411. doi:10.1016/j.mcn.2006.08.009.
- Pannasch, U. and Rouach, N.** (2013) Emerging role for astroglial networks in information processing: from synapse to behavior. *Trends Neurosci* **36**, 405-417. doi:10.1016/j.tins.2013.04.004.
- Parenti, R., Campisi, A., Vanella, A. and Cicirata, F.** (2002) Immunocytochemical and RT-PCR analysis of connexin36 in cultures of mammalian glial cells. *Arch Ital Biol* **140**, 101-108.
- Pastor, A., Chvatal, A., Sykova, E. and Kettenmann, H.** (1995) Glycine- and GABA-activated currents in identified glial cells of the developing rat spinal cord slice. *Eur J Neurosci* **7**, 1188-1198.
- Perry, V. H. and O'Connor, V.** (2010) The role of microglia in synaptic stripping and synaptic degeneration: a revised perspective. *ASN Neuro* **2**, e00047. doi:10.1042/AN20100024.

- Rash, J. E.** (2010) Molecular disruptions of the panglial syncytium block potassium siphoning and axonal saltatory conduction: pertinence to neuromyelitis optica and other demyelinating diseases of the central nervous system. *Neuroscience* **168**, 982-1008. doi:10.1016/j.neuroscience.2009.10.028.
- Rouach, N., Koulakoff, A., Abudara, V., Willecke, K. and Giaume, C.** (2008) Astroglial metabolic networks sustain hippocampal synaptic transmission. *Science* **322**, 1551-1555. doi:10.1126/science.1164022.
- Saab, A. S., Tzvetanova, I. D. and Nave, K. A.** (2013) The role of myelin and oligodendrocytes in axonal energy metabolism. *Curr Opin Neurobiol* **23**, 1065-1072. doi:10.1016/j.conb.2013.09.008.
- Saederup, N., Mizutani, M., Pino, P. A., Charo, I. F., Ransohoff, R. M. and Cardona, A. E.** (2012) The fractalkine receptor but not CCR2 is present on microglia from embryonic development throughout adulthood. *J Immunol* **188**, 29-36. doi:10.4049/jimmunol.1100421.
- Saez, J. C., Retamal, M. A., Basilio, D., Bukauskas, F. F. and Bennett, M. V.** (2005) Connexin-based gap junction hemichannels: gating mechanisms. *Biochim Biophys Acta* **1711**, 215-224. doi:S0005-2736(05)00052-0 [pii]  
10.1016/j.bbamem.2005.01.014.
- Saez, P. J., Shoji, K. F., Retamal, M. A., Harcha, P. A., Ramirez, G., Jiang, J. X., von Bernhardi, R. and Saez, J. C.** (2013) ATP is required and advances cytokine-induced gap junction formation in microglia in vitro. *Mediators Inflamm* **2013**, 216402. doi:10.1155/2013/216402.
- Sasmono, R. T., Oceandy, D., Pollard, J. W., Tong, W., Pavli, P., Wainwright, B. J., Ostrowski, M. C., Himes, S. R. and Hume, D. A.** (2003) A macrophage colony-stimulating factor receptor-green fluorescent protein transgene is expressed throughout the mononuclear phagocyte system of the mouse. *Blood* **101**, 1155-1163. doi:10.1182/blood-2002-02-0569.
- Seifert, S., Pannell, M., Uckert, W., Farber, K. and Kettenmann, H.** (2011) Transmitter- and hormone-activated Ca(2+) responses in adult microglia/brain macrophages in situ recorded after viral transduction of a recombinant Ca(2+) sensor. *Cell Calcium* **49**, 365-375. doi:10.1016/j.ceca.2011.03.005.
- Streit, W. J.** (2013) *Neuroglia - Microglial Cells*. Oxford University Press.
- Sutor, B. and Hagerty, T.** (2005) Involvement of gap junctions in the development of the neocortex. *Biochim Biophys Acta* **1719**, 59-68. doi:10.1016/j.bbamem.2005.09.005.
- Szulzewsky, F., Pelz, A., Feng, X., Synowitz, M., Markovic, D., Langmann, T., Holtman, I. R., Wang, X., Eggen, B. J., Boddeke, H. W., Hambardzumyan, D., Wolf, S. A. and Kettenmann, H.** (2015) Glioma-associated microglia/macrophages display an expression profile different from M1 and M2 polarization and highly express *Gpnmb* and *Spp1*. *PLoS One* **10**, e0116644. doi:10.1371/journal.pone.0116644  
PONE-D-14-27058 [pii].
- Tambuyzer, B. R., Ponsaerts, P. and Nouwen, E. J.** (2009) Microglia: gatekeepers of central nervous system immunology. *J Leukoc Biol* **85**, 352-370. doi:jlbb.0608385 [pii]  
10.1189/jlb.0608385.
- Teubner, B., Michel, V., Pesch, J., Lautermann, J., Cohen-Salmon, M., Sohl, G., Jahnke, K., Winterhager, E., Herberhold, C., Hardelin, J. P., Petit, C. and Willecke, K.** (2003) Connexin30 (*Gjb6*)-deficiency causes severe hearing impairment and lack of endocochlear potential. *Hum Mol Genet* **12**, 13-21.

- Teubner, B., Odermatt, B., Guldenagel, M., Sohl, G., Degen, J., Bukauskas, F., Kronengold, J., Verselis, V. K., Jung, Y. T., Kozak, C. A., Schilling, K. and Willecke, K. (2001) Functional expression of the new gap junction gene connexin47 transcribed in mouse brain and spinal cord neurons. *J Neurosci* **21**, 1117-1126. doi:10.1523/JNEUROSCI.0392-12.2012.
- Tress, O., Maglione, M., May, D., Pivneva, T., Richter, N., Seyfarth, J., Binder, S., Zlomuzica, A., Seifert, G., Theis, M., Dere, E., Kettenmann, H. and Willecke, K. (2012) Panglial gap junctional communication is essential for maintenance of myelin in the CNS. *J Neurosci* **32**, 7499-7518. doi:10.1523/JNEUROSCI.0392-12.2012.
- Tress, O., Maglione, M., Zlomuzica, A., May, D., Dicke, N., Degen, J., Dere, E., Kettenmann, H., Hartmann, D. and Willecke, K. (2011) Pathologic and phenotypic alterations in a mouse expressing a connexin47 missense mutation that causes Pelizaeus-Merzbacher-like disease in humans. *PLoS Genet* **7**, e1002146. doi:10.1371/journal.pgen.1002146.
- Trotter, J., Karram, K. and Nishiyama, A. (2010) NG2 cells: Properties, progeny and origin. *Brain Res Rev* **63**, 72-82. doi:10.1016/j.brainresrev.2009.12.006.
- Venance, L., Piomelli, D., Glowinski, J. and Giaume, C. (1995) Inhibition by anandamide of gap junctions and intercellular calcium signalling in striatal astrocytes. *Nature* **376**, 590-594. doi:10.1038/376590a0.
- Verkhratsky, A., Orkand, R. K. and Kettenmann, H. (1998) Glial calcium: homeostasis and signaling function. *Physiol Rev* **78**, 99-141.
- Verkhratsky, A. and Steinhauser, C. (2000) Ion channels in glial cells. *Brain Res Brain Res Rev* **32**, 380-412.
- Vinnakota, K., Hu, F., Ku, M. C., Georgieva, P. B., Szulzewsky, F., Pohlmann, A., Waiczies, S., Waiczies, H., Niendorf, T., Lehnardt, S., Hanisch, U. K., Synowitz, M., Markovic, D., Wolf, S. A., Glass, R. and Kettenmann, H. (2013) Toll-like receptor 2 mediates microglia/brain macrophage MT1-MMP expression and glioma expansion. *Neuro Oncol* **15**, 1457-1468. doi:10.1093/neuonc/not115.
- Von Blankenfeld, G., Ransom, B. R. and Kettenmann, H. (1993) Development of cell-cell coupling among cells of the oligodendrocyte lineage. *Glia* **7**, 322-328. doi:10.1002/glia.440070407.
- Wallraff, A., Kohling, R., Heinemann, U., Theis, M., Willecke, K. and Steinhauser, C. (2006) The impact of astrocytic gap junctional coupling on potassium buffering in the hippocampus. *J Neurosci* **26**, 5438-5447. doi:10.1523/JNEUROSCI.0037-06.2006.
- Wallraff, A., Odermatt, B., Willecke, K. and Steinhauser, C. (2004) Distinct types of astroglial cells in the hippocampus differ in gap junction coupling. *Glia* **48**, 36-43. doi:10.1002/glia.20040.
- Wang, L. P., Cheung, G., Kronenberg, G., Gertz, K., Ji, S., Kempermann, G., Endres, M. and Kettenmann, H. (2008) Mild brain ischemia induces unique physiological properties in striatal astrocytes. *Glia* **56**, 925-934. doi:10.1002/glia.20660.
- Wasseff, S., Abrams, C. K. and Scherer, S. S. (2010) A dominant connexin43 mutant does not have dominant effects on gap junction coupling in astrocytes. *Neuron Glia Biol* **6**, 213-223. doi:10.1017/S1740925X11000019.
- Wasseff, S. K. and Scherer, S. S. (2011) Cx32 and Cx47 mediate oligodendrocyte:astrocyte and oligodendrocyte:oligodendrocyte gap junction coupling. *Neurobiol Dis* **42**, 506-513. doi:10.1016/j.nbd.2011.03.003.
- Wasseff, S. K. and Scherer, S. S. (2014) Activated microglia do not form functional gap junctions in vivo. *J Neuroimmunol* **269**, 90-93. doi:10.1016/j.jneuroim.2014.02.005.

- Wen, P. Y. and Kesari, S.** (2008) Malignant gliomas in adults. *N Engl J Med* **359**, 492-507. doi:10.1056/NEJMra0708126.
- Wender, R., Brown, A. M., Fern, R., Swanson, R. A., Farrell, K. and Ransom, B. R.** (2000) Astrocytic glycogen influences axon function and survival during glucose deprivation in central white matter. *J Neurosci* **20**, 6804-6810.
- Willecke, K., Eiberger, J., Degen, J., Eckardt, D., Romualdi, A., Guldenagel, M., Deutsch, U. and Sohl, G.** (2002) Structural and functional diversity of connexin genes in the mouse and human genome. *Biol Chem* **383**, 725-737. doi:10.1515/BC.2002.076.
- Zhang, W., Couldwell, W. T., Simard, M. F., Song, H., Lin, J. H. and Nedergaard, M.** (1999) Direct gap junction communication between malignant glioma cells and astrocytes. *Cancer Res* **59**, 1994-2003.